PB-233 252

AIR POLLUTION TRANSPORT IN STREET CANYONS

Los Alamos Scientific Laboratory

Prepared for
Environmental Protection Agency

June 1973

DISTRIBUTED BY:

NTIS
National Technical Information Service
U. S. DEPARTMENT OF COMMERCE

BIBLIOGRAPHIC DATA SHEET	1. Report No. EPA-R4-73-029	2.	PB 233 252

4. Title and Subtitle Air Pollution Transport in Street Canyons	5. Report Date June 1973 6.
7. Author(s) R. S. Hotchkiss and F. H. Harlow	8. Performing Organization Rept. No.
9. Performing Organization Name and Address University of California Los Alamos Scientific Laboratory Los Alamos, New Mexico 87544	10. Project/Task/Work Unit No. 11. Contract/Grant No. EPA-IAG-0122 (D)
12. Sponsoring Organization Name and Address EPA, Meteorology Laboratory National Environmental Research Center Research Triangle Park, North Carolina 27711	13. Type of Report & Period Covered Final Report 14.

15. Supplementary Notes

16. Abstracts

This project was conducted to demonstrate the applicability of numerically modeling the transport of pollution in street canyons. The numerical model employs the solutions of the fully nonlinear, three-dimensional Navier-Stokes equations along with a transport equation for pollutants, for regions of space in which obstacles or buildings cause strong distortions in the flow fields.

The numerical technique is used to model three-dimensional flows for which some experimental data have been obtained. This includes calculating the distribution of pollutants in the Broadway Street Canyon in downtown St. Louis, Missouri. Also, the numerical method is used to calculate pollutant distributions in a non-specific street canyon; that is, a street canyon in which the geometry and other important non-dimensional flow parameters give rise to solutions that are applicable, in a general sense, to a variety of street canyons.

17. Key Words and Document Analysis. 17a. Descriptors

17b. Identifiers/Open-Ended Terms

Reproduced by
NATIONAL TECHNICAL
INFORMATION SERVICE
U S Department of Commerce
Springfield VA 22151

17c. COSATI Field/Group

18. Availability Statement	19. Security Class (This Report) UNCLASSIFIED	21. No. of Pages 128
	20. Security Class (This Page UNCLASSIFIED	22. Price $4.75/1.45

EPA-R4-73-029

AIR POLLUTION TRANSPORT IN STREET CANYONS

by

R.S. Hotchkiss and F.H. Harlow

University of California
Los Alamos Scientific Laboratory
Los Alamos, New Mexico 87544

Interagency Agreement No. EPA-IAG-0122(D)
Program Element No. 1A1009

EPA Project Officer: William H. Snyder

Meteorology Laboratory
National Environmental Research Center
Research Triangle Park, North Carolina 27711

Prepared for

OFFICE OF RESEARCH AND MONITORING
U.S. ENVIRONMENTAL PROTECTION AGENCY
WASHINGTON, D.C. 20460

June 1973

1-A

This report has been reviewed by the Environmental Protection Agency and approved for publication. Approval does not signify that the contents necessarily reflect the views and policies of the Agency, nor does mention of trade names or commercial products constitute endorsement or recommendation for use.

ABSTRACT

This report presents the results of a study to determine the applicability of numerically modeling the transport of pollution in street canyons. The numerical model employs the solutions of the fully non-linear, three-dimensional Navier-Stokes equations along with a transport equation for pollutants, for regions of space in which obstacles or buildings cause strong distortions in the flow fields.

An analytic formulation of a two-dimensional street canyon is presented to illustrate the linear theory and the associated principles of flow in a notch. These results are then compared to the numerically obtained non-linear solutions to determine the regions of validity for linear theory.

The numerical technique is also used to model three-dimensional flows for which some experimental data have been obtained. This includes calculating the distribution of pollutants in the Broadway Street Canyon in downtown St. Louis, Missouri.

Finally, the numerical method is used to calculate pollutant distributions in a non-specific street canyon; that is, a street canyon in which the geometry and other important nondimensional flow parameters give rise to solutions that are applicable, in a general sense, to a variety of street canyons.

This report was submitted in fulfillment of Contract Number EPA-IAG-0122(D), by the University of California, Los Alamos Scientific Laboratory, under the partial sponsorship of the Environmental Protection Agency. Work was completed as of March, 1973.

CONTENTS

		Page
Abstract		ii
List of Figures		iv
List of Tables		viii
Acknowledgments		ix
Sections		
I	Conclusions	1
II	Recommendations	2
III	Introduction	3
IV	Analytical Derivation	6
V	Comparison with the Model of Johnson, et.al.	14
VI	The Numerical Approach	15
VII	Two-Dimensional Results	19
VIII	Three-Dimensional Results	41
IX	A Generalized Street Canyon	60
X	Computer Requirements	77
XI	References	78
XII	Appendix	79

FIGURES

No.		Page
1.	Steady velocity field established in a two dimensional square street canyon.	20
2.	Experimental flow field observed by Wang, Chang and Lin for a Reynold's number of 2.1×10^4.	21
3.	Steady pressure distribution isobars for the flow depicted in Fig. 1.	22
4.	Steady particle distribution resulting from a line source in the bottom of the canyon.	24
5.	Isopleths of Fig. 4 showing concentration distribution within the canyon.	25
6.	Steady particle distribution resulting from a point source located at the bottom center of the canyon.	26
7.	Isopleths of Fig. 6 showing concentration distributions in the canyon.	27
8.	Isopleths predicted by the analytic model for concentration distribution in the canyon.	28
9.	Steady particle distribution resulting from a line source in the bottom of the canyon. Results reflect a smaller diffusivity.	33
10.	Isopleths of Fig. 9 showing concentration distribution within the canyon.	34
11.	Steady particle distribution obtained from modeling the experiment of Wang, Chang and Lin.	36
12.	Isopleths of numerically calculated concentrations in the plane of the source of Fig. 11.	37
13.	Isopleths drawn through the data reported by Wang, Chang and Lin.	38
14.	Isopleths of numerically calculated concentrations for a plane slightly off the plane of the source in Fig. 11.	39

FIGURES (continued)

No.		Page
15.	Computing mesh for Broadway Street Canyon - St. Louis, Missouri.	42
16.	Perspective view of velocity vectors in a plane perpendicular to the z axis at a distance of 15 feet from the origin. Location of the coordinate system is shown.	43
17.	Perspective view of velocity vectors in a plane perpendicular to the z axis at a distance of 65 feet from the origin.	44
18.	Perspective view of velocity vectors in a plane perpendicular to the z axis at a distance of 115 feet from the origin.	45
19.	Plane view of velocity vectors in a plane perpendicular to the y axis at a distance of 55 feet from the origin.	46
20.	Plane view of velocity vectors in a plane perpendicular to the y axis at a distance of 105 feet from the origin.	46
21.	Plane view of velocity vectors in a plane perpendicular to the y axis at a distance of 155 feet from the origin. The intersection of this plane with the buildings is shown.	47
22.	Plane view of velocity vectors in a plane perpendicular to the x axis at a distance of 175 feet from the origin.	48
23.	Steady particulate distribution in Broadway Street Canyon resulting from real sources on Broadway, Locust and Olive Streets.	49
24.	Isopleths in a plane perpendicular to the x axis at a distance of 155 feet from the origin. This plot corresponds to the measuring station of Ludwig and Dabberdt.	50
25.	Distribution of CO concentration in Broadway Street Canyon measured by Ludwig and Dabberdt.	51

FIGURES (continued)

No.		Page
26.	Isopleths in a plane perpendicular to the z axis at a distance of 15 feet from the origin.	54
27.	Isopleths in a plane perpendicular to the z axis at a distance of 65 feet from the origin.	55
28.	Isopleths in a plane perpendicular to the y axis at a distance of 55 feet from the origin.	56
29.	Isopleths in a plane perpendicular to the y axis at a distance of 105 feet from the origin.	57
30.	Isopleths in a plane perpendicular to the x axis at a distance of 95 feet from the origin.	58
31.	Isopleths in a plane perpendicular to the x axis at a distance of 205 feet from the origin.	59
32.	Generalized street canyon configuration in perspective with velocity vectors shown in a plane perpendicular to the z axis at a distance of 5.5 units from the origin. Location of the coordinate system is shown.	62
33.	Plane views of velocity vectors in a plane perpendicular to the y axis at a distance of 9.5 units from the origin.	63
34.	Steady particle distribution in the generalized street canyon, as viewed from above, resulting from a line source perpendicular to the incoming flow.	64
35.	Same particle distribution as that shown in Fig. 34, only viewed from the top of the buildings at mid-block.	65
36.	Isopleths in a plane perpendicular to the z axis at a distance of 1.5 units from the origin. (Source perpendicular to inflow).	66
37.	Isopleths in a plane perpendicular to the z axis at a distance of 5.5 units from the origin. (Source perpendicular).	67

FIGURES (continued)

No.		Page
38.	Isopleths in a plane perpendicular to the z axis at a distance of 10.5 units from the origin. (Source perpendicular).	68
39.	Isopleths in a plane perpendicular to the y axis at a distance of 1.5 units from the origin. (Source perpendicular).	69
40.	Isopleths in a plane perpendicular to the y axis at a distance of 13.5 units from the origin. (Source perpendicular).	70
41.	Isopleths in a plane perpendicular to the x axis at a distance of 8.5 units from the origin. (Source perpendicular).	71
42.	Isopleths in a plane perpendicular to the x axis at a distance of 16.5 units from the origin. (Source perpendicular).	72
43.	Steady particle distribution in the generalized street canyon as viewed from above, resulting from a line source parallel to the incoming flow.	73
44.	Isopleths in a plane perpendicular to the z axis at a distance of 1.5 units from the origin. (Source perpendicular).	74
45.	Isopleths in a plane perpendicular to the y axis at a distance of 13.5 units from the origin. (source parallel).	75
46.	Isopleths in a plane perpendicular to the x axis at a distance of 8.5 units from the origin. (Source parallel).	76

TABLES

No.		Page
1.	Numerically obtained concentration values associated with isopleths of Fig. 5.	30
2.	Analytically predicted concentration values associated with isopleths of Fig. 4.	31

ACKNOWLEDGMENTS

The authors would like to express their appreciation to T. D. Butler for his valuable technical assistance during this study.

This work was performed, in part, under the auspices of the United States Atomic Energy Commission and supported, in part, by the Environmental Protection Agency under contract (EPA-IAG-0122(D)).

SECTION I

CONCLUSIONS

The transport of air and pollutants in street canyons can be effectively modeled with numerical techniques that employ solutions to the full Navier-Stokes equations and pollutant transport equations in regions where obstacles occur. With a constant eddy diffusivity turbulence model, we find that the results of calculating flows in street canyons compare well with experiment. This is most probably due to the fact that the additional turbulence produced in street canyons by automobiles and by warm rising gases (plumes), coupled with the vortical flow structure, causes turbulence to be more nearly uniformly distributed throughout the canyon than occurs, for example, for flows in a plain notch. That flow in a notch is extremely dependent on turbulence intensity distribution is verified by comparing calculational results with experimental results.

The applicability of numerical calculations to generalized street canyon configurations is valuable in the understanding of the complicated flow fields that exist in various geometries of city street canyons. Such techniques can be used as an aid in the development of more sophisticated analytic models.

SECTION II

RECOMMENDATIONS

As seen from the text, it is evident that numerical calculations are very useful in modeling flows in street canyons. However, it has also been shown that the modeling of turbulence by a constant eddy viscosity causes inaccuracies in the calculated pollutant dispersal in pure notch flow. The distributed effects of a turbulent viscosity in such situations therefore, must be included in the numerical technique. These effects can be included if either a set of mass or momentum diffusivities are available from experiments, or a full turbulence model is included in the numerical method from which a distribution of turbulence energies can be obtained.

In addition to the above recommendation, further refinements could be made to the numerical technique that would allow greater flexibilities and accuracies in computing the structure of a wide variety of flows. Such refinements include a variable mesh that would allow for the inclusion of arbitrarily shaped obstacles, finer resolution of specific regions of interest and along with a set of turbulence transport equations, better resolution of the spatially distributed mass diffusivities.

SECTION III

INTRODUCTION

The transport of pollution in the air can be significantly affected by the presence of terrain sculpture of buildings. The dispersal properties of a noxious plume depend quite strongly on the position of the source relative to surrounding structures, for example, a source in a valley surrounded by hills. Likewise the distribution of carbon monoxide from automobile exhaust depends in complicated fashion on the modifying effects that adjacent buildings have on both the mean wind pattern and the turbulence.

The primary source of information on these effects is derived from experimental observations, both in the field and from laboratory models. To correlate these observations requires a combination of both theoretical and empirical reasoning. The value of such rules of correlation is maximal if they can be applied to a wide range of circumstances, but at the same time are simple and convenient to use. Confidence in their wide applicability requires extensive testing with as much data as possible, while simplicity and convenience implies formulation in terms of short analytical or tabular expressions.

The purpose of this study is to develop correlation expressions for a particular class of circumstances, namely the dispersal and/or buildup of pollution concentration in street canyons (i.e., the gaps carved by streets in high density metropolitan areas) mainly as a result of automobile exhaust and smoke or fumes from the buildings. To this end, our investigation has consisted of three parts, as follows:

1. As a basis of insuring realism, we have gathered together the available field data that are essential to the accomplishment of discriminating comparison. Especially valuable for this purpose

have been the measurements conducted in St. Louis.[1]

2. Because the amount of field data is severely restricted, however, we have also developed and utilized computer generated data derived from solutions of the full Navier-Stokes equations in three dimensional configurations, coupled with the full transport equations for pollution dispersal in a turbulent atmosphere. Confidence in these results has been inspired by their favorable comparisons with the available field data, and use of them has been made both for the investigation of circumstances not covered by those data, and as a basis for testing predictions from the correlation formulas.

3. We have used a combination of analysis and empiricism for the formulation of analytical expressions and rules by which to describe and/or predict the pollution levels to be expected in various street-canyon configurations. The goal has been to achieve a compromise between analytical elegance and completeness on the one hand, versus simplicity and convenience on the other. The latter attributes, however, have not been allowed to override the requirements of applicability and accuracy.

These three topics are presented in reverse order. We first discuss the derivation of an equation for the pollution concentration in a simple notch. The result is quite similar to an empirical formula proposed by Johnson, et. al.[2] The present derivation serves, however, to show more clearly the basis for their formula, modifies the form to increase accuracy and applicability, and enables a more critical appraisal of the limitations that can be expected from such models. In addition, it is shown how the analysis might be extended to other configurations, by a combination of analytical and heuristic reasoning.

The second topic is a discussion of the numerical method employed for the complete three-dimensional solutions. The goal has been to provide data for circumstances not easily amenable to the collection

of field data, the results being used both as an end in themselves (to illustrate the nature of pollution dispersal in various commonly-occurring street-canyon configurations), and for comparison purposes (with both the field data and the correlation formulas). This discussion then blends into the third topic in which the results and comparisons are brought together. Finally we discuss the conclusions from the study so far, and indicate the directions that appear appropriate for extension.

SECTION IV

ANALYTICAL DERIVATION

This analysis is addressed to the problem of determining the distribution of pollutant in a simple notch, this being the idealization of a street canyon with automobile exhaust emitted at the bottom and a cross wind passing over the top. While a complete analysis requires numerical solution of the appropriate equations, the approximate derivations presented here are useful in showing how the principal features can be parameterized, as well as the manner by which previous semi-empirical formulas can be extended.

The specific configuration is described as follows. The origin of coordinate is located at the upper-left corner of the notch, with x positive to the right and y positive upwards into the overlying external flow. The velocity components in these two directions are u and v, respectively. The width of the notch is W, and its depth is D (the bottom lying at $y = -D$). We define $k \equiv \pi/W$. The walls of the notch allow free slip of the fluid. Across the bottom there is a prescribed flux of pollutant, S, resulting in a concentration field, $\phi(x,y)$, which becomes equal to the external concentration at $y = 0$.

The velocity distribution in the notch is obtained from the incompressibility condition

$$\frac{\partial u}{\partial x} + \frac{\partial v}{\partial y} = 0 \quad ,$$

and the linearized steady-state momentum equations,

$$-\frac{\partial (p/\rho)}{\partial x} + \nu_1 \nabla^2 u = 0 \ ,$$

$$- \frac{\partial (p/\rho)}{\partial y} + \nu_1 \nabla^2 v = 0 \quad ,$$

in which ν_1 is the (constant) coefficient of kinematic eddy viscosity. Eliminating the pressure and defining

$$\omega \equiv \frac{\partial u}{\partial y} - \frac{\partial u}{\partial x} \quad ,$$

we get

$$\nabla^2 \omega = 0 \quad .$$

A suitable solution is

$$\omega = \omega_o \left(e^{ky} - \beta e^{-ky}\right) \sin kx \quad ,$$

which, because of the free-slip boundary conditions, vanishes on the bottom and sides of the notch. Together with the incompressibility condition and the definition of ω, the particular solution for ω can be used to derive the following approximate solution for the velocity components:

$$u = \frac{A}{k}\left[e^{ky}\,(1 + ky) - \beta e^{-ky}\,(1 - ky)\right] \sin kx \quad , \qquad (1)$$

$$v = - Ay \left(e^{ky} - \beta e^{-ky}\right) \cos kx \quad , \qquad (2)$$

where

$$\beta = e^{-2kD} \quad , \qquad (3)$$

$$A = k u_o / (1 - \beta) \quad . \qquad (4)$$

As described below, we use this approximate form for the benefit of simplicity, rather than the full solution, which we have found to produce an extremely complicated concentration formula without, however, the virtue of significantly greater accuracy.

It may be observed that this solution gives a non-uniform (sinusoidal) horizontal velocity profile across the top of the notch, of which the maximum has been equated to the speed of the external flow.

To solve for the pollutant concentration within the notch, we utilized the combined convection-diffusion equation

$$u \frac{\partial \phi}{\partial x} + v \frac{\partial \phi}{\partial y} = \nu \left(\frac{\partial^2 \phi}{\partial x^2} + \frac{\partial^2 \phi}{\partial y^2} \right) \quad , \tag{5}$$

in which ν is a (constant) coefficient of eddy diffusivity, closely related in value to the kinematic eddy viscosity coefficient, ν_1.

Our procedure is to derive the solution as a power series in u_o:

$$\phi = \phi_b + \phi_o + u_o \phi_1 + \cdots \quad , \tag{6}$$

in which ϕ_b is the background concentration level carried by the external flow. Within the notch, the boundary conditions on ϕ are

$$\phi = \phi_b \qquad \text{at } y = 0, \tag{7}$$

$$\frac{\partial \phi}{\partial x} = 0 \qquad \text{at } x = 0 \text{ and } x = W, \tag{8}$$

$$- \nu \frac{\partial \phi}{\partial y} = S \qquad \text{at } y = - D. \tag{9}$$

This last describes a constant, uniform flux of pollutant across the entire bottom. For reasons to be discussed below, however, the uniformity of flux will be required only in the zero-order part of the ϕ solution. Equation (8), which forbids a flux of pollutant into the walls of the notch, is easily satisfied to first order.

Substitution of Eqs. (1), (2) and (6) into Eq. (5) leads to

$$\frac{\partial^2 \phi_o}{\partial x^2} + \frac{\partial^2 \phi_o}{\partial y^2} = 0 \quad ,$$

for which the appropriate solution is

$$\phi_o = - \frac{Sy}{\nu} \quad . \tag{10}$$

To the next order in u_o,

$$\frac{\partial^2 \phi_1}{\partial x2} + \frac{\partial^2 \phi_1}{\partial_y 2} = - \frac{Sv}{\nu^2 u_o} \quad . \tag{11}$$

For this, a particular solution can be found of the form

$$\phi_1^P = f(y) \cos kx \quad . \tag{12}$$

With

$$R \equiv \frac{AS}{\nu^2 u_o} = \frac{kS}{\nu^2 (1 - \beta)} \quad , \tag{13}$$

the equation for f becomes

$$\frac{d^2f}{dy^2} - k^2F = Ry\ (e^{ky} - \beta e^{-ky}) \quad ,$$

for which the following solution is appropriate:

$$f = \frac{Ry}{4k^2}\left[e^{ky}\ (1 - ky) - \beta e^{-ky}\ (1 + ky)\right] .$$

Accordingly, the solution for ϕ becomes at this stage

$$\phi = \phi_b - \frac{Sy}{\nu} - \frac{Ru_o y \cos kx}{4k^2}\left[e^{ky}\ (1 - ky) - \beta e^{-ky}\ (1 + ky)\right] \quad . \quad (14)$$

Although this solution satisfied the boundary conditions in Eqs. (7) and (8), it departs from the requirement of Eq. (9), in that

$$-\nu\left(\frac{\partial\phi}{\partial y}\right)_{y = -D} = S\left[1 + \frac{u_o D \cos kx}{2\nu\ (1 - \beta)}\ e^{-kD}\right] . \quad (15)$$

This could be remedied by adding an appropriate part of the reduced (homogeneous) solution, but the added complexity does not seem necessary for the purpose at hand. Indeed, the non-uniform flux is no greater an error than several others that have been introduced for the sake of tractability. Equations (1) and (2) could, for example, be replaced with the exact solution for the velocity profile that results from the stated vorticity solution. While this, in itself, is not severely more complicated, the resulting ϕ distribution is described by a vastly more lengthy expression, not warranted by the circumstances at hand. In addition, the non-uniformity of flux described by Eq. (15) is not inconsistent with the

experimental observations of a strong low-level non-uniformity in concentration from surface winds at the bottom of the notch, and accordingly we continue with the derivation from Eq. (14), without requiring further refinements.

The next step in the analysis is to determine ϕ_b, described previously as the background concentration level carried by the external flow. From the viewpoint of the notch, ϕ_b means the concentration lying just above. This is composed of two parts, the ambient concentration carried to the region from far upstream and the spilled-out concentration coming from the notch itself. The first of these contributes an additive level of concentration that is easily superimposed onto the final solution. The second, which is assumed to be constant across the level of the notch top, is to be determined by the following derivations.

Neglecting diffusion in the x direction above the notch, we write, analogous to Eq. (5).

$$u_o \frac{\partial \phi}{\partial x} = \nu \frac{\partial^2 \phi}{\partial y^2} \quad ,$$

and look for a solution subject to the conditions

$$\phi = 0 \qquad \text{at } x = 0$$

$$\phi = 0 \qquad \text{at } y = \infty$$

$$\phi = \phi_b \qquad \text{at } y = 0, \text{ for } x > 0$$

$$-\nu \int_o^W \frac{\partial \phi}{\partial y}\, dx = SW \qquad \text{at } y = 0 \, .$$

The analysis is easily accomplished, proves to be over determined, and

therefore allows us to derive the result

$$\phi_b = S\left(\frac{W}{\nu u_o}\right)^{\frac{1}{2}} + \phi_a \quad , \tag{16}$$

in which ϕ_a has been added to describe the far upstream ambient concentration in the wind approaching the notch region.

With all of this, Eq. (14) can be written in the useful form

$$\phi = \phi_a + S\left(\frac{W}{\nu u_o}\right)^{\frac{1}{2}} - \frac{Sy}{\nu}\left\{1 + \frac{u_o \cos kx}{4k\nu\,(1-\beta)}\left[e^{ky}\,(1-ky) - \beta e^{-ky}\,(1+ky)\right]\right\} \quad . \tag{17}$$

For comparison with the street-canyon models of other authors, however, it is convenient to identify some of the factors in this equation in terms of a somewhat different set of parameters.

The simplest theories of turbulence eddy diffusivity show that

$$\left(\frac{\nu}{L}\right)^2 = q \quad , \tag{18}$$

in which L is the integral scale of the turbulence, q is the turbulence energy per unit mass, and a factor of order unity has been omitted. The magnitude of q, in turn, can be related to the wind speed, u_o, and the stirring speed, (from vehicle motion), u_s, by

$$q = \gamma_1 u_o^2 + \gamma_2 u_s^2 \quad . \tag{19}$$

The factor, γ_1, describes the relative stability of the external atmosphere; for a very stable atmosphere, $\gamma_1 \approx 0$, while for a very

unstable atmosphere, γ_1 can be as large as 0.1, perhaps even larger. In contrast, γ_2 is independent of the atmospheric stability properties, and should in principle depend on the distance away from the vehicle path. Having ignored the spatial dependence of ν, however, we must postulate a constant, effective value for γ_2, which will require empirical determination. Note, incidentally, that the presence of u_s in Eq. (19) is crucial, both to avoid a singularity as $u_o \to 0$ as well as to represent the observed contrast between idling traffic and rapidly moving traffic. The magnitude of L will be given further consideration below.

The modified concentration distribution equation thus becomes

$$\phi = \phi_a + S\left[\frac{W}{u_o L\left(\gamma_1 u_o^2 + \gamma_2 u_s^2\right)^{1/2}}\right]^{1/2} - \frac{Sy}{L\left(\gamma_1 u_o^2 + \gamma_2 u_s^2\right)^{1/2}}\left\{1\right.$$

$$\left. + \frac{\cos kx}{4kL\ (1-\beta)\left(\gamma_1 + \gamma_2\, u_s^2/u_o^2\right)^{1/2}}\left[e^{ky}\ (1-ky) - \beta e^{-ky}\ (1+ky)\right]\right\} \qquad (20)$$

SECTION V

COMPARISON WITH THE MODEL OF JOHNSON, ET. AL

Johnson and associates have proposed a street canyon model that bears some similarity to Eq. (20), and has been proven to agree moderately well with experimental data. For the leeward side of the building, they write, in the present nomenclature,

$$\phi = \phi_a + \frac{\alpha S}{(u_o + u_c)\left\{d_o + \left[\left(\frac{W}{2} - x\right)^2 + \left(D + y\right)^2\right]^{\frac{1}{2}}\right\}} \qquad (21)$$

in which $u_c = 0.5$ m/sec, $d_o = 2$ m, and α is a constant. On the windward side,

$$\phi = \phi_a + \frac{\alpha S}{(u_o + u_c)\, W} \quad . \qquad (22)$$

The result is a discontinuity in concentration at $x = W/2$. Apart from this discrepancy, there is agreement with Eq. (20) in the dependence upon S, and qualitatively in the dependence on u_o. The nature of that agreement suggests that we follow their prescription for the turbulence scale, and choose L proportional to W. Actually, the scale of turbulence produced by the vehicles should be significantly smaller than W, whereas that carried by the external flow depends upon meteorological conditions and may be somewhat larger than W. As in the case of γ_2, the factor, ε, in the relation $L = \varepsilon W$, will probably require empirical determination.

SECTION VI

THE NUMERICAL APPROACH

The street canyon problem involves very complex phenomena. For a complete understanding, much more experimental data will have to be obtained and analyzed. These data will need to be extensive in content, not only measuring pollution distributions, but velocity, temperature and turbulence intensity distributions as well, with significant spatial resolution to account for the complex interactions that occur between buildings and fluid. Even with this large amount of data, the fact still remains that no two street canyons are exactly alike, thus implying that the categorization of street canyon results will require more than a single extensive experiment. Not only are data such as these difficult to obtain, they are also very expensive.

The use of three dimensional computer programs to model such flows can greatly alleviate the need for many of the costly experiments and reinforce those experiments that are needed, by indicating the basic structures of these flows and their related implications to pollution dispersal. Data generated in this way not only familiarize the experimentalist with flow patterns for which he must be concerned, but allow him to concentrate his efforts on those portions of the street canyon for which there is interest, with cognizance of the complications of the nearby flow. Data generated in this way also give the analyst information with which to compare and extend his analytic models of these complicated phenomena at significantly reduced costs.

A numerical technique that can be used to perform such calculations at these, allows the detailed consideration of flows of incompressible, buoyant fluids in and around three-dimensional obstacles and their associated effects on pollutant dispersal. The equations used

to calculate the motions of such fluids are the continuity equation,

$$\frac{\partial u_i}{\partial x_i} = 0 \quad , \tag{23}$$

the Navier-Stokes equation with buoyancy,

$$\frac{\partial u_i}{\partial t} + \frac{\partial}{\partial x_j}(u_i u_j) = g_i + \beta g_i (T_o - T) - \frac{\partial p}{\partial x_i} + \nu \frac{\partial^2 u_i}{\partial x_j \partial x_j} \tag{24}$$

and the heat equation,

$$\frac{\partial T}{\partial t} + \frac{\partial}{\partial x_j}(T u_j) = \alpha \frac{\partial^2 T}{\partial x_j \partial x_j} \tag{25}$$

in which

i,j = 1, 2 or 3

t = time

u_i = the component of velocity in the x_i direction

g_i = the acceleration of gravity in the x_i direction

p = the pressure per unit constant density

ν = a kinematic molecular or eddy viscosity, here assumed constant, but easily generalized to include space-time variations

T = temperature

α = thermal diffusivity

T_o = a reference temperature

β = coefficient of volumetric expansion

and the summation convention of repeated indices is implied.

The method by which numerical solutions for these equations are obtained is described by Hirt and Cook[3] (a preprint of which is included in this report as an appendix) and is an extension of the Marker-and-Cell method originated by Harlow and Welch.[4] This method approximates the above equations with finite differences by dividing the calculational region spanning the problem, into Eulerian cells. After initial and boundary conditions are specified, the dependent variables, recorded at specific locations on each cell, are advanced through time in short time steps thus providing the time dependent solution.

Obstacles, which may occur anywhere in the mesh, are specialized cells that never contain fluid and which impose internal boundary conditions on the fluid. Since obstacles are constructed by denoting any desired combination of cells as these specialized cells, this technique can be used to study a wide variety of complex flow problems.

In this technique, pollutants are represented as discrete particles, each particle being spherical in shape and having the mass of a prescribed amount of pollutant. Particle motions are influenced by such forces as gravity, Stokes drag and a diffusive force that statistically represents the drag force exerted on a particle by the turbulent eddy spectrum. The movement of particles is governed by the particulate transport equations,

$$\frac{d\vec{u}_p}{dt} = \vec{g} + \alpha_m(\vec{u} - \vec{u}_p) + \alpha_m \vec{u}_{diff}$$

with

$\vec{u}_p$ = particle velocity

$\vec{u}$ = the fluid velocity evaluated at the position of the particle

$\vec{g}$ = the acceleration of gravity

$\vec{u}_{diff}$ = a random diffusion velocity

$\alpha_m = 4.5 \frac{\rho\nu}{\rho_m r_m^2}$ = the coefficient of Stokes drag divided by the mass of the m^{th} particle species.

ρ = fluid density

ρ_m = density of the m^{th} particle species

r_m = radius of the m^{th} particle species

A species of particles is defined by the species' size and density. It is evident that particle transport is coupled to fluid transport through the fluid velocity $\vec{u}$ in Eqs. (24) and (26). The manner in which $\vec{u}_{diff}$ is calculated and the details of the particulate transport scheme are described by Hotchkiss and Hirt.[5] Basically, $\vec{u}_{diff}$ is chosen to have randomly generated components that are Gaussian distributed in each coordinate direction.

SECTION VII

TWO-DIMENSIONAL RESULTS

Various problems have been studied numerically, not only to compare numerical results with experimental results and demonstrate credibility in the numerical technique, but to generate information with which analytic model results can be compared.

Shown below are the results from a series of calculations on a two-dimensional street canyon problem. Fig. 1 shows the steady, state flow velocity distribution resulting from a uniform inflow of unit magnitude velocity from the left and existing the mesh on the right. Even though the picture is shown in perspective, the problem is two-dimensional. The velocity vectors shown indicate the magnitude and direction of the flow in the notch. Comparison of this figure with the observed results of Wang, Chang and Lin,[6] Fig. 2, shows excellent correlation of flow structure. Note, for example, the location of the vortex center in the two figures. Also comparison of Fig. 1 with the experimental results of Reiman and Sabersky[7] and Mills[8] shows excellent agreement. The Reynolds number for the flow of Fig. 1 was 100 while that of Fig. 2 was 2.1×10^4, however, Jacobs and Sutton[9] have shown that there is no appreciable difference in flow structure, at least calculationally, for the two cases. The Reynolds number reported by Reiman and Sabersky is 143.2, while that of Mills is 10^5. The calculation depicted in Fig. 1 was performed with uniform inflow and free slip walls. Thus any secondary vortices that appear in experimental results do not appear here, although the overall flow structure is very similar. The steady pressure distribution for this flow is shown in Fig. 3. The contour values for the isobars are in non-dimensional units measured relative to an ambient value of zero.

With this flow field established, particles are fluxed into the system from various sources, with varying amounts of diffusion and

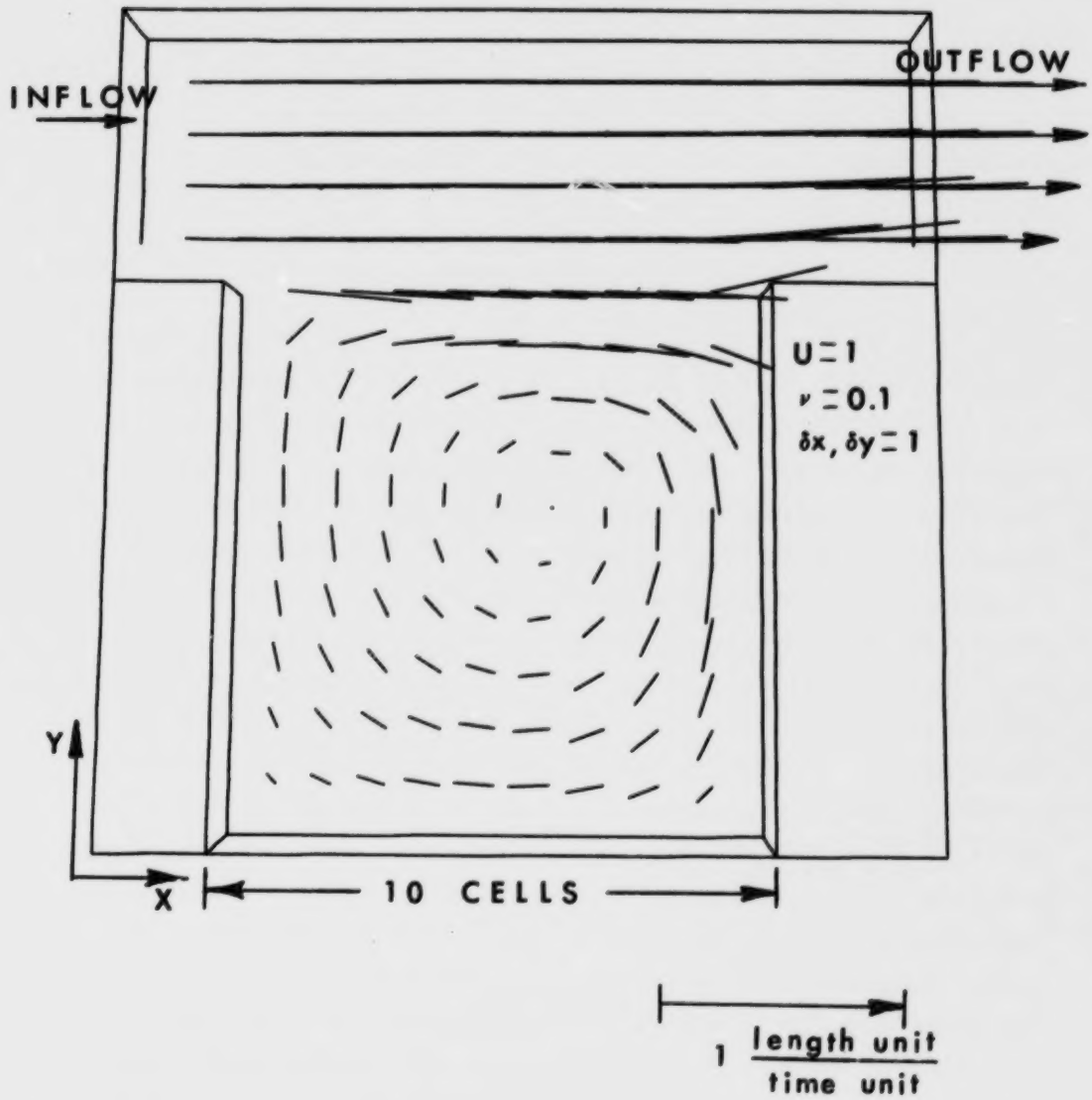

Fig. 1. Steady velocity field established in a two-dimensional square street canyon.

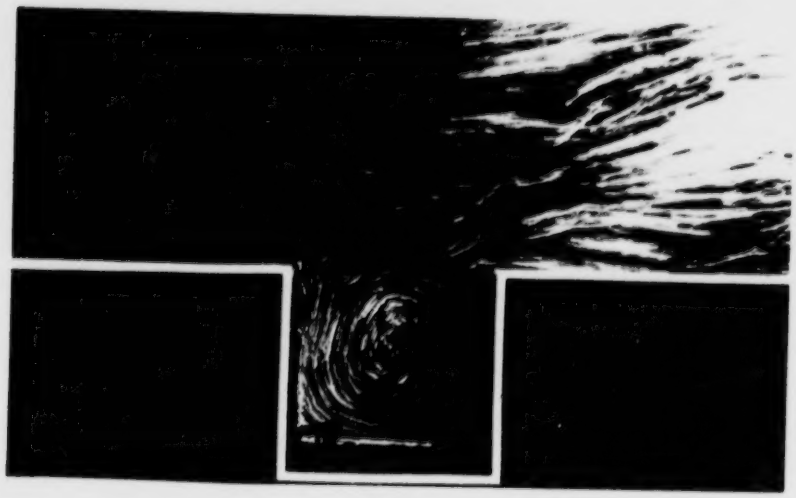

Fig. 2. Experimental flow field observed by Wang, Chang, and Lin for a Reynold's number of 2.1×10^4 Reproduced with the permission of Prof. P. C. Chang.

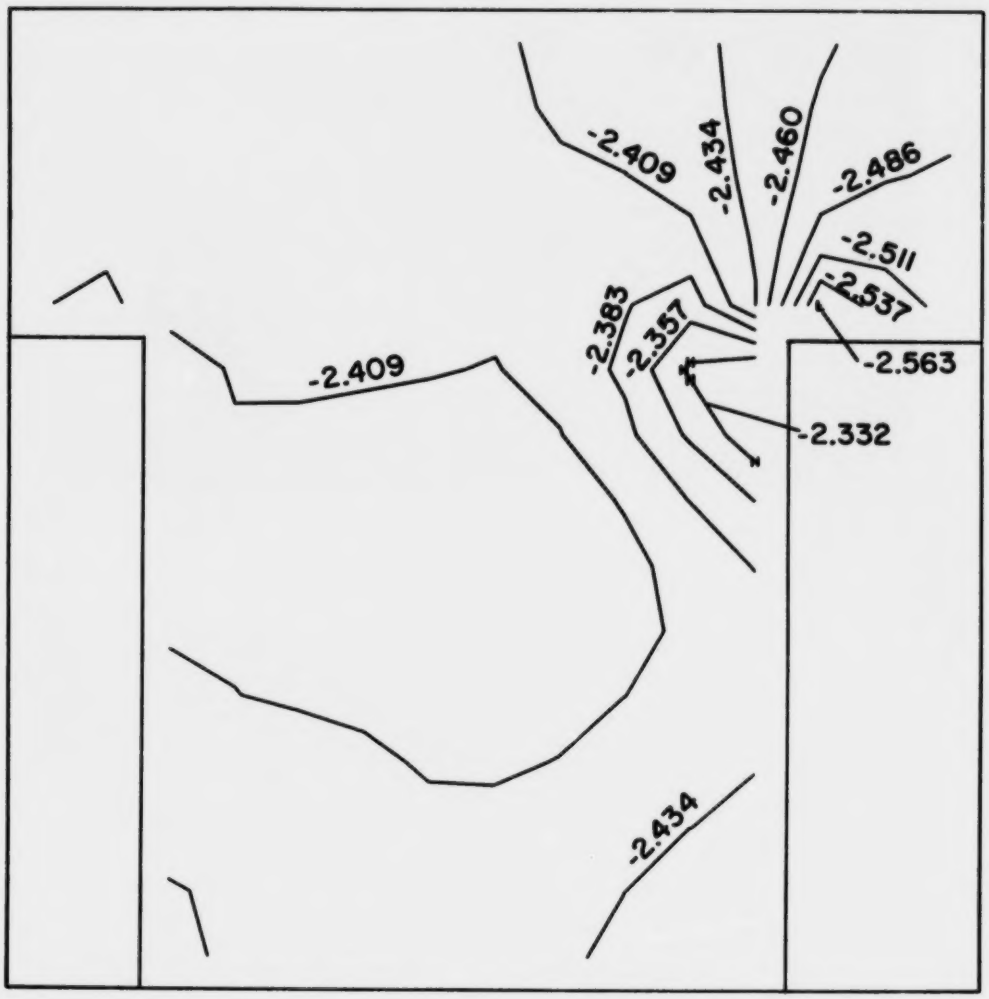

Fig. 3. Steady pressure distribution isobars for the flow depicted in Fig. 1. Pressures are in non-dimensional units relative to an ambient pressure of zero.

allowed to move to a statistically steady distribution. For example, Fig. 4 shows the steady distribution of pollutants input from a line source at a rate of 40 particles per unit time into the velocity field established in Fig. 1. Each particle has a non-dimensional mass of 1 mass unit. The line source, is across the bottom of the street canyon corresponding to a uniform area source for the street of which this is a cross section. This resulting distribution is more specifically analyzed in Fig. 5 which shows the isopleths of Fig. 4 within the canyon. These lines of constant concentration, measured in units of mass per unit volume of space, are labeled in the figure and show the effect of the notch vortex on the pollutants' distribution. The circulating vortex convects a large amount of pollution to the lee side of the canyon causing higher concentrations there than on the side with a downwash wind in front.

It must be noted here that all of the isopleth plots presented in this paper reflect the averaging of instantaneous particle distributions over relatively long periods of time at steady state. The results in Fig. 5, for example, were averaged over 50 time units. This procedure is performed since instantaneous distributions are dependent upon time varying random fluctuations and therefore never come to a true steady state. The contour plots in this paper are produced directly with the aid of the CDC 7600 computer and a Stromberg-Carlson 4020 microfilm printer. Since contour lines are scaled and drawn automatically by placing ten contour lines between the maximum and minimum contour values to be plotted, the contour lines usually have fractional numbers associated with them.

Figure 6 shows the particle distribution from a similar calculation to those shown in Figs. 4 and 5, except here a point source is positioned at the bottom center of the canyon. As before, 40 mass units per unit time are input into the steady velocity field shown in Fig. 1. The isopleths in Fig. 7 show contours of the number of mass

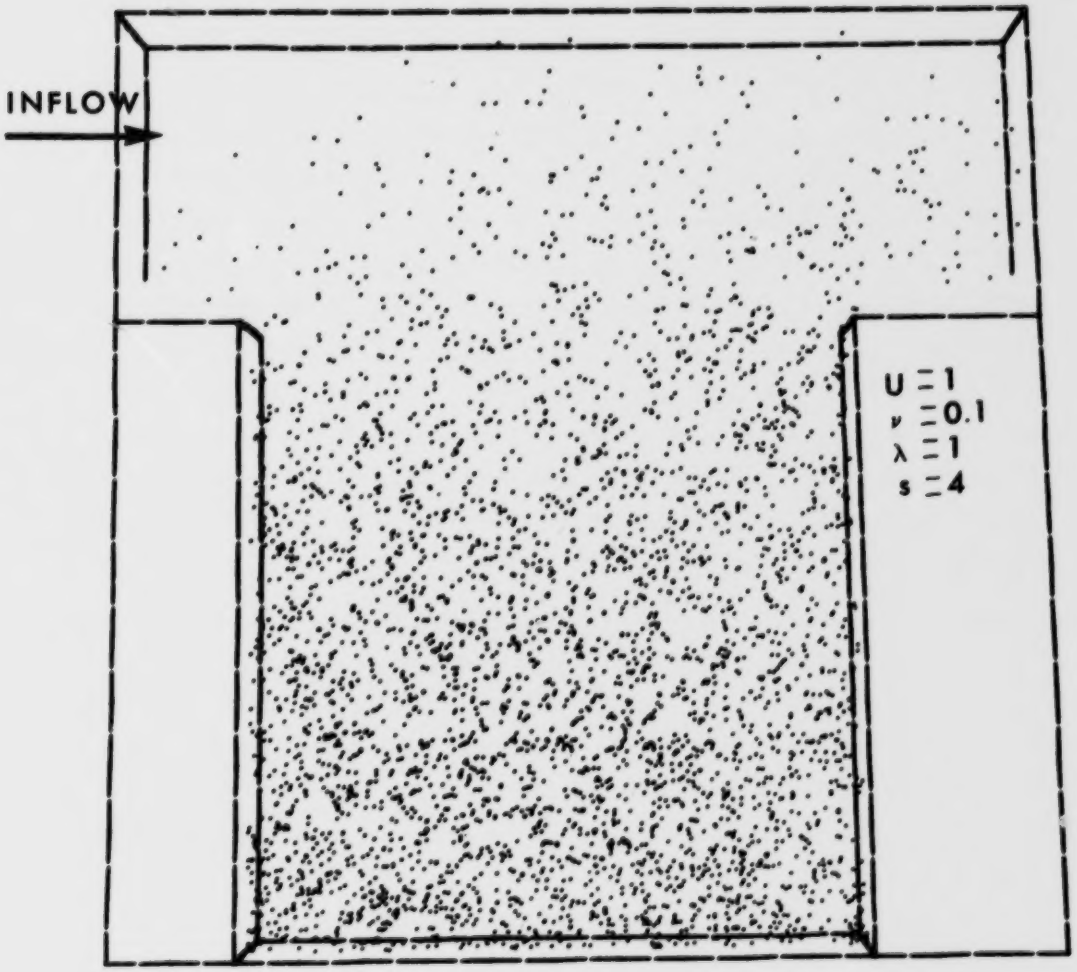

Fig. 4. Steady particle distribution resulting from a line source in the bottom of the canyon.

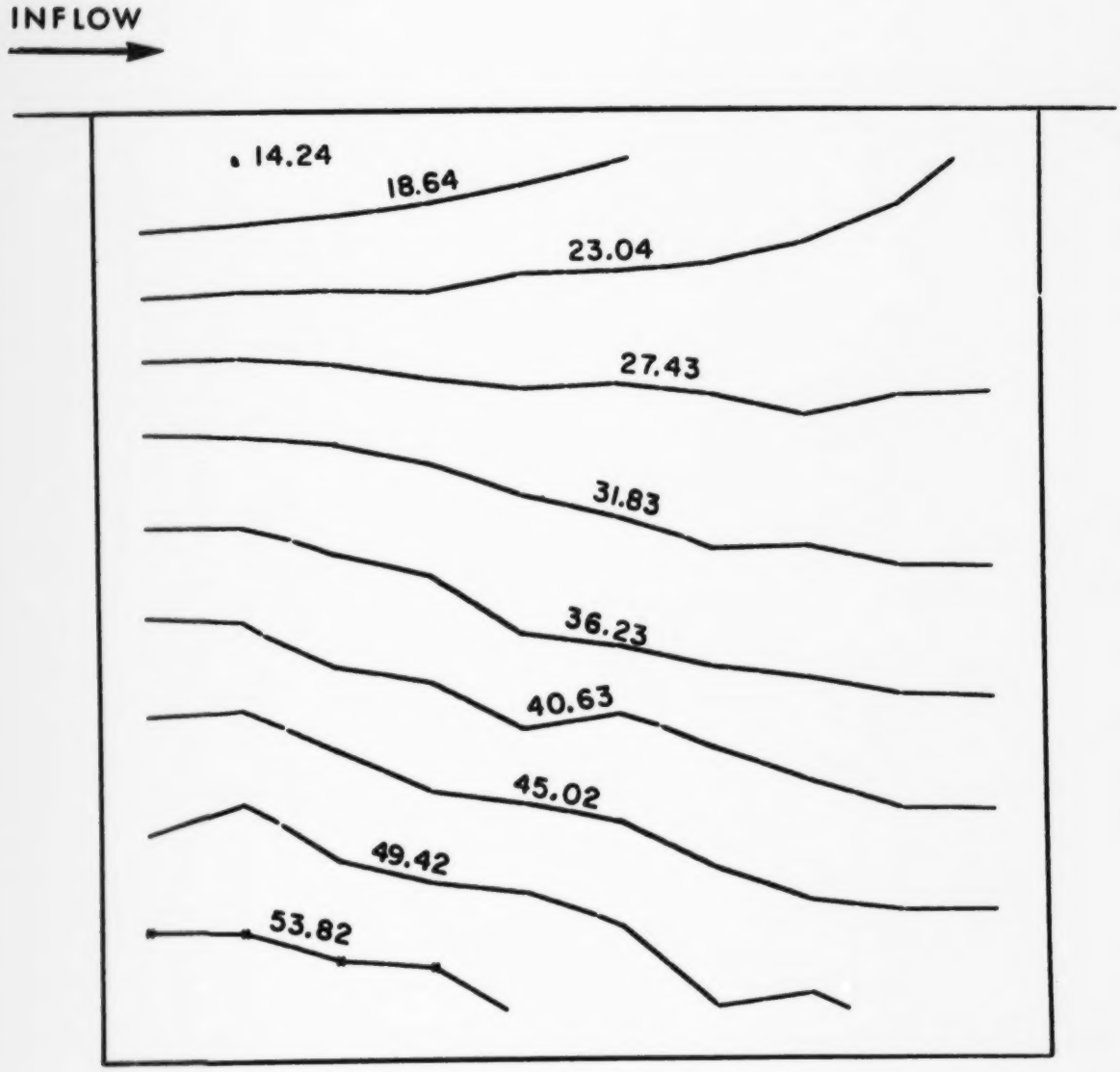

Fig. 5. Isopleths of Fig. 4 showing concentration distribution within the canyon. Units are particles per cell volume.

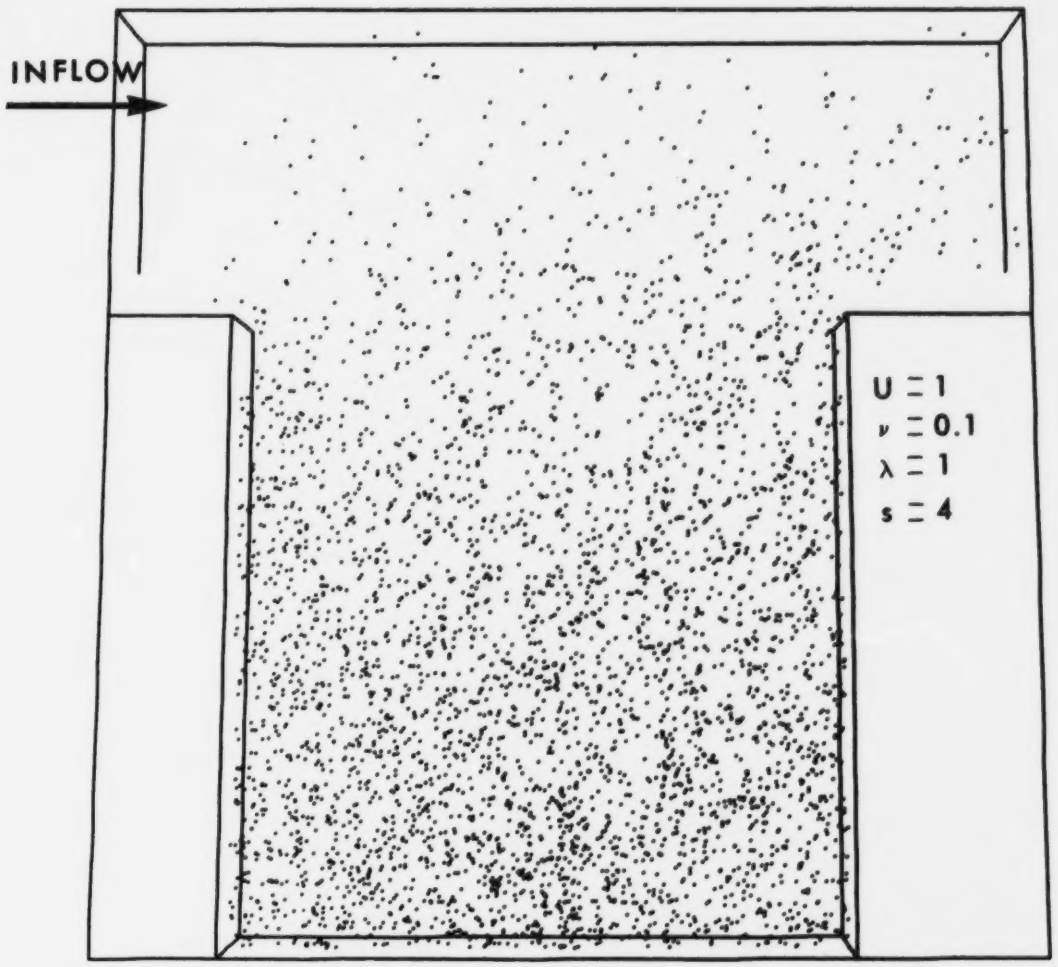

Fig. 6. Steady particle distribution resulting from a point source located at the bottom center of the canyon.

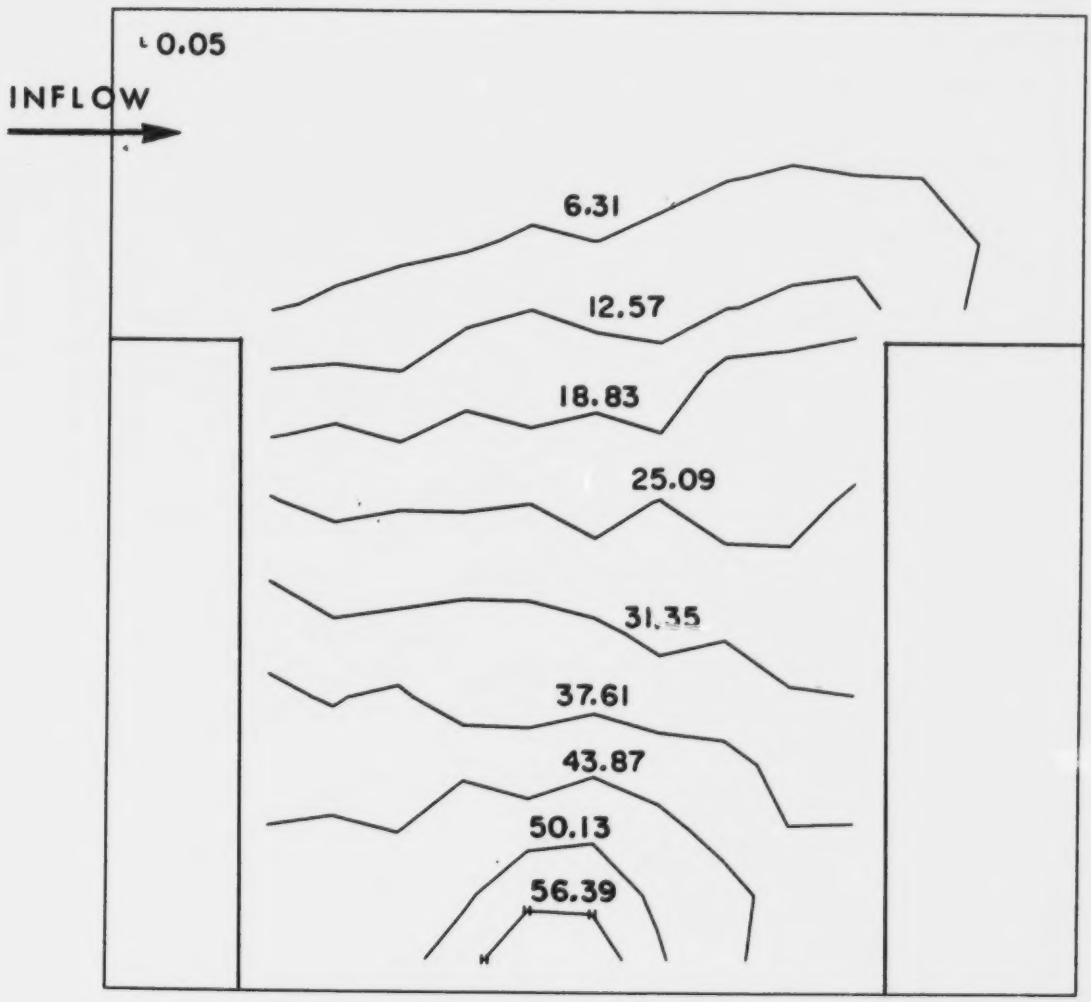

Fig. 7. Isopleths of Fig. 6 showing concentration distributions in the canyon in units of particles per cell volume.

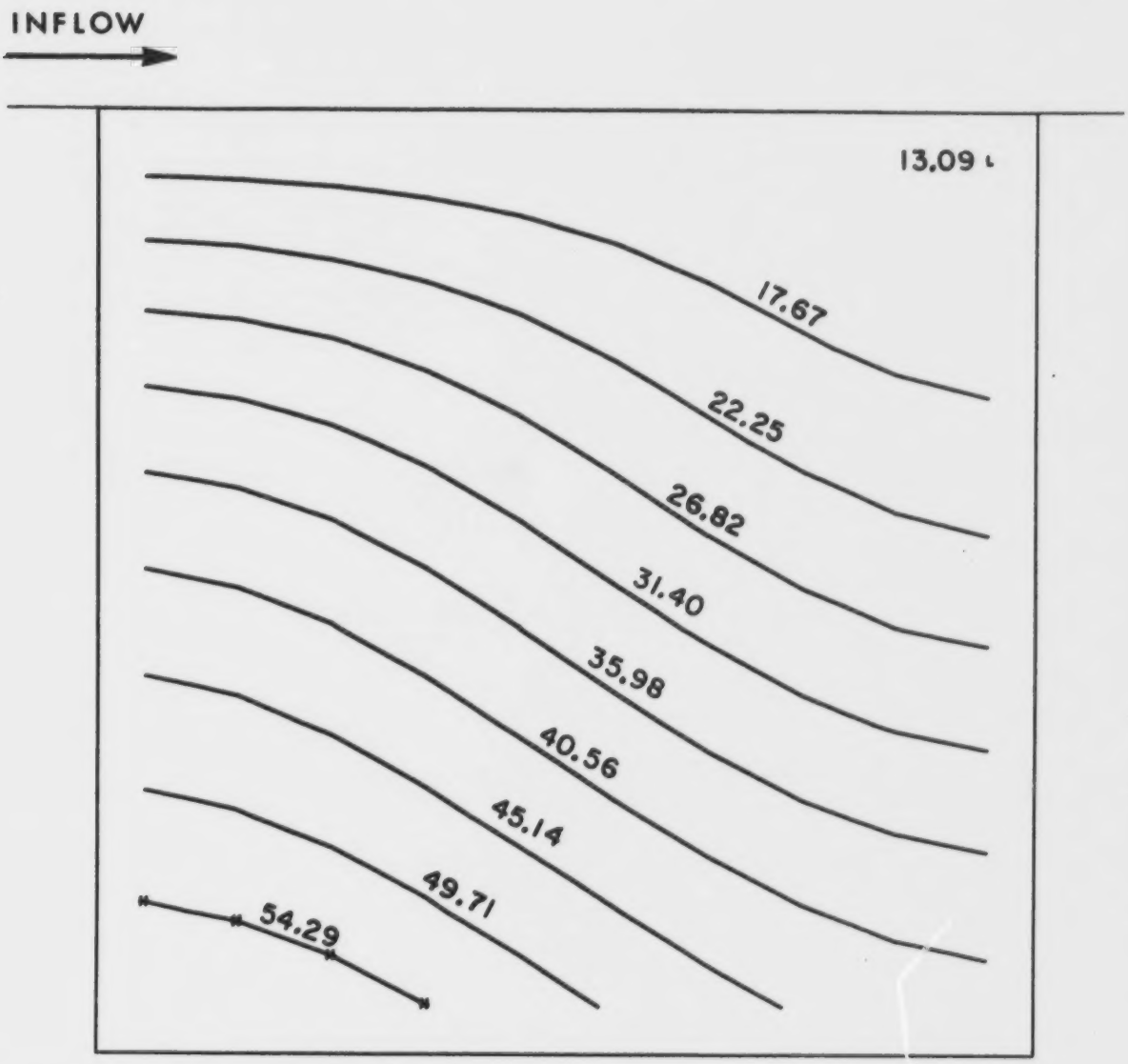

Fig. 8. Isopleths predicted by the analytic model for concentration distribution in the canyon. Units are the same as those in Figs. 5 and 7.

units per unit volume that result at statistically steady state from this type of source. (Here, we are looking at the effects of a single lane of traffic in the center of the canyon.) Comparison of the results in Figs. 7 and 5 show similarities between the two source types. Comparison of the two particle distributions reveals that the contour lines from the lower middle portion of the canyon ($\approx$ 36 mass units per unit volume) on up to the top of the canyon have not only very similar shapes but very nearly equal magnitudes as well. The similarities of these two results are not too surprising since they both were performed with an enhanced particle diffusivity $\lambda = 1.0$ as compared to the fluid diffusivity of $\nu = 0.1$. These calculations do, however, present the solution to a well posed mathematical problem with which the analytic results as shown in Fig. 8 can be compared. These isopleths exhibit the solution of Eq. (20) with $S = 4.0$, $W = D = 10.0$, $u_o = 1.0$,

$$\lambda = L\sqrt{\gamma_1 u_o^2 + \gamma_2 u_s^2} = 1.0 \text{ and } \phi_a = 0.0 \ .$$

The agreement between analytic results and the numerical results of Fig. 5 are extremely good on the left side of the canyon with increasing divergence in agreement on the right side. The reason for the disagreement on the right side, however, arises from the boundary condition given by Eq. (7) which prohibits the concentration generated within the cavity from being convected away at the top in the analytic model. A detailed comparison of concentration distribution for the two cases is enabled with the uses of Tables 1 and 2, which shown concentrations in mass units per unit volume throughout the canyon. The numerical results are concentrations that have been averaged over a long period of time after a statistically steady particle distribution has been obtained.

It should be pointed out that the analytic model, as previously formulated, gives valid results only when the coefficient,

TABLE 1

U = 1 →

14.3	14.2	15.4	16.3	17.2	18.4	19.5	20.1	21.4	23.9
20.1	20.6	20.9	21.2	22.2	22.2	22.7	23.4	24.6	24.6
26.9	27.0	26.6	25.8	26.0	26.6	25.5	25.4	25.9	26.6
32.5	32.2	31.8	31.0	29.4	28.9	29.4	28.3	29.0	28.4
36.8	36.8	35.8	35.0	33.8	32.6	31.5	31.5	31.0	31.5
41.4	41.2	38.7	38.2	36.2	35.4	34.2	34.6	33.8	32.5
45.5	45.9	44.0	42.9	40.5	41.4	39.6	37.9	37.4	37.8
48.9	50.3	48.0	46.0	46.1	45.0	43.8	42.6	41.0	41.0
53.0	53.0	51.5	51.5	50.5	49.0	46.3	45.4	45.2	45.2
58.2	57.9	56.4	56.0	53.2	52.4	49.5	50.2	48.2	49.1

Numerically obtained concentration values associated with isopleths of Fig. 5. $S = 4$, $\lambda = 1$.

TABLE 2

U = 1 →

16.2	16.1	15.8	15.4	14.9	14.4	13.9	13.5	13.2	13.1
23.0	22.6	21.8	20.6	19.3	18.0	16.7	15.5	14.7	14.3
29.1	28.4	27.2	25.6	23.7	21.6	19.7	18.1	16.9	16.2
34.4	33.6	32.2	30.2	27.9	25.4	23.1	21.1	19.7	18.7
39.0	38.2	36.6	34.5	32.0	29.3	26.8	24.7	23.1	22.3
43.2	42.3	40.8	38.6	36.0	33.3	30.7	28.5	27.0	26.1
47.0	46.2	44.7	42.5	40.0	37.3	34.8	32.6	31.1	30.3
50.8	50.0	48.5	46.4	43.9	41.4	38.9	36.8	35.3	34.5
54.7	53.9	52.4	50.3	41.9	45.4	43.0	40.9	39.4	38.6
58.9	58.1	56.5	54.4	52.0	49.3	46.9	44.8	43.2	42.4

Analytically predicted concentration values associated with isopleths of Fig. 4. $S = 4$, $\lambda = 1$.

$u_o/4k\lambda(1 - \beta)$, is less than unity (by virtue of the solution's expansion in u_o). In other words, the analytic model can only be applied with confidence to problems in which the horizontal variation of concentration, as predicted by the model, does not differ by more than about a factor of 2 from one side to the other. Since the analytic model was derived from first principles and only has a limited range of applicability, the implication can be made that the analogous Johnson model cannot be applied to generalized circumcumstances without taking cautions to ensure proper normalizations.

A street canyon with smaller diffusivity, modeled in two dimensions, is depicted in Fig. 9. In this calculation, particles are input uniformly along the bottom of the canyon at a rate of 40 particles (i.e., mass units) per time unit. The particle diffusivity and the kinematic eddy viscosity of the fluid are equal: $\lambda = \nu = .1$. The steady flow field used for particle movement is again that shown in Fig. 1. The concentrations produced by this calculation are considerably greater than those presented in the previous results. The overall concentration distribution is also somewhat different as shown in Fig. 10. The effects of the vortical flow structure on pollution distribution are now extremely evident. This purely two-dimensional case should be able to be compared with two-dimensional experimental results, however, purely two-dimensional experiments in which concentrations are measured are not easily accomplished. The water tunnel experiment performed by Wang, Chang and Lin involved three-dimensional phenomena as far as the concentration measurements were concerned. Since a dye was injected at a single point beneath the surface of the water, diffusion proceeded in all three directions, thus reflecting much lower concentrations in the plane of the source than a truly two-dimensional experiment would have produced. Additional complications to the flow field can be expected in their experiment, as a vertical flow structure, produced by an Eckman layer on the floor of the water tunnel, was most

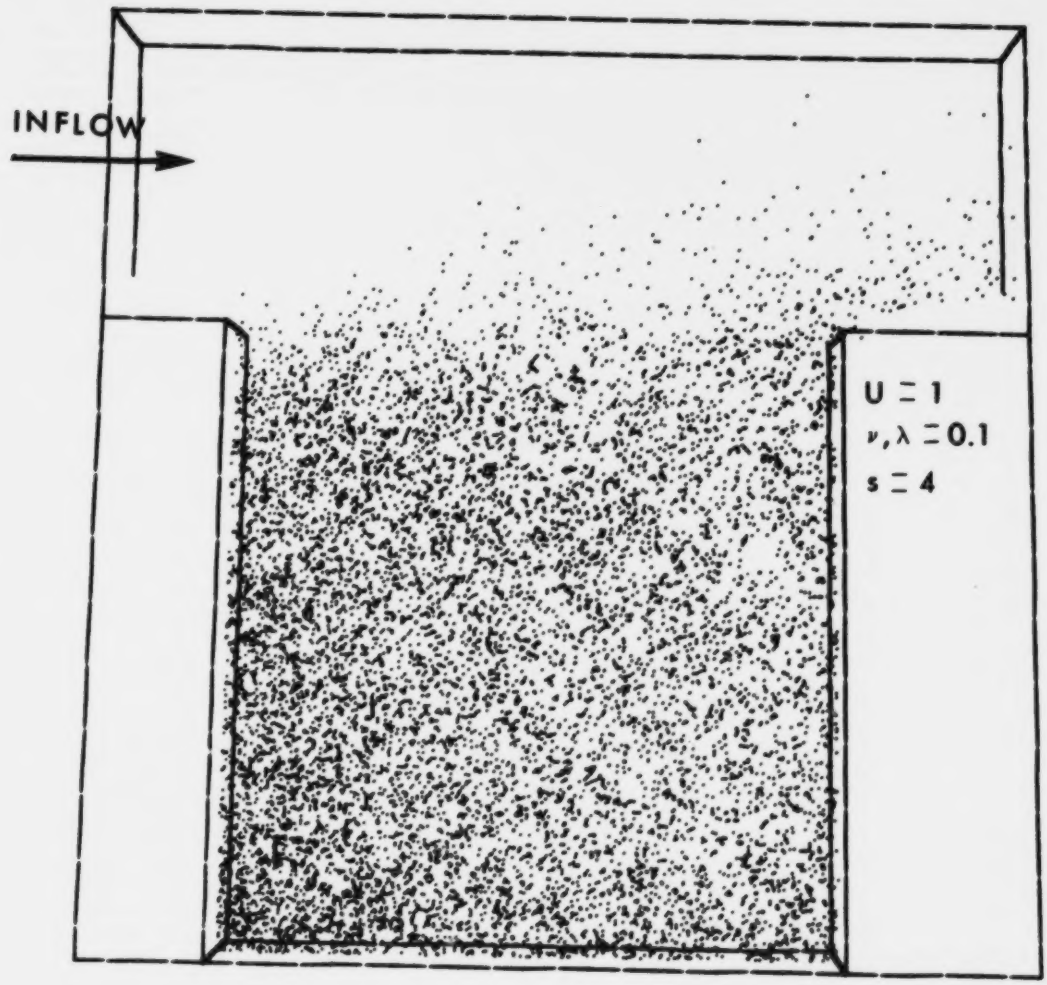

Fig. 9. Steady particle distribution resulting from a line source in the bottom of the canyon. Results reflect a smaller diffusivity.

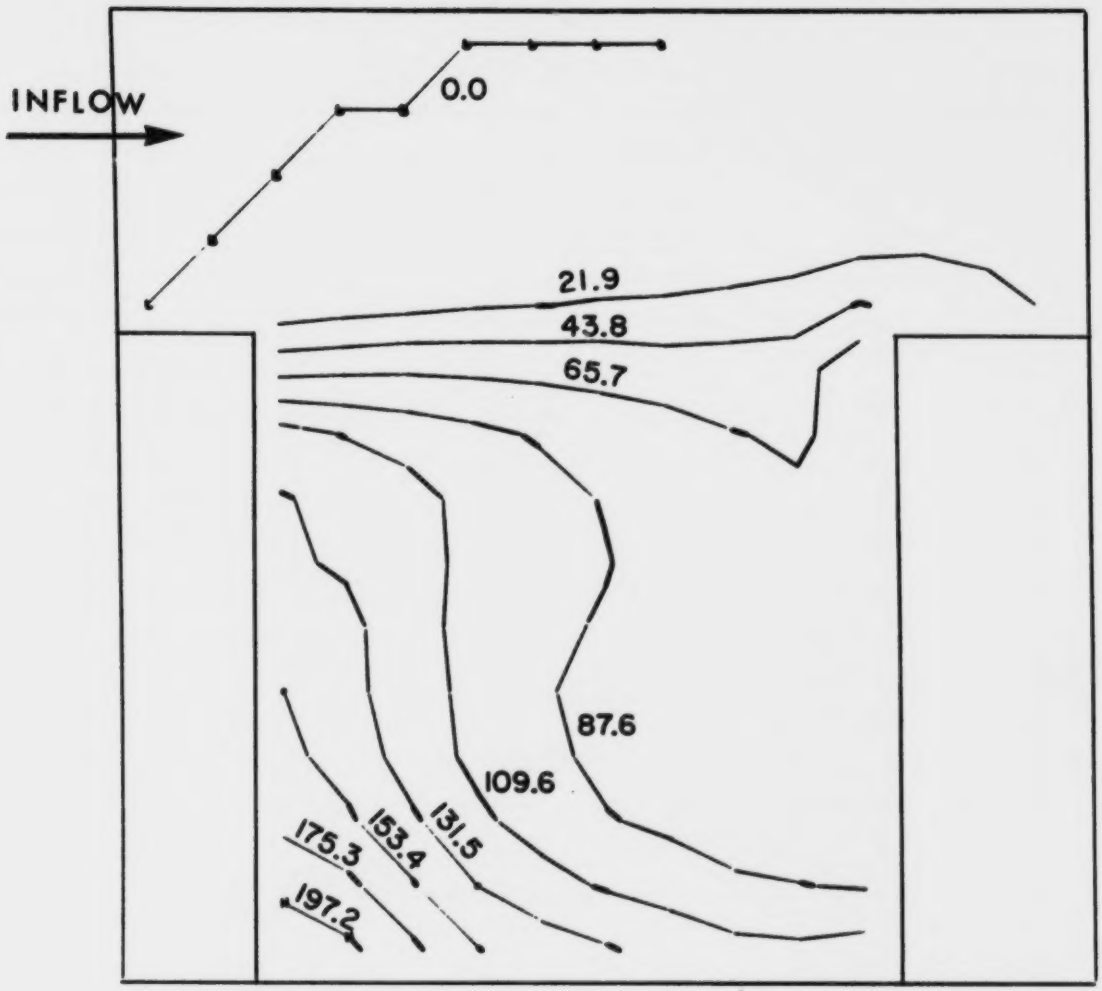

Fig. 10. Isopleths of Fig. 9 showing concentration distribution within the canyon in units of particles per cell volume.

probably present thus distributing concentration by a vertical convective process.

Since the two-dimensional results previously reported cannot be compared with the experimental data obtained by Wang, Chang and Lin, a three-dimensional version of the problem was modeled as shown in Fig. 11. Here, a steady particulate distribution resulting form a point source, located midway between the front and back of the mesh (which is seven cells deep), is shown. Diffusion in all three directions is allowed, however, the mean-flow field is actually two-dimensional because all walls are assumed to be free slip and the acceleration of gravity is assumed to be zero, hence, convection only occurs in two dimensions. A comparison of Fig. 12, which contains the numerically calculated contour lines of concentration (in ppb) in the plane of the source, with Fig. 13, which contains contour lines for the experimentally obtained concentrations at various points throughout the canyon, shows the areas of agreement and areas of disagreement between calculation and experiment. It is evident that the calculated concentrations in the plane of the source are considerably higher than the experimentally obtained values. However, it is interesting to note Fig. 14, which contains contour lines of concentration for a plane parallel to but slightly off the plane of the source. Here the agreement is much better.

It is clear from the calculation, that all of the physics of the flow is not being properly modeled. For example, a calculation of this type confirms the fact that a constant eddy diffusivity scheme has certain limitations and that the selection of a proper variation for λ is a critical step in the calculation. Clearly, a full set of turbulence equations that would automatically couple the turbulent shear stresses with particulate motions would alleviate this problem considerably.[10]

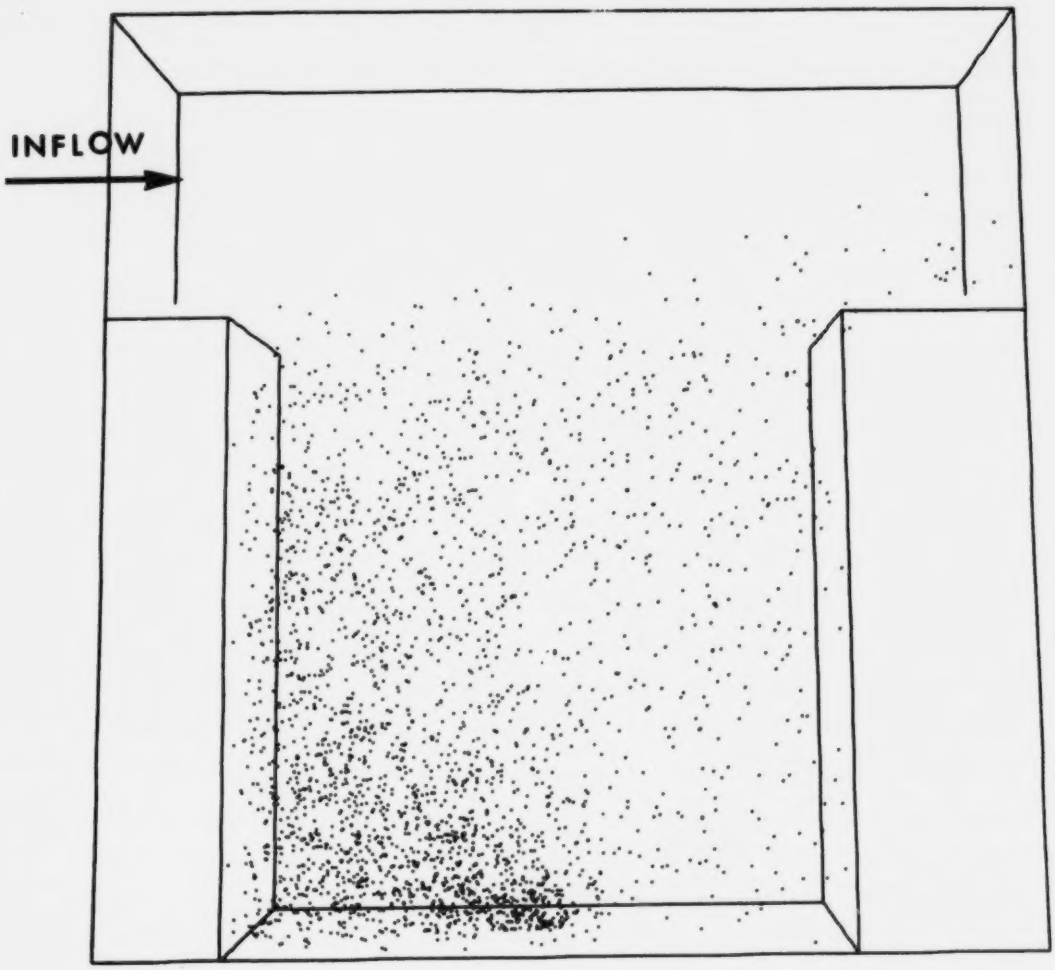

Fig. 11. Steady particle distribution obtained from modeling the experiment of Wang, Chang and Lin.

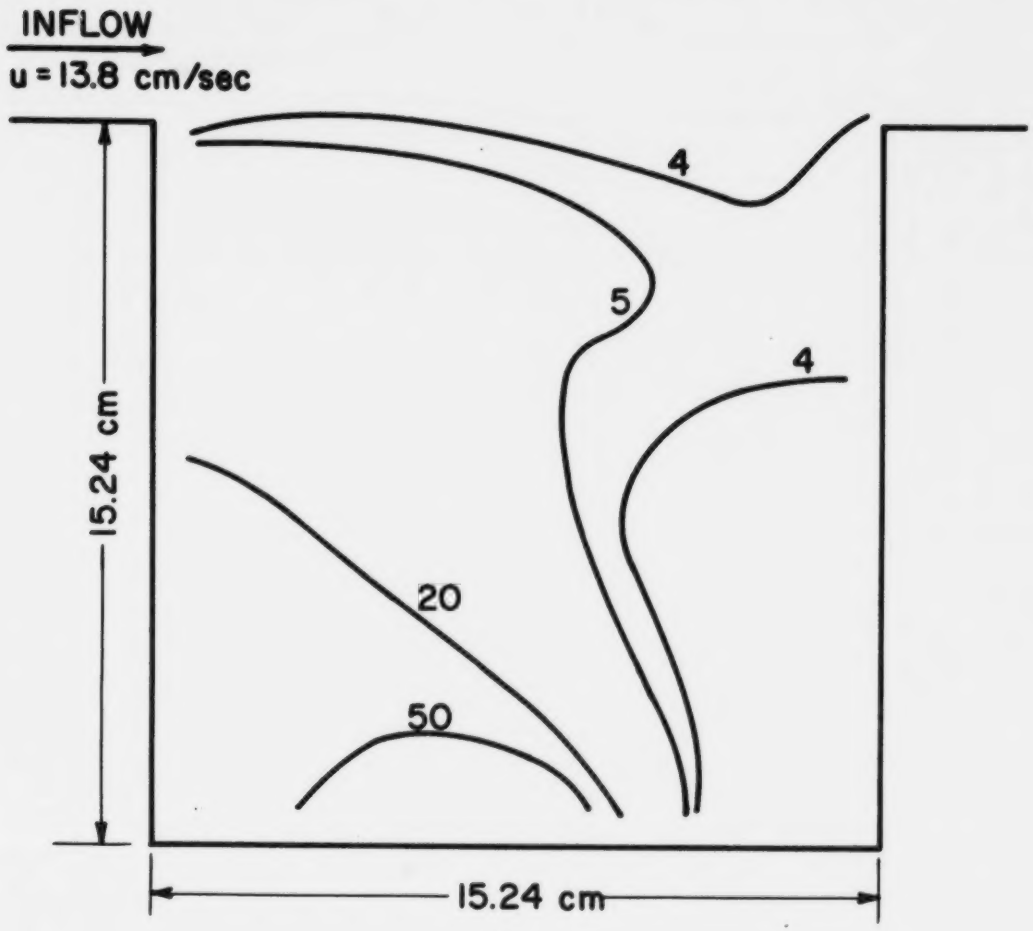

Fig. 12. Isopleths of numerically calculated concentrations (in ppb) in the plane of the source of Fig. 11.

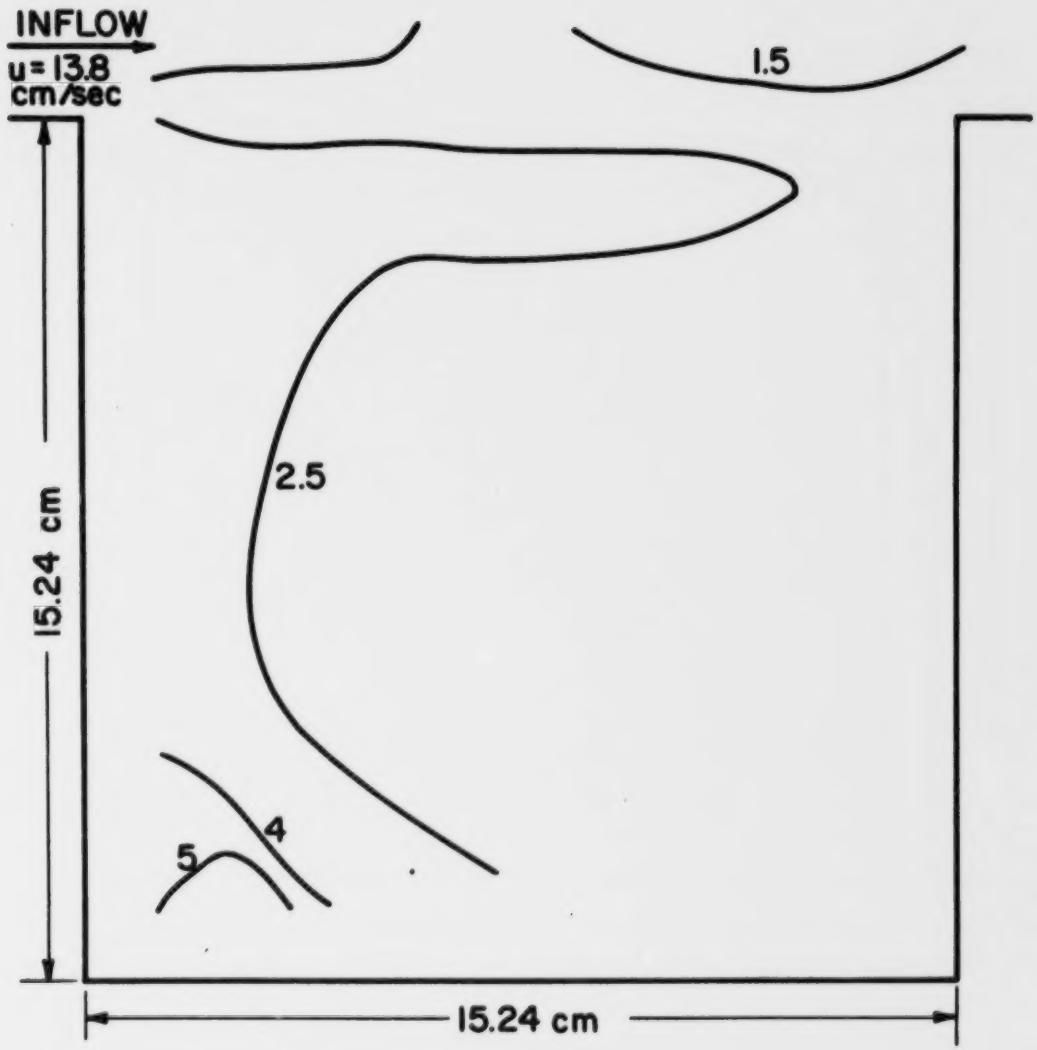

Fig. 13. Isopleths drawn through the data reported by Wang, Chang and Lin (in ppb) (results approximate).

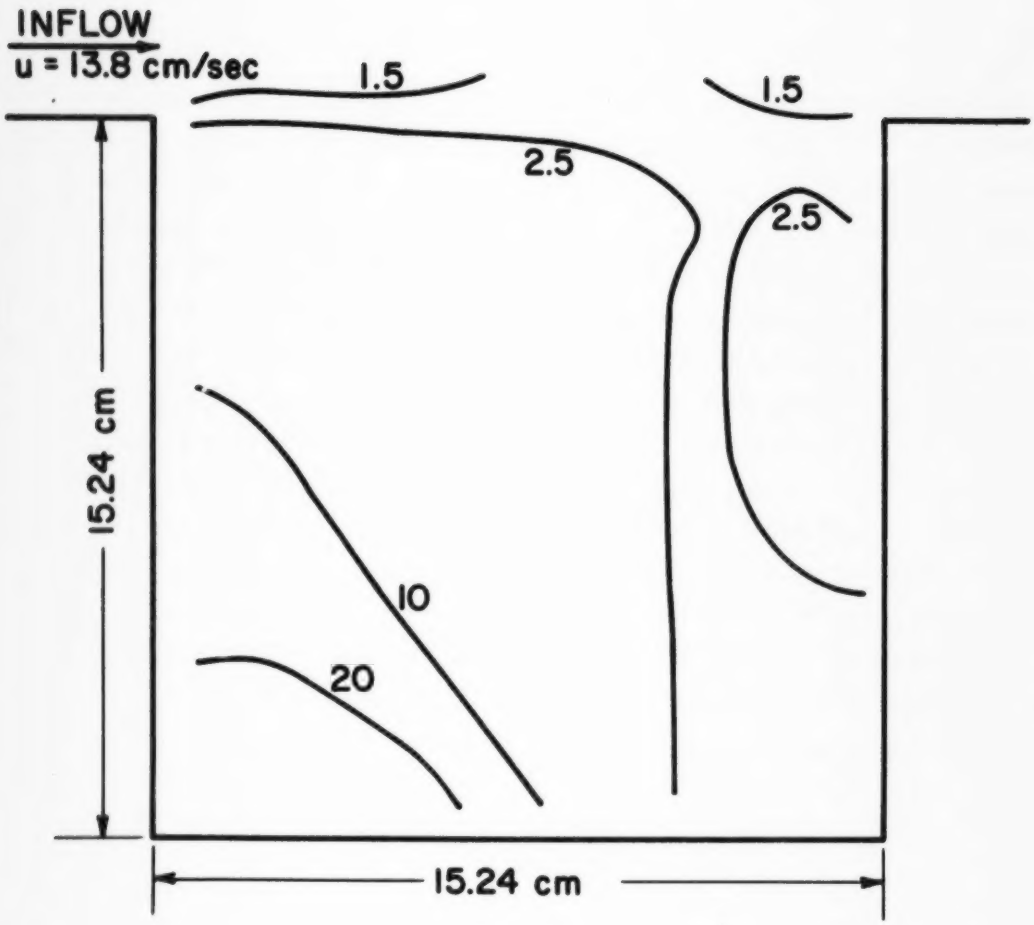

Fig. 14. Isopleths of numerically calculated concentrations (in ppb) for a plane slightly off the plane of the source in Fig. 11.

Since the source strength in the experiment was 3.8×10^4 ppb, one would initially expect to find extremely large concentrations in the vicinity of the source. Consequently, since these high concentrations are not found, it becomes evident that the pollutants remain near the wall for some distance away from the source before they become dissipated throughout the rest of the fluid. The measuring technique of the experimentalists did not allow them to see these high concentration areas because their measurements were taken fairly far from the wall. However, calculationally the particles near the wall are still considered to contribute to the concentration in the layer of cells next to the wall thus explaining the difference between the large calculated concentrations and the relatively small experimentally obtained concentrations near the walls. The remainder of the field, however, does show a relatively good comparison between calculations and experiment; it is evident that a distributed mass diffusivity would allow even better correlation.

SECTION VIII

THREE-DIMENSIONAL RESULTS

A fully three-dimensional investigation of the Broadway Street canyon in St. Louis, Missouri was made in order to compare numerical predictions with the experimental results obtained by Ludwig and Dabberdt.[1] The case chosen for comparison involved an incoming wind (at approximately 2 m/sec) perpendicular to Broadway over the top of the First National Bank and down Locust and Olive Streets. The computing mesh was selected to span the space between the center of Locust Street and the center of Olive Street as indicated in Fig. 15. The lateral span of the mesh only encompasses portions of the buildings (approximately forty feet) on both sides of Broadway and the height of the mesh is the equivalent of 16 stories. Actually, using the coordinate system specified in Fig. 16, the mesh extends 300 feet (30 cells) in the x direction, 160 feet (16 cells) in the y direction and 160 feet (16 cells) in the z direction.

The incoming wind, flowing from left to right in Fig. 16, causes an extremely complex velocity field to exist in the canyon at steady state as shown in Fig. 16 through 22. These figures show various views of velocity vectors in planes perpendicular to the direction indicated at a distance (in feet) from the origin of the coordinate system. Mental superposition of the various figures indicates the overall flow field structure.

Traffic exhaust emissions are assumed to originate uniformly at ground level on each street. The equivalent number of particles input per unit time for Broadway was 66.7 while Locust and Olive were assumed to have forty percent of Broadway's input rate. Particles were uniformly distributed at height $z = 0$ as they modeled continuous area sources. They were allowed to be convected by the steady velocity field and randomly diffused until they reached a statistically

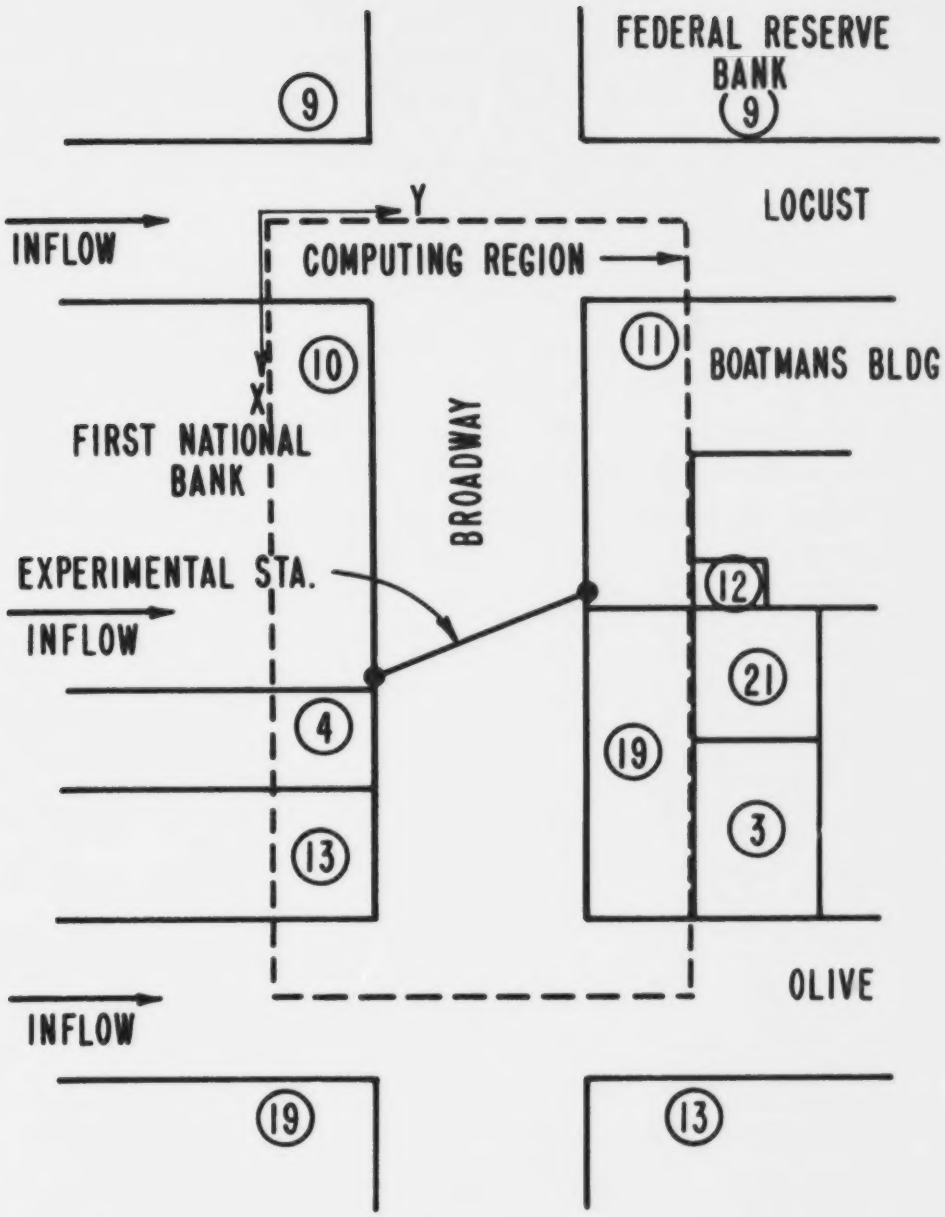

Fig. 15. Computing mesh for Broadway Street Canyon St. Louis, Missouri. Circled numbers represent building heights in stories.

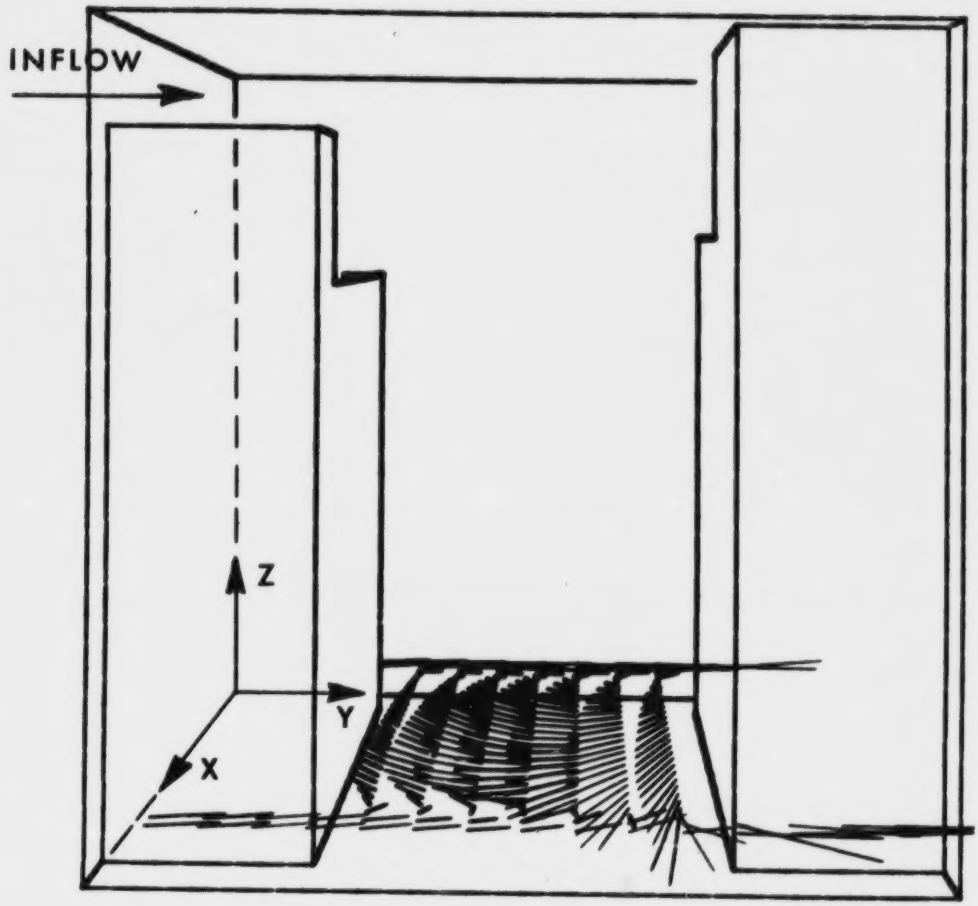

Fig. 16. Perspective view of velocity vectors in a plane perpendicular to the z axis at a distance of 15 feet from the origin. Location of the coordinate system is shown.

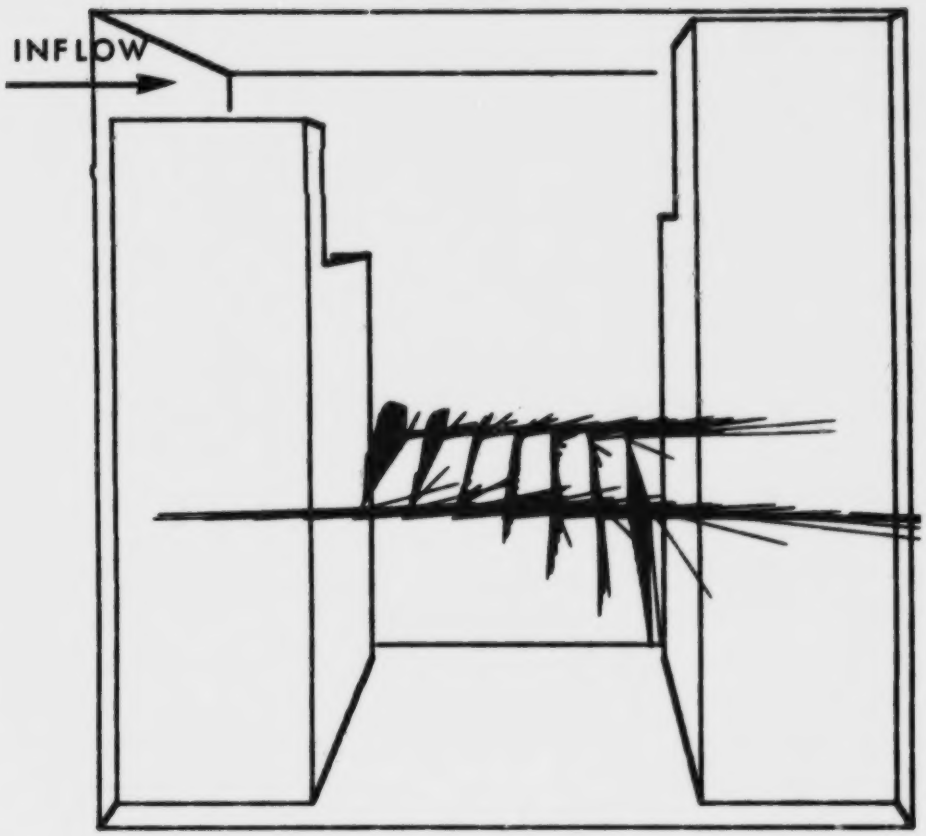

Fig. 17. Perspective view of velocity vectors in a plane perpendicular to the z axis at a distance of 65 feet from the origin.

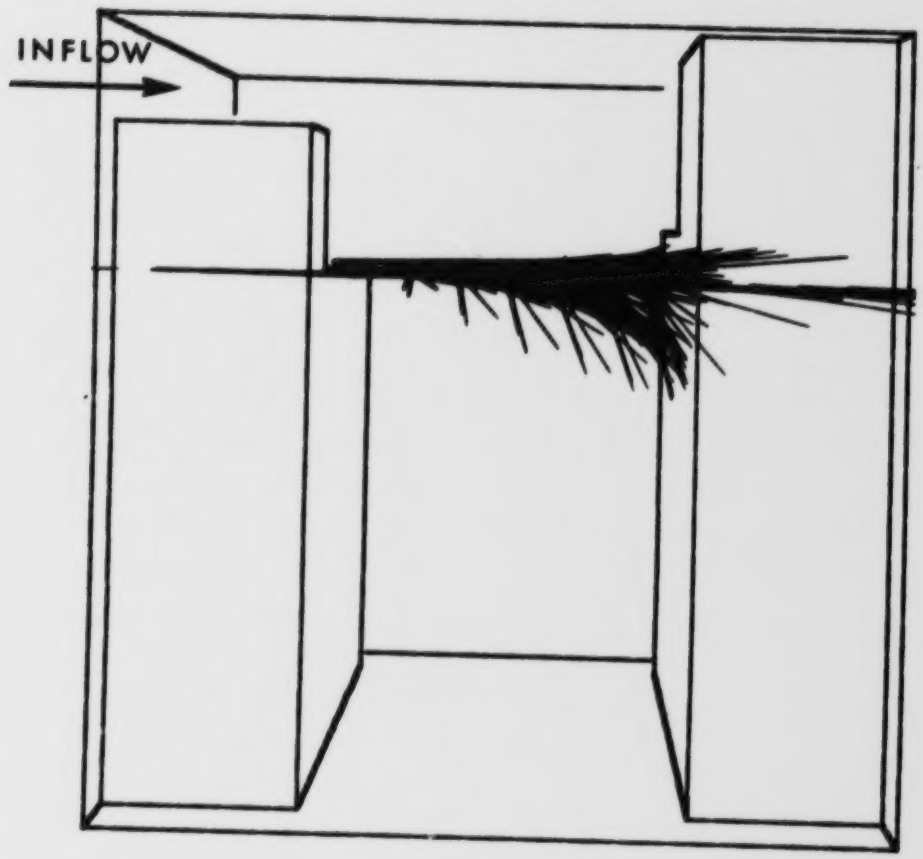

Fig. 18. Perspective view of velocity vectors in a plane perpendicular to the z axis at a distance of 115 feet from the origin.

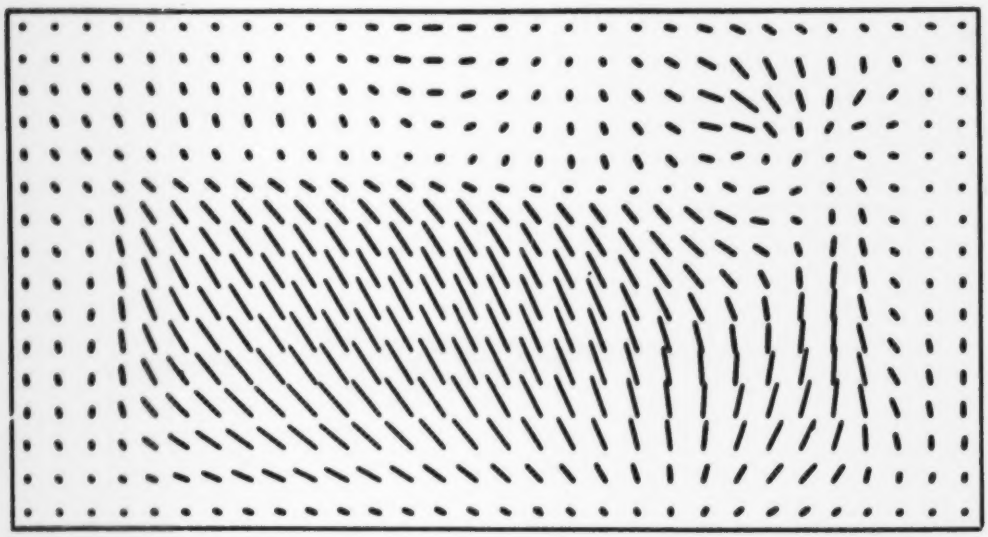

Fig. 19. Plane view of velocity vectors in a plane perpendicular to the y axis at a distance of 55 feet from the origin.

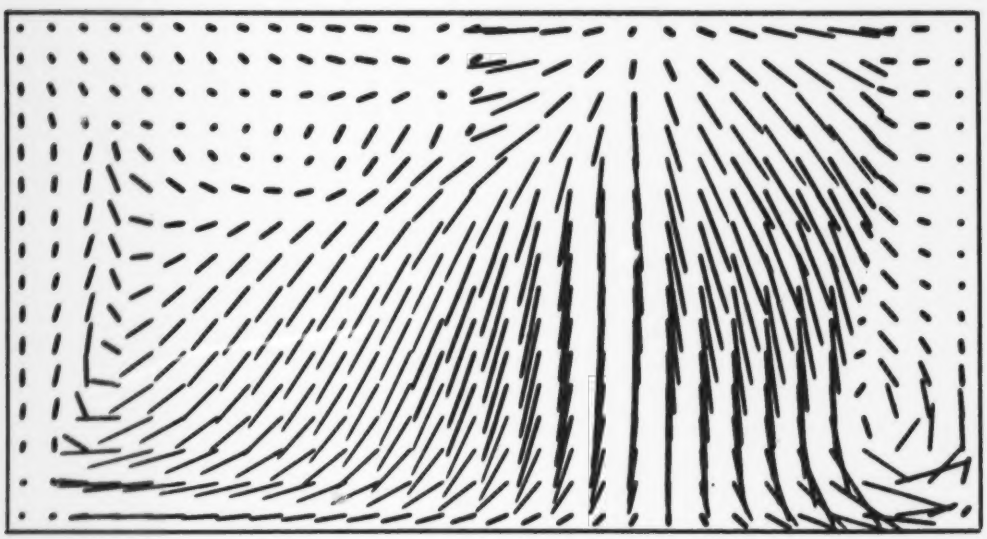

Fig. 20. Plane view of velocity vectors in a plane perpendicular to the y axis at a distance of 105 feet from the origin.

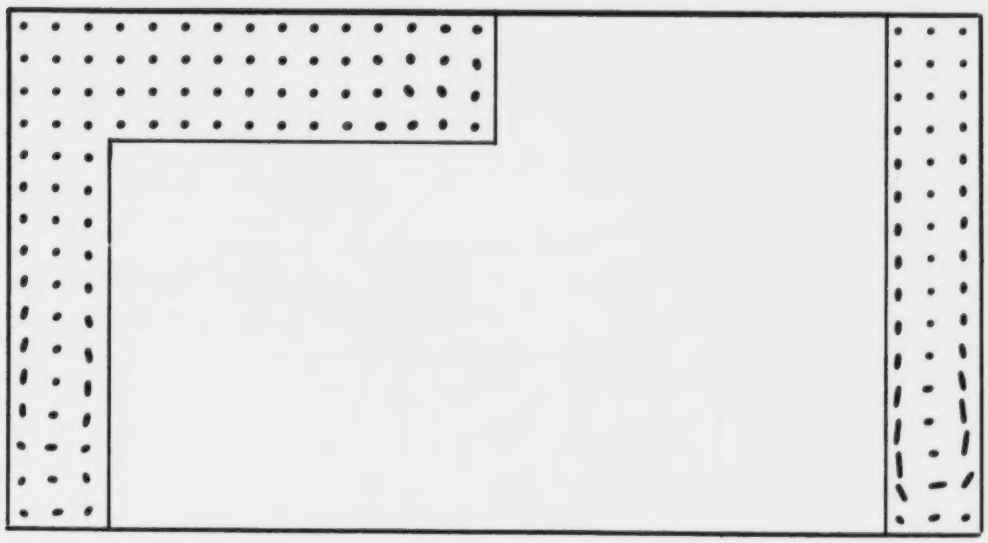

Fig. 21. Plane view of velocity vectors in a plane perpendicular to the y axis at a distance of 155 feet from the origin. The intersection of this plane with the buildings is shown.

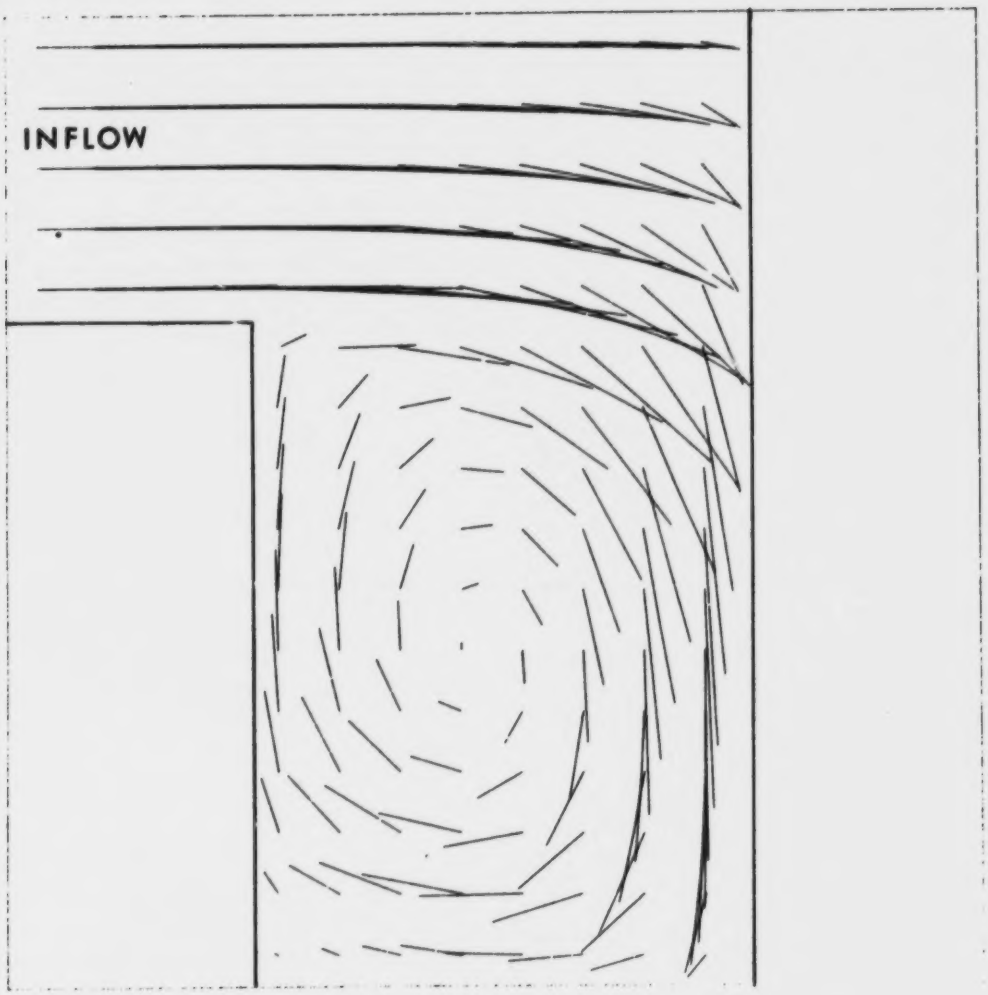

Fig. 22. Plane view of velocity vectors in a plane perpendicular to the x axis at a distance of 175 feet from the origin.

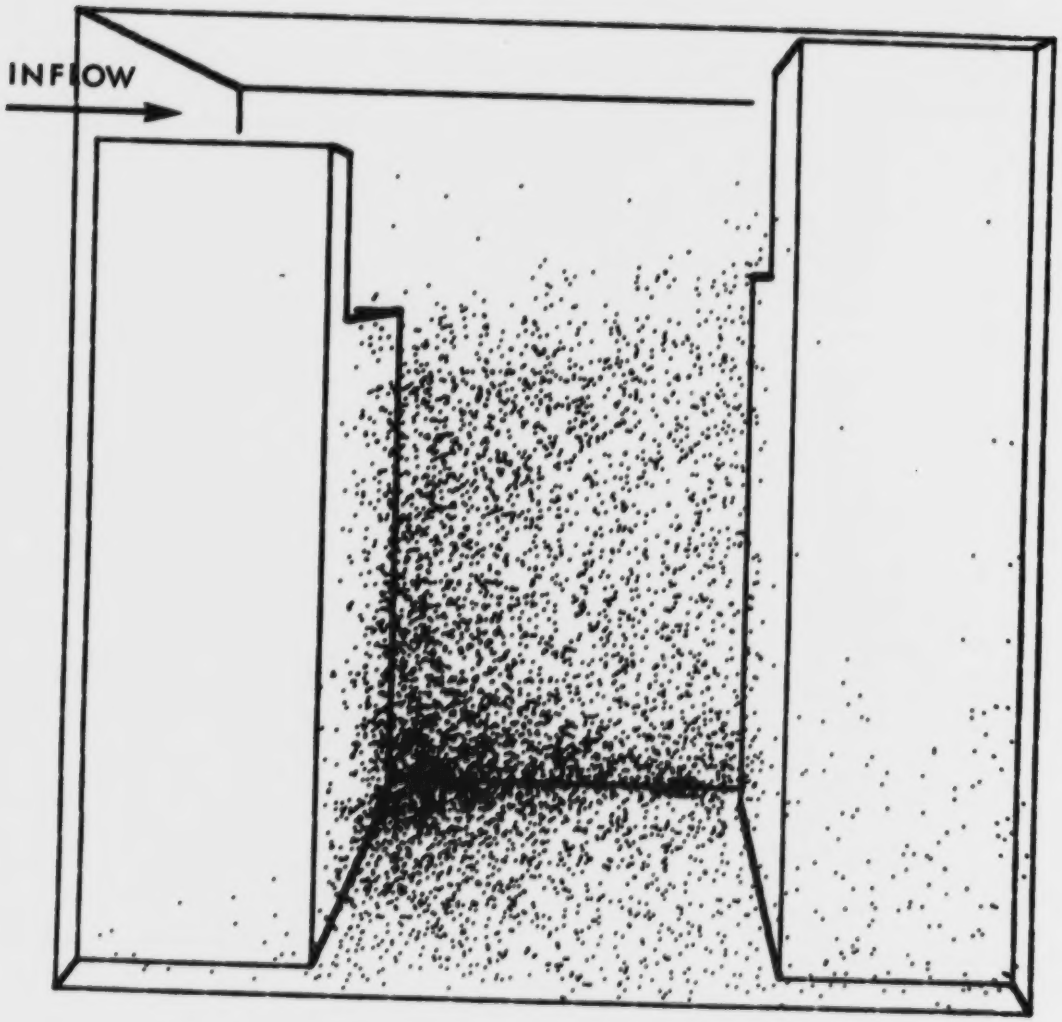

Fig. 23. Steady particular distribution in Broadway Street Canyon resulting from real sources on Broadway, Locust and Olive Streets.

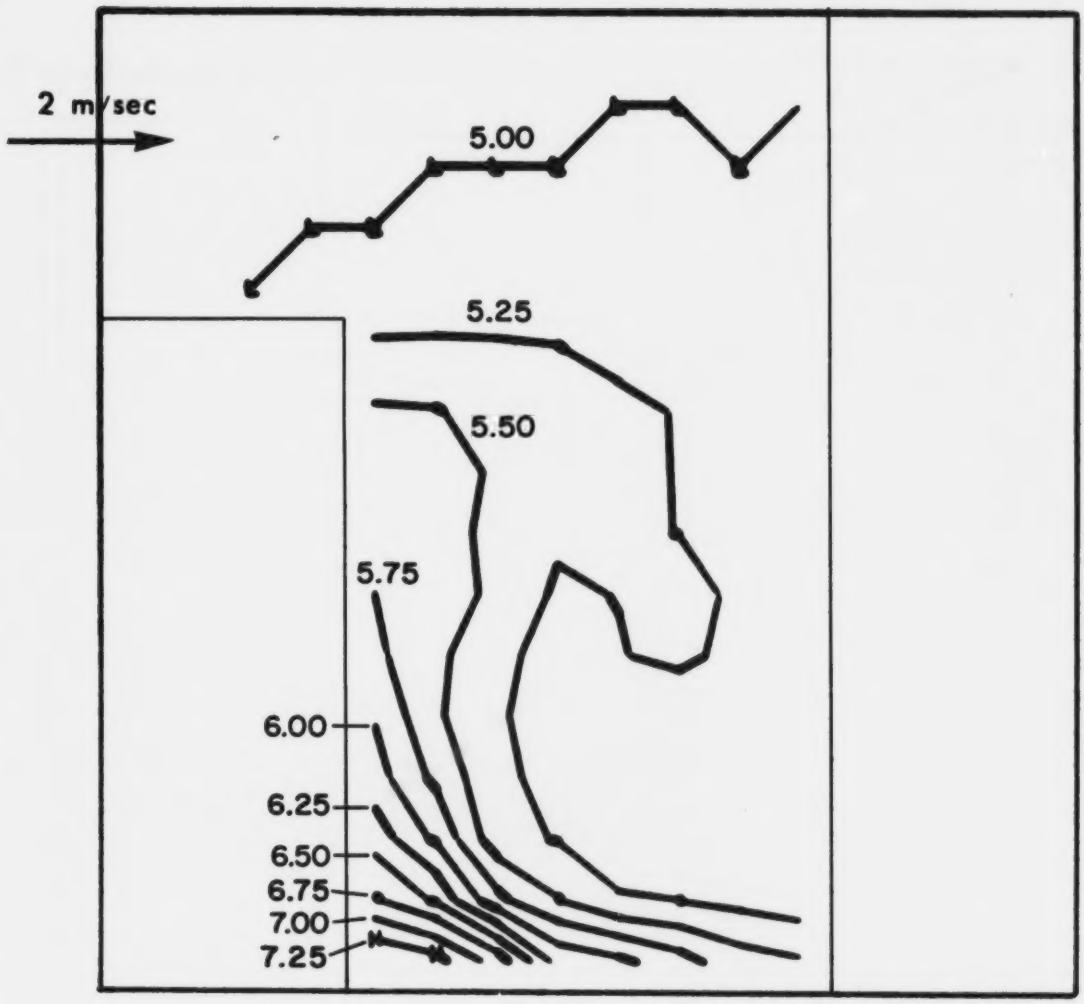

Fig. 24. Isopleths in a plane perpendicular to the x axis at a distance of 155 feet from the origin. This plot corresponds to the measuring station of Ludwig and Dabberdt. (Units in ppm of CO).

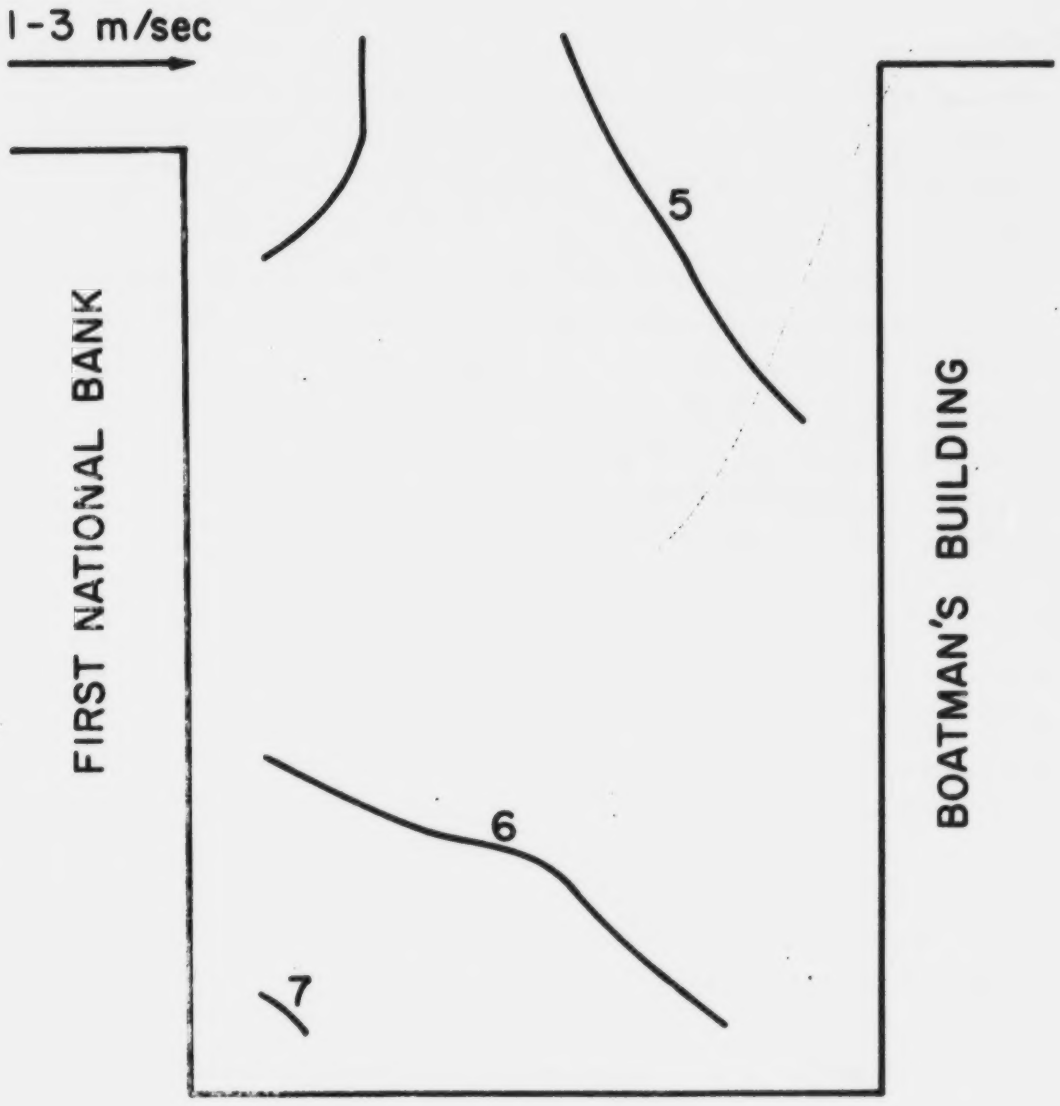

Fig. 25. Distribution of CO concentration in Broadway Street Canyon (in ppm) measured by Ludwig and Dabberdt.

steady distribution. This final distribution is pictured in Fig. 23. Isopleths of this distribution in the same plane as that measured by Ludwig and Dabberdt are shown in Fig. 24 in the units of parts per million.

In order to determine the proper units for these numerical results, it is necessary to know two of the parameters involved in the experiment. These may include, for example, a source strength in equivalent units of mass per unit area and time and a background concentration, a value of concentration at any point within the street canyon and a background concentration or any other pair of similar values. Since a background concentration does nothing more than elevate the entire concentration field by that same amount, a numerical calculation may proceed without a background concentration, and the results elevated accordingly. The calculation previously depicted proceeded in this way.

In order to scale our results to the units reported by Ludwig and Dabberdt, an experimental value of concentration (in ppm) from the CO-detector at the lower corner of Broadway and the First National Bank was chosen equal to our calculated concentration (in particles per cell volume) at the same point after all concentrations had been elevated by their experimentally determined background concentration. Thus we were able to determine the mass of pollutant that was being represented by each particle. This approach was taken since it was not possible to determine the flux of pollutants at the street level pertinent to those results presented in Fig. 21 of their referenced paper. A comparison of Fig. 24 with their results as presented in Fig. 25 with the wind between 1-3 m/sec shows excellent correlation.

As a matter of fact, the above approach proves to be an advantage if one elected to use a numerical technique of this type to monitor CO levels in downtown street canyons. Time dependent CO-detectors

located at two points within the street canyon could be used with the numerical technique to monitor the levels of CO at every point within the street canyon over long periods of time.

After having determined the mass of pollutant per particle in this way, we can calculate the average value of the source flux as being approximately 4.3×10^{-3} gm-CO/m^2 sec (based on properties of air at standard temperature and pressure) in the Broadway street canyon during the data taking phase of this experiment.

The concentration plots in Figs. 26 and 31 show the distribution of pollution in planes, again perpendicular to the direction indicated and at distances from the coordinate system, as previously discussed. The presence of buildings on the sides of the streets shows how pollutants are allowed to build up in the canyon. However, at the intersections of Locust and Olive, it is evident that the concentrations are greatly reduced as they are swept out of the computing region.

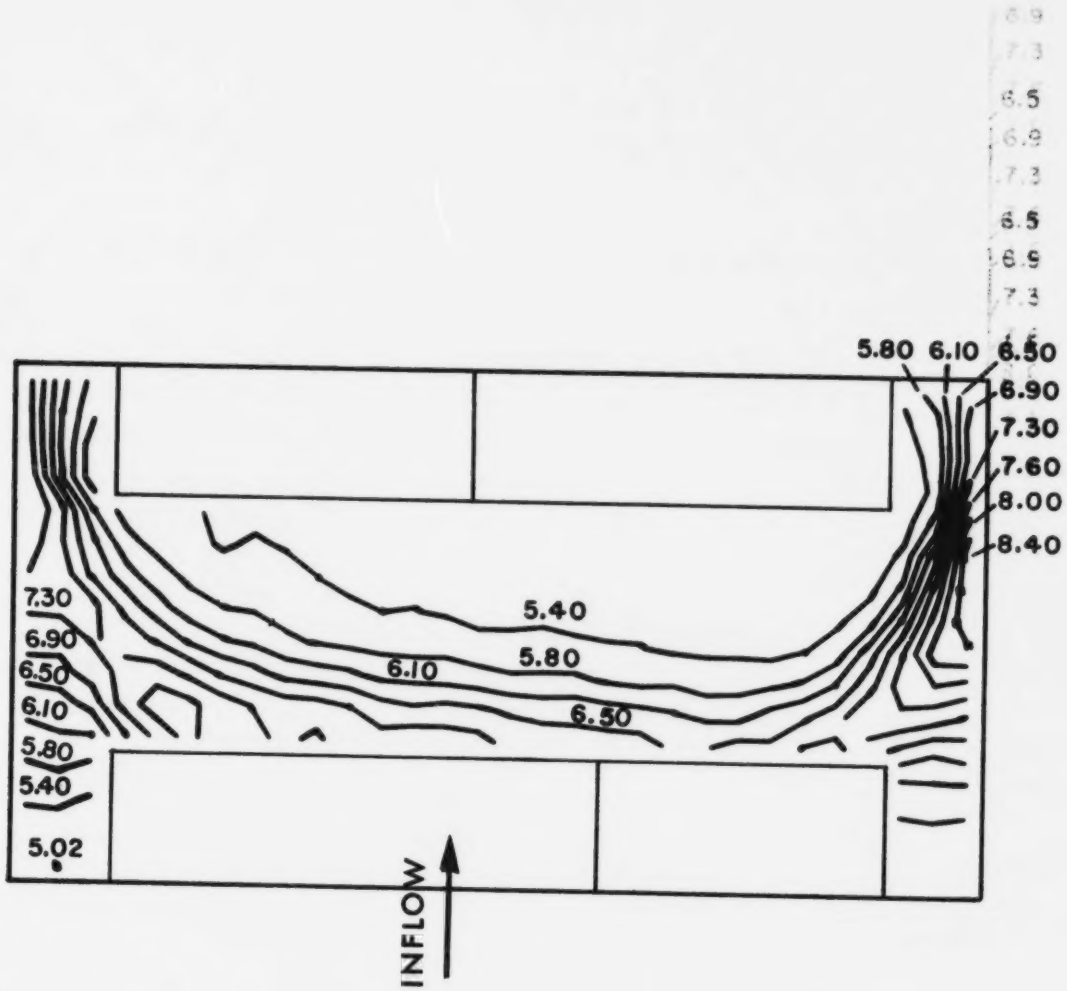

Fig. 26. Isopleths in a plane perpendicular to the z axis at a distance of 15 feet from the origin (ppm).

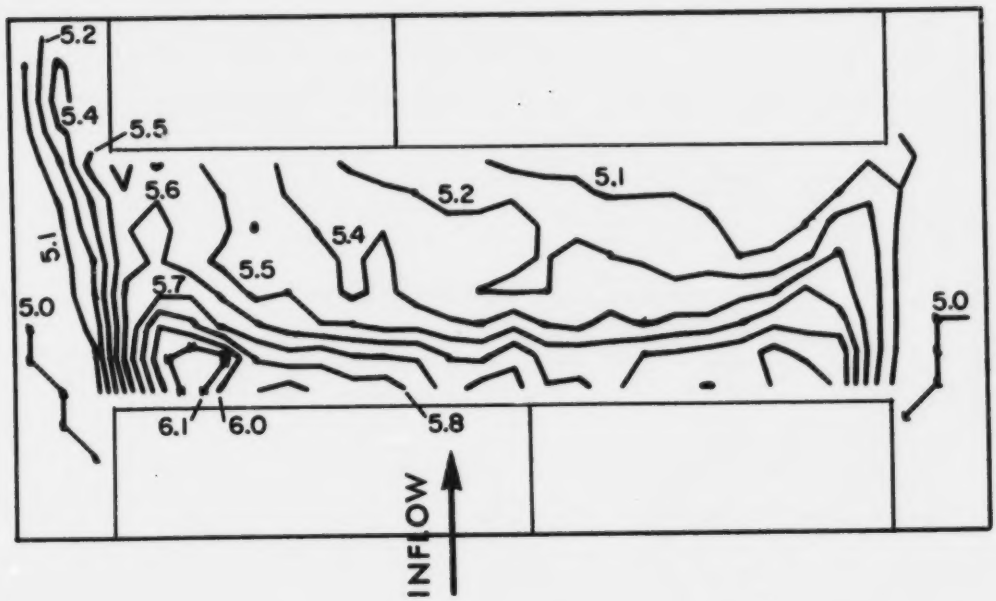

Fig. 27. Isopleths in a plane perpendicular to the z axis at a distance of 65 feet from the origin (ppm).

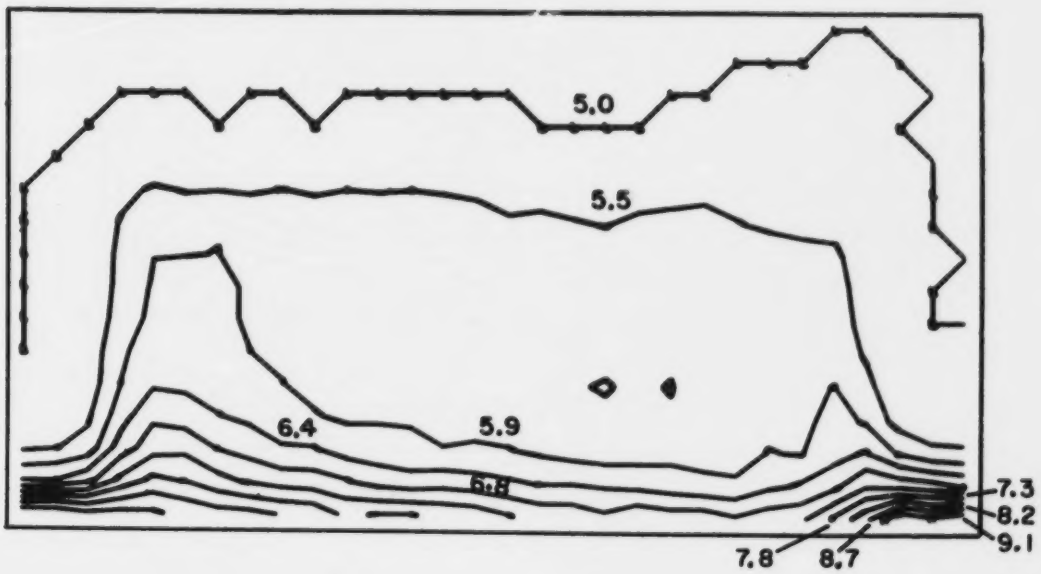

Fig. 28. Isopleths in a plane perpendicular to the y axis at a distance of 55 feet from the origin (ppm).

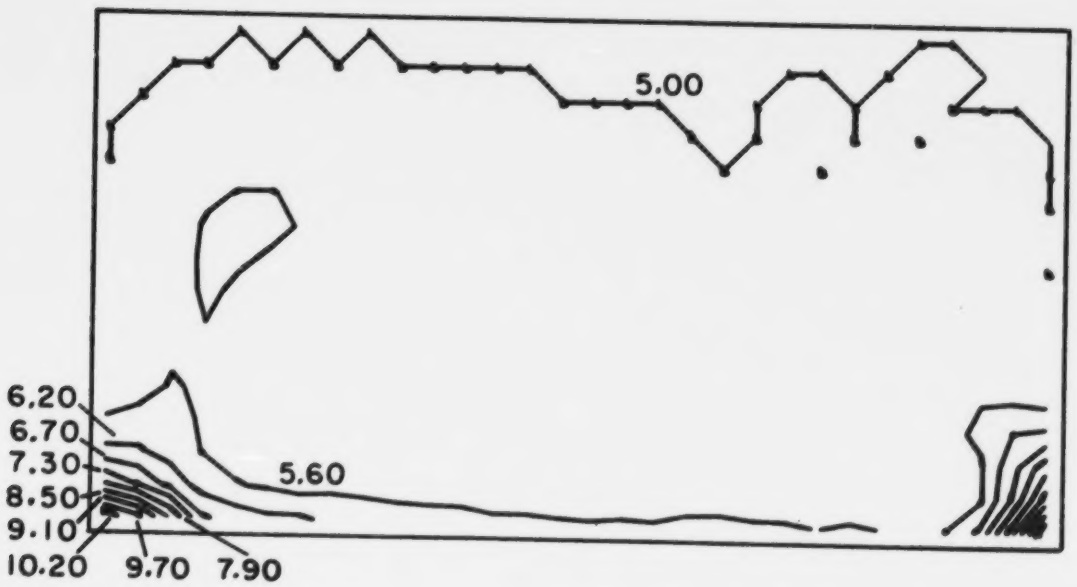

Fig. 29. Isopleths in a plane perpendicular to the y axis at a distance of 105 feet from the origin (ppm).

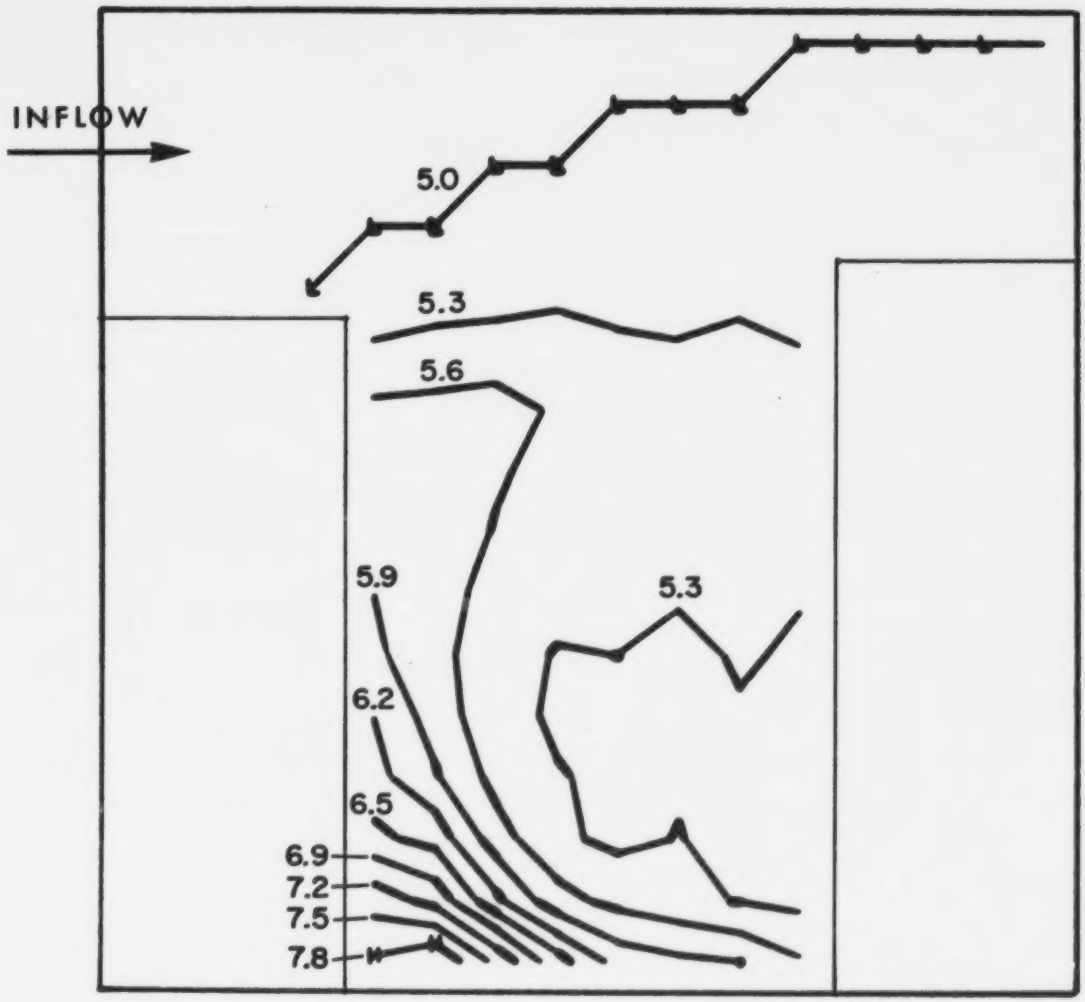

Fig. 30. Isopleths in a plane perpendicular to the x axis at a distance of 95 feet from the origin (ppm).

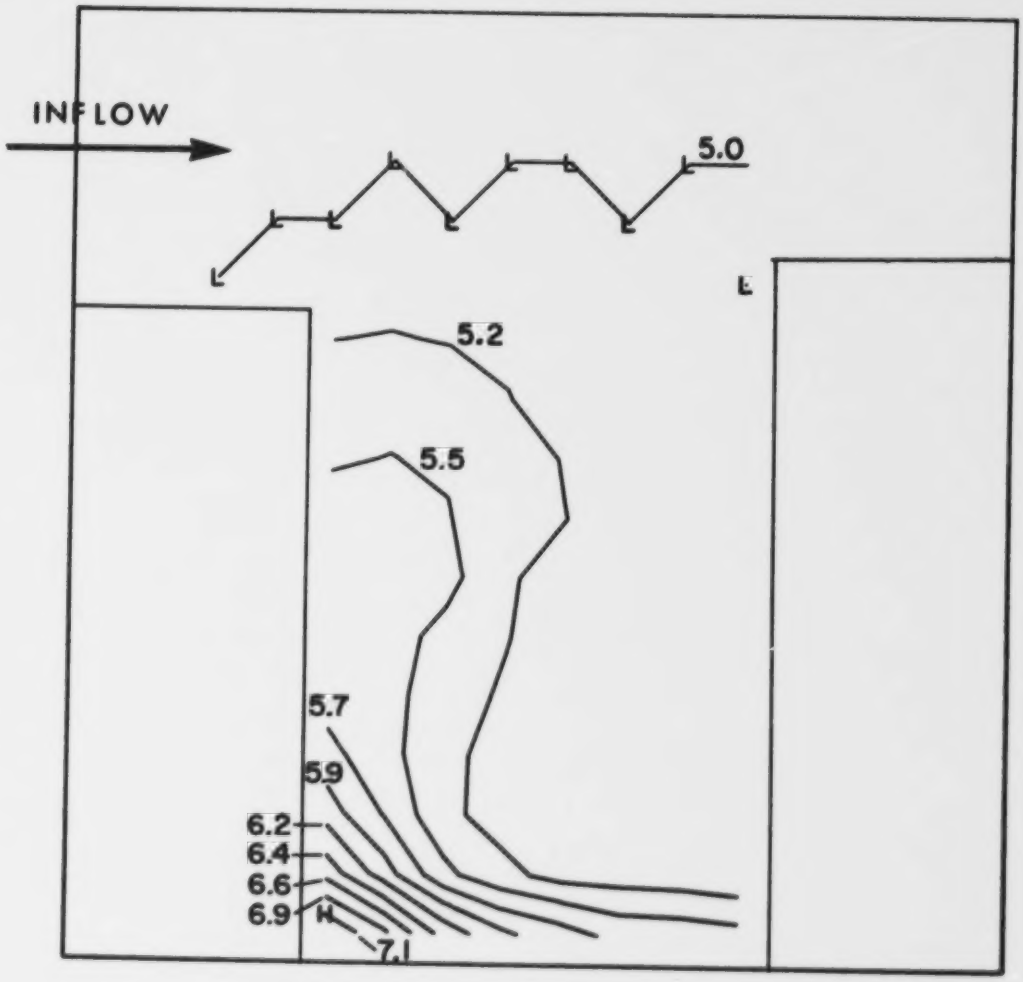

Fig. 31. Isopleths in a plane perpendicular to the x axis at a distance of 205 feet from the origin (ppm).

SECTION IX

A GENERALIZED STREET CANYON

As previously mentioned, the uniqueness of each street canyon geometry complicates analysis of flow patterns and pollution transport since each canyon must be analyzed separately. However, an alternate approach to such analyses is to generalize street canyons in categories defined by height to width ratios, incoming wind velocities, source strengths, etc., and then calculate the flow and pollution dispersal patterns for such a class of problems. For example, geometries such as that depicted in Fig. 32 can pertain to a large class of problems for which an effective canyon height to width ratio is unity and for which the building heights on both sides of the street are nearly equal. Since half of the canyon block is being modeled, the front and back planes in Fig. 32 are chosen to be planes of symmetry, implying that mirror images of the geometry viewed exist on the opposite side of those planes. The incoming wind is chosen to be perpendicular to the main canyon, not only for simplicity in the calculational setup but for witnessing the "worst case" type of problem. The steady velocity distribution resulting from the uniform inflow of unit magnitude is presented in Figs. 32 and 33 in a similar manner to the previous results. The calculational region is 18 cells in the x direction, 18 cells in the y direction and 15 cells in the z direction with each cell having unit length in each coordinate dimension. Thus with the appropriate selection of length and time scales, the calculation can be made to apply to any desired situation involving this geometry.

A line source of pollutants, placed along the bottom center of the longitudinal street, influxes 360 particles per unit time uniformly along the length of the street in the velocity field previously presented. At statistically steady state, the particle distribution in the canyon as viewed looking downwards and from mid-block is shown in

Figs. 34 and 35. Concentration plots, in units of particles per unit cell volume, are given in Figs. 36 and 42 for various planes within the canyon. Again these contour lines can be scaled to any appropriate units by assigning a mass of pollutant to each particle, and dividing this number by the true length scale cubed.

Another line source, parallel to the incoming wind, is placed along the bottom of the plane of symmetry at the street intersection and emits pollutants into the steady velocity field. The steady distribution from this source and the associated concentration contour plots are shown in Figs. 43 through 46. The mass diffusivity for particle motion in each of these cases was chosen to be $\lambda = .25$ while the turbulent eddy viscosity of the fluid was $\nu = .1$, however, as previously mentioned, the proper choice of λ is somewhat uncertain.

After having scaled each of these results to the appropriate units, a superposition of the two produces the distribution of concentration in the canyon for the cases in which traffic density is different along each of the two streets. Although a single line source in each street may not be the appropriate type of source for most common studies, the technique is very flexible to allow area, volume or even point sources to be considered along with the previously calculated steady velocity field, in a fairly efficient manner.

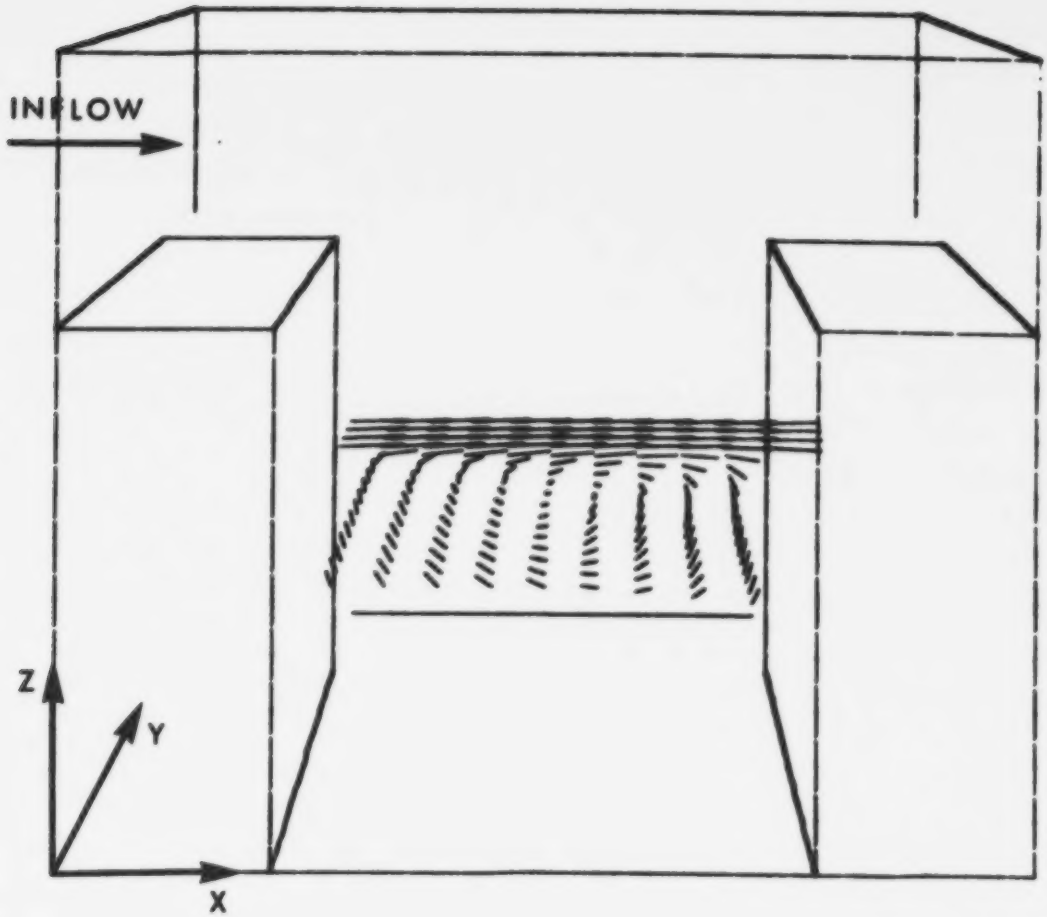

Fig. 32. Generalized street canyon configuration in perspective with velocity vectors shown in a plane perpendicular to the z axis at a distance of 5.5 units from the origin. Location of the coordinate system is shown.

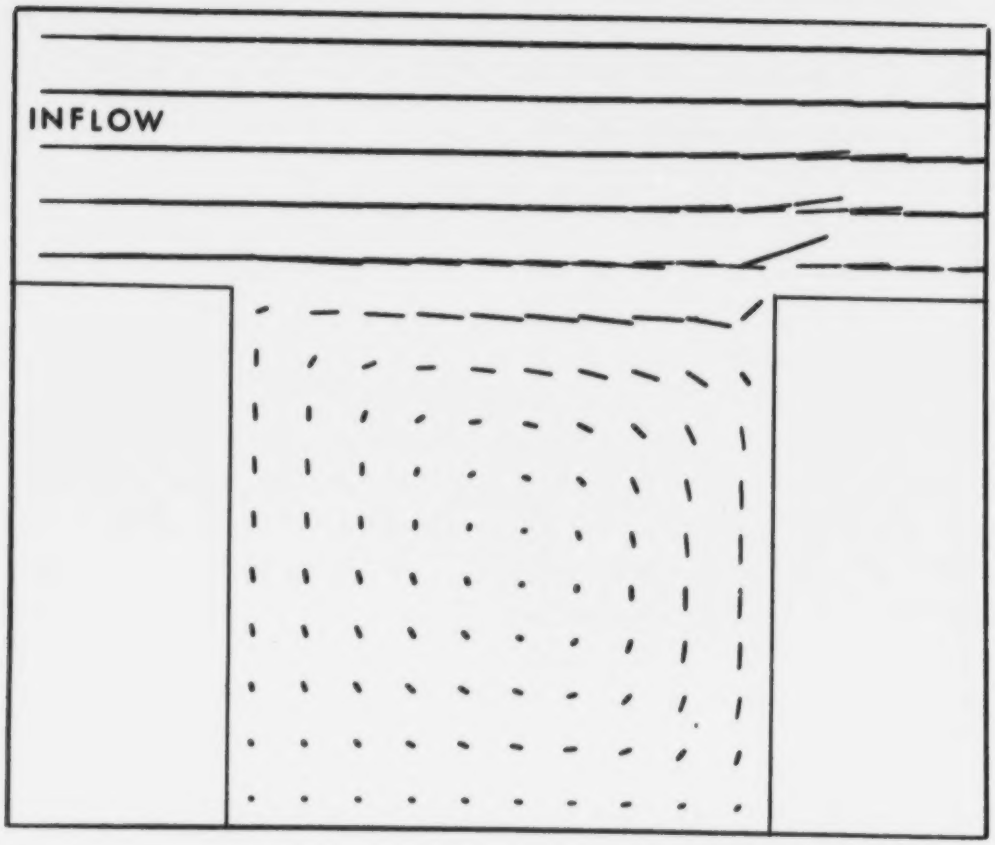

Fig. 33. Plane views of velocity vectors in a plane perpendicular to the y axis at a distance of 9.5 units from the origin.

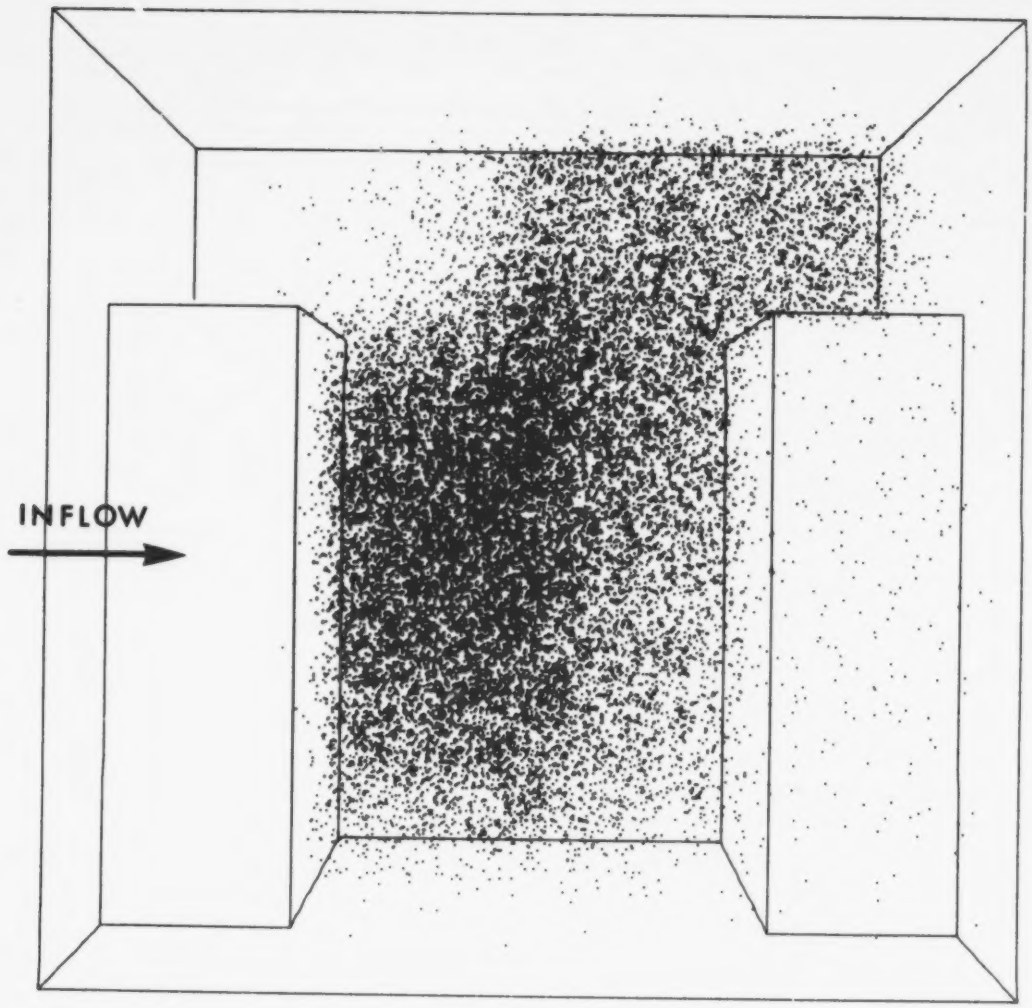

Fig. 34. Steady particle distribution in the generalized street canyon, as viewed from above, resulting from a line source perpendicular to the incoming flow.

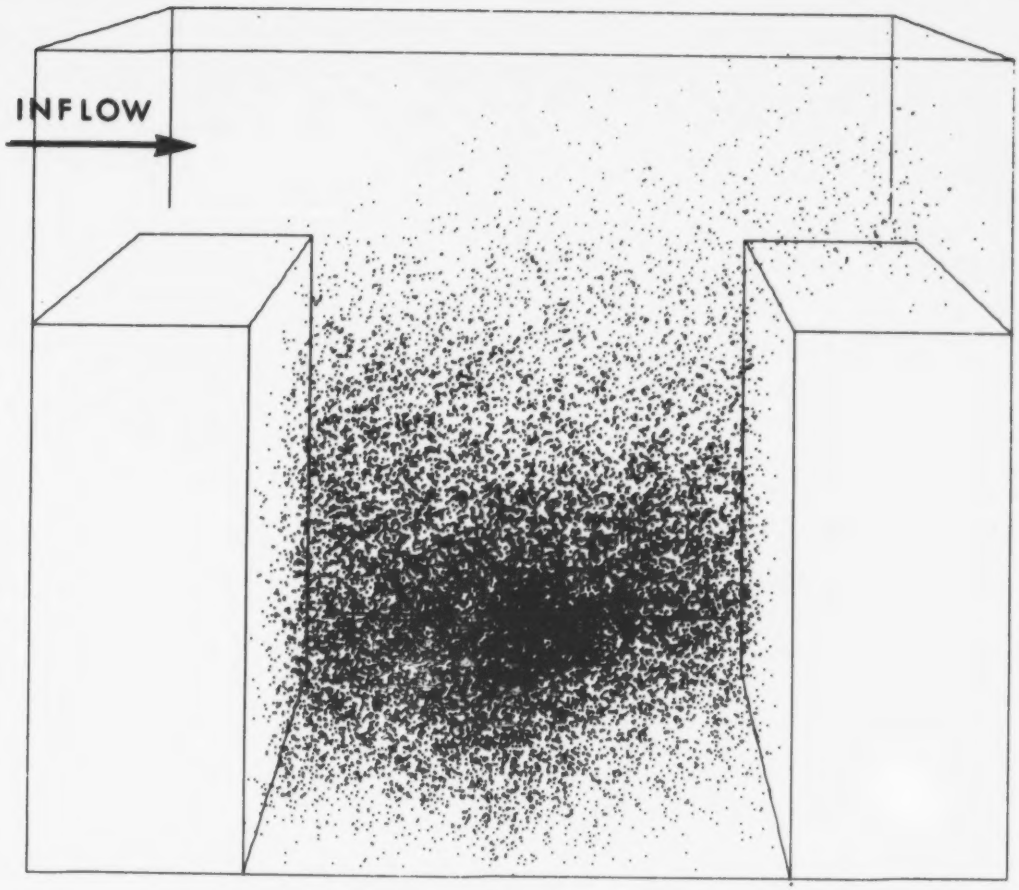

Fig. 35. Same particle distribution as that shown in Fig. 34, only viewed from the top of the buildings at mid-block.

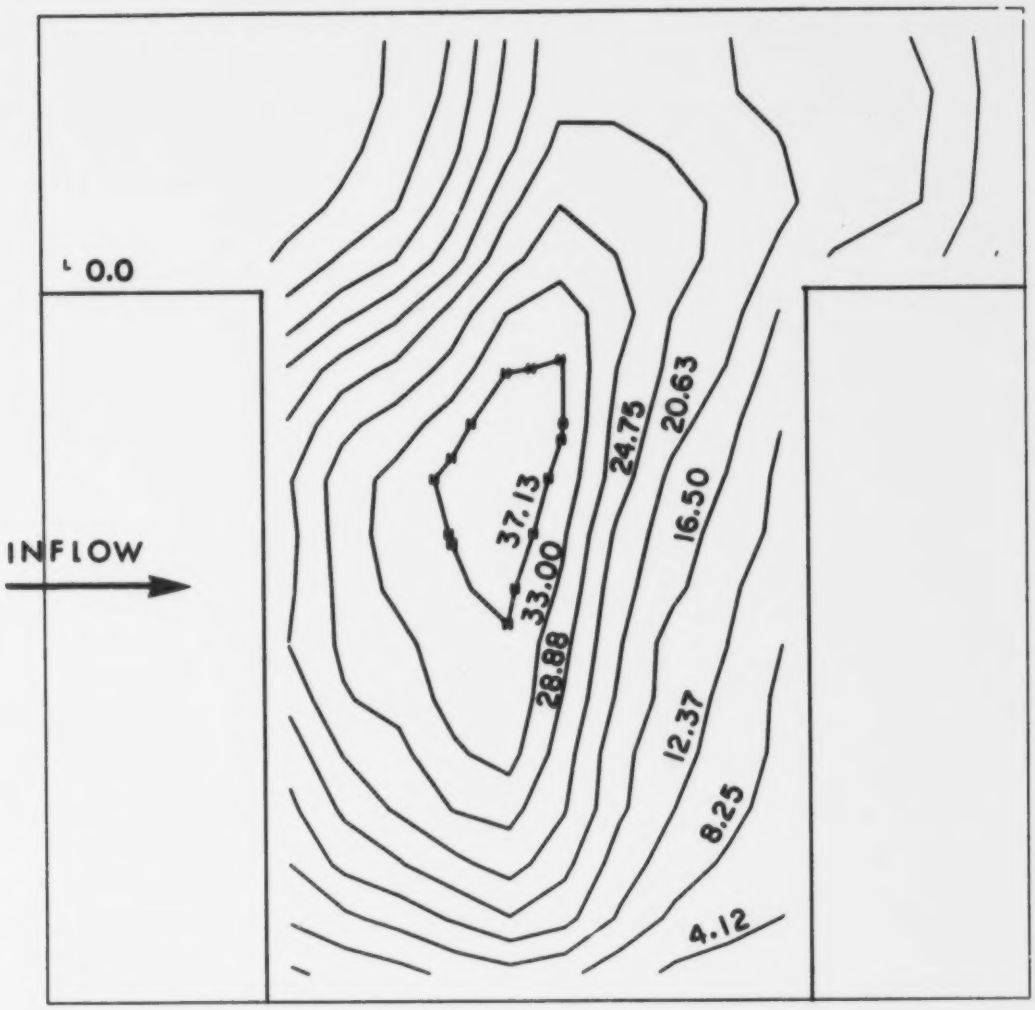

Fig. 36. Isopleths in a plane perpendicular to the z axis at a distance of 1.5 units from the origin. (Source perpendicular to inflow). Concentrations in particles per cell volume.

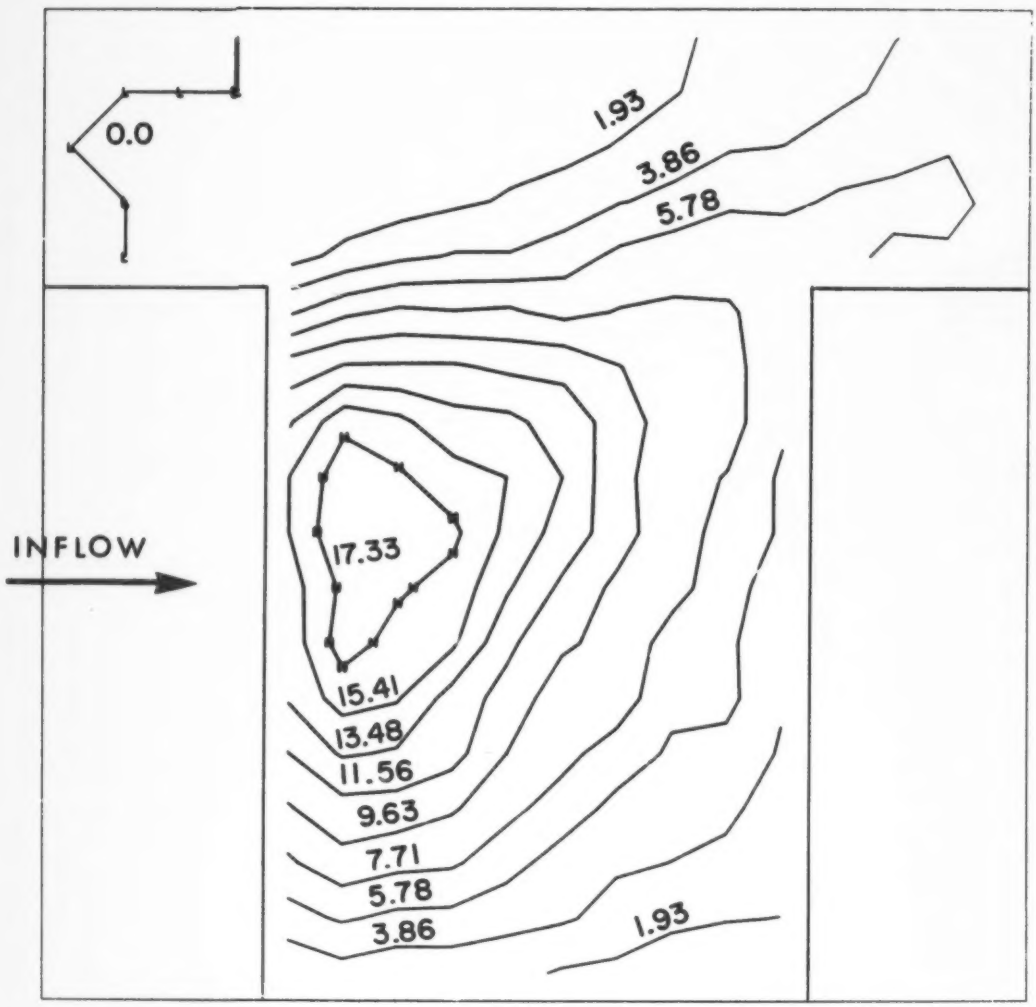

Fig. 37. Isopleths in a plane perpendicular to the z axis at a distance of 5.5 units from the origin. (Source perpendicular).

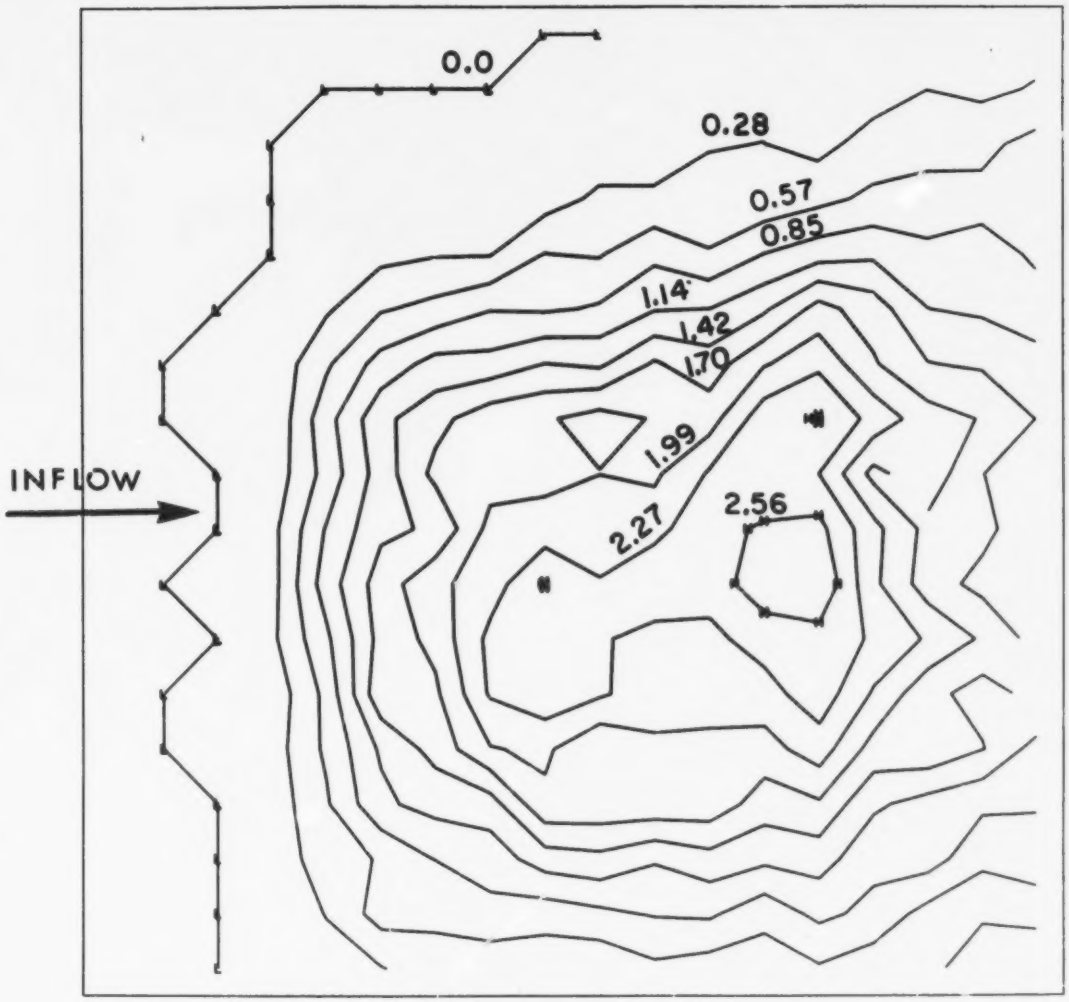

Fig. 38. Isopleths in a plane perpendicular to the z axis at a distance of 10.5 units from the origin. (Source perpendicular).

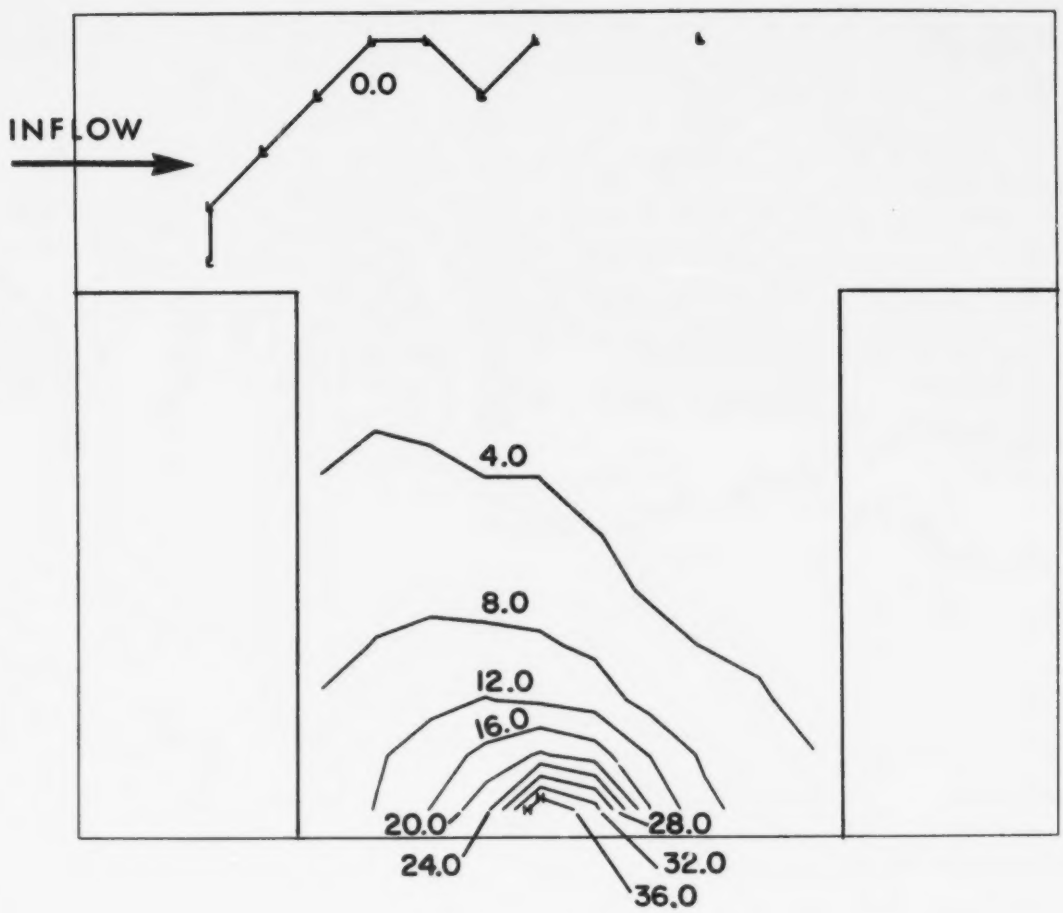

Fig. 39. Isopleths in a plane perpendicular to the y axis at a distance of 1.5 units from the origin. (Source perpendicular).

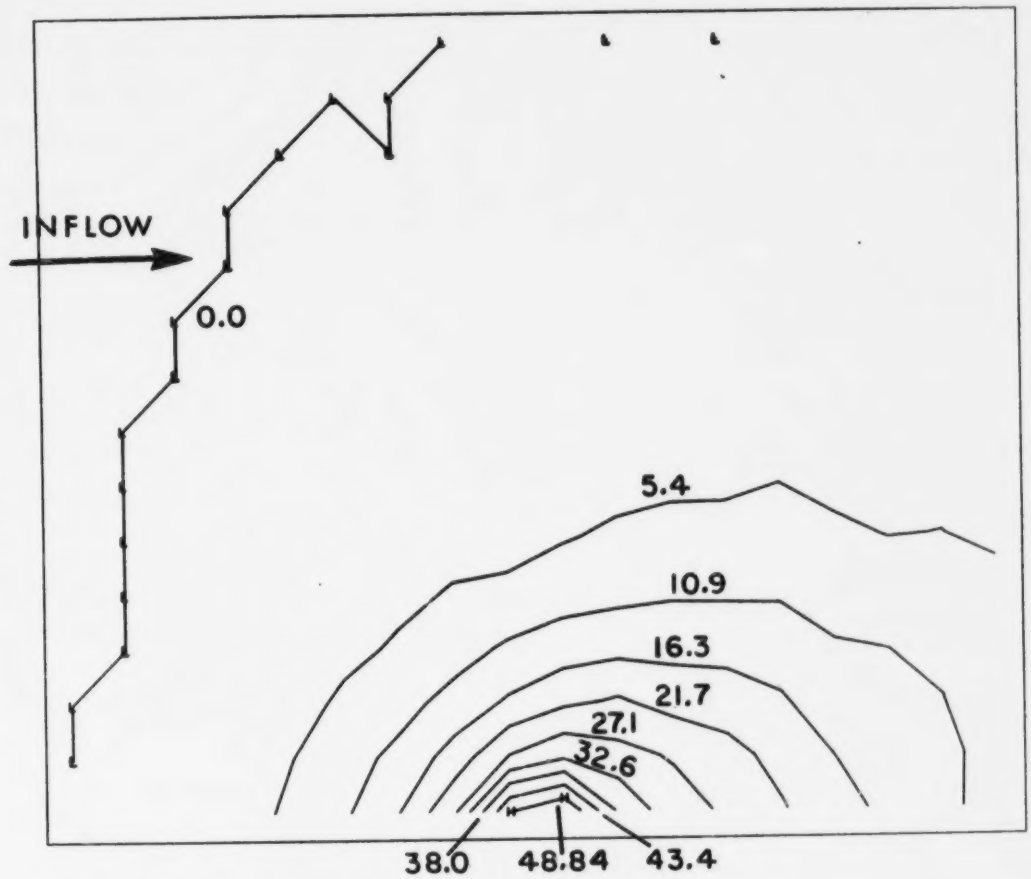

Fig. 40. Isopleths in a plane perpendicular to the y axis at a distance of 13.5 units from the origin. (Source perpendicular).

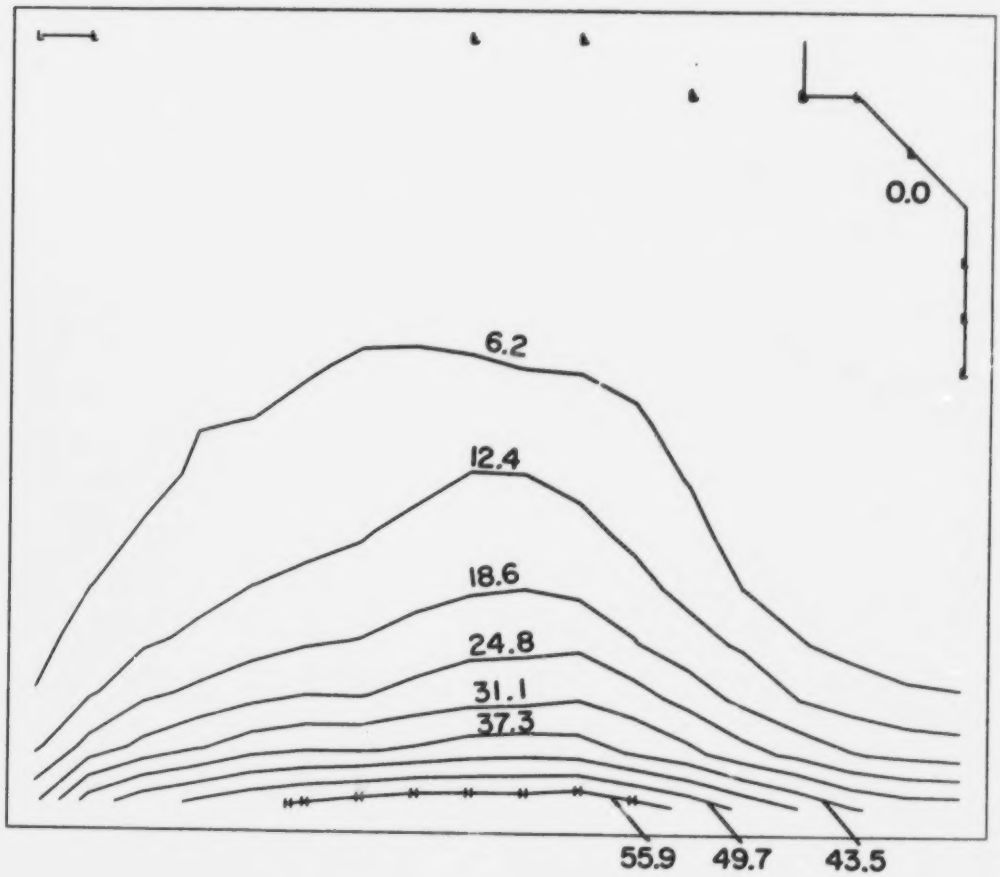

Fig. 41. Isopleths in a plane perpendicular to the x axis at a distance of 8.5 units from the origin. (Source perpendicular).

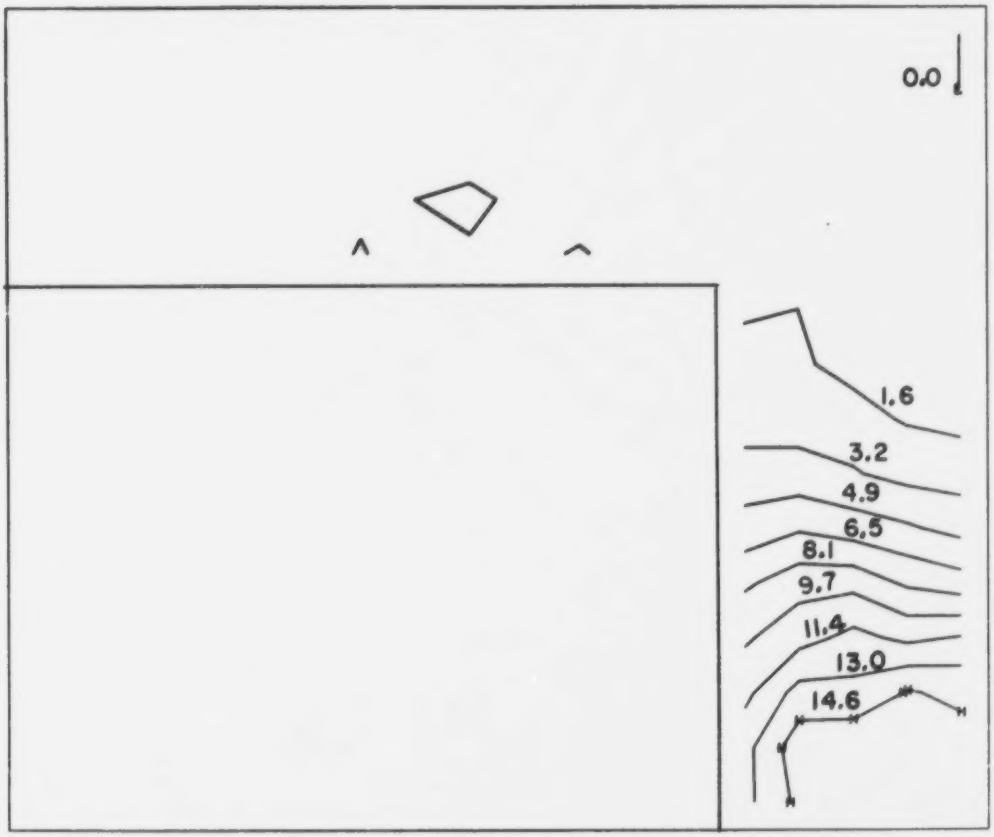

Fig. 42. Isopleths in a plane perpendicular to the x axis at a distance of 16.5 units from the origin. (Source perpendicular).

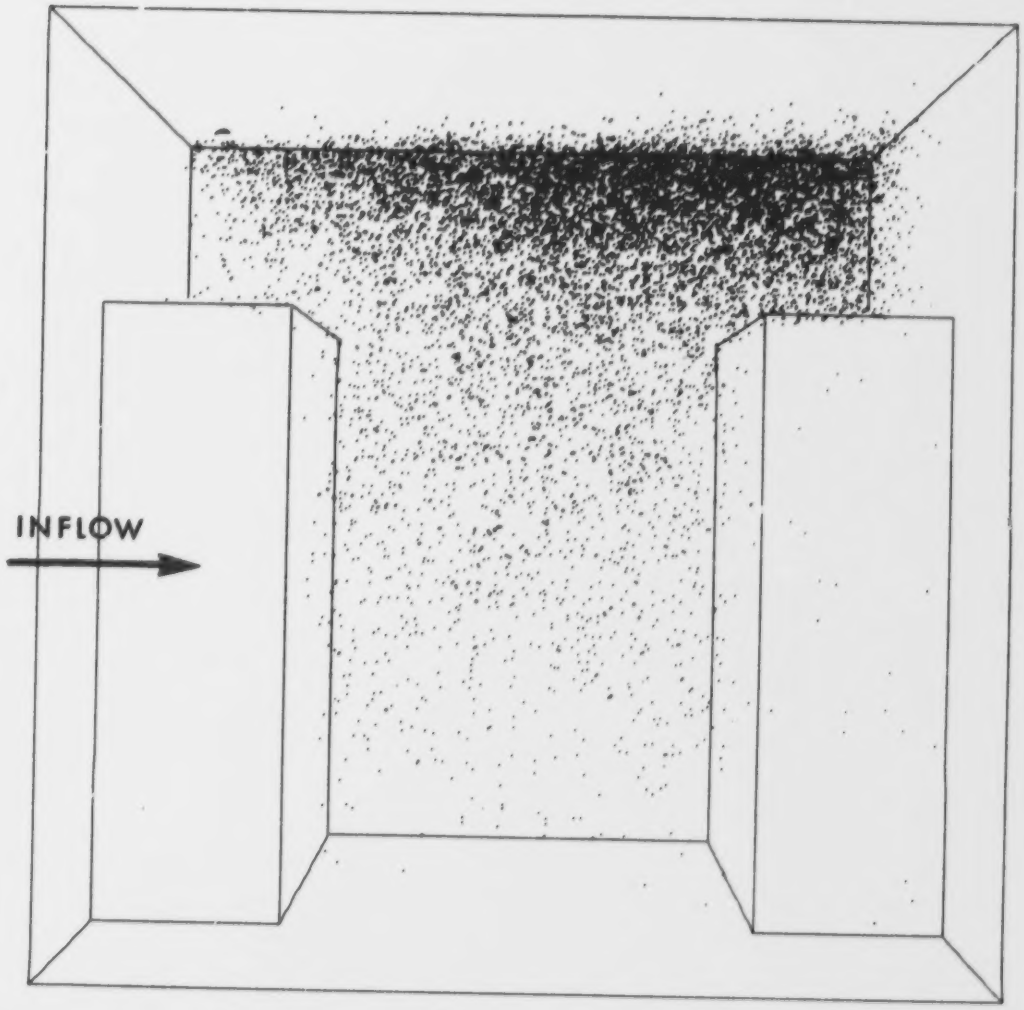

Fig. 43. Steady particle distribution in the generalized street canyon as viewed from above, resulting from a line source parallel to the incoming flow.

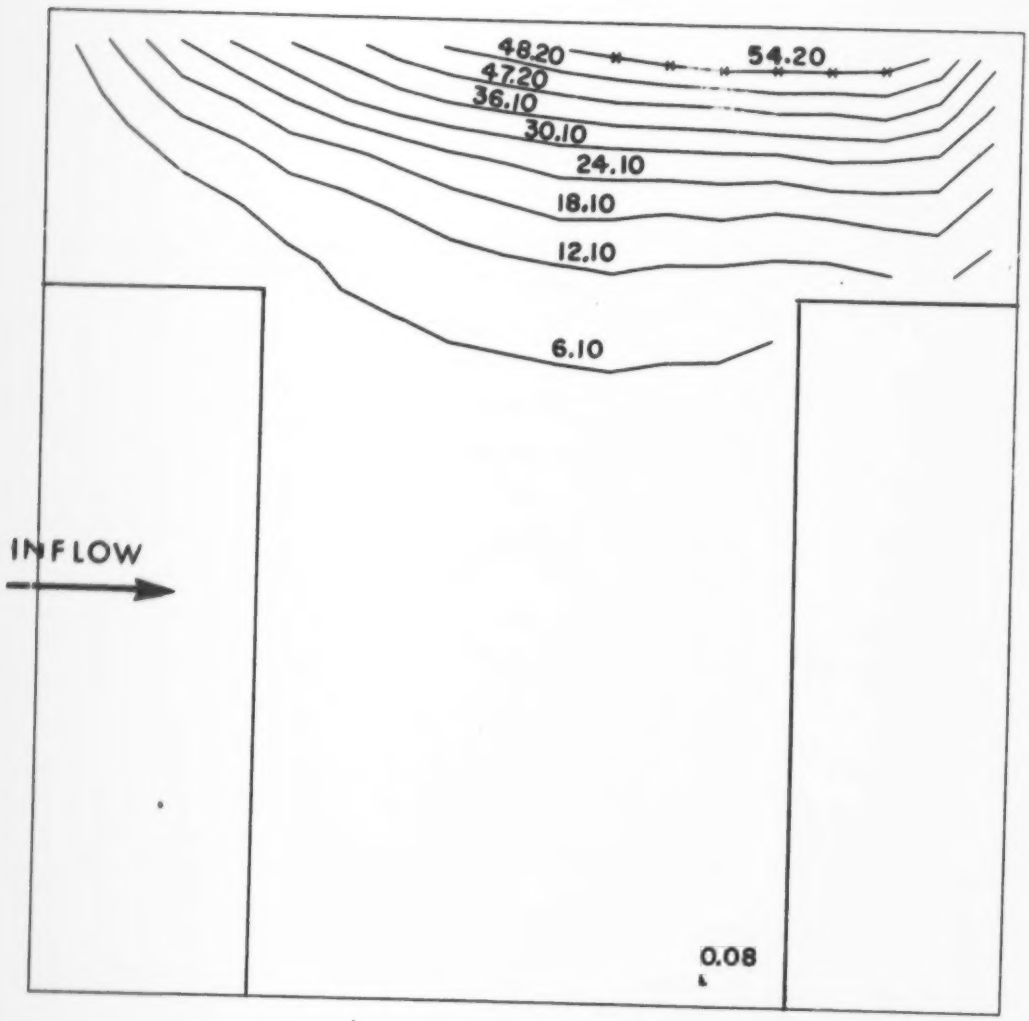

Fig. 44. Isopleths in a plane perpendicular to the z axis at a distance of 1.5 units from the origin. (Source perpendicular).

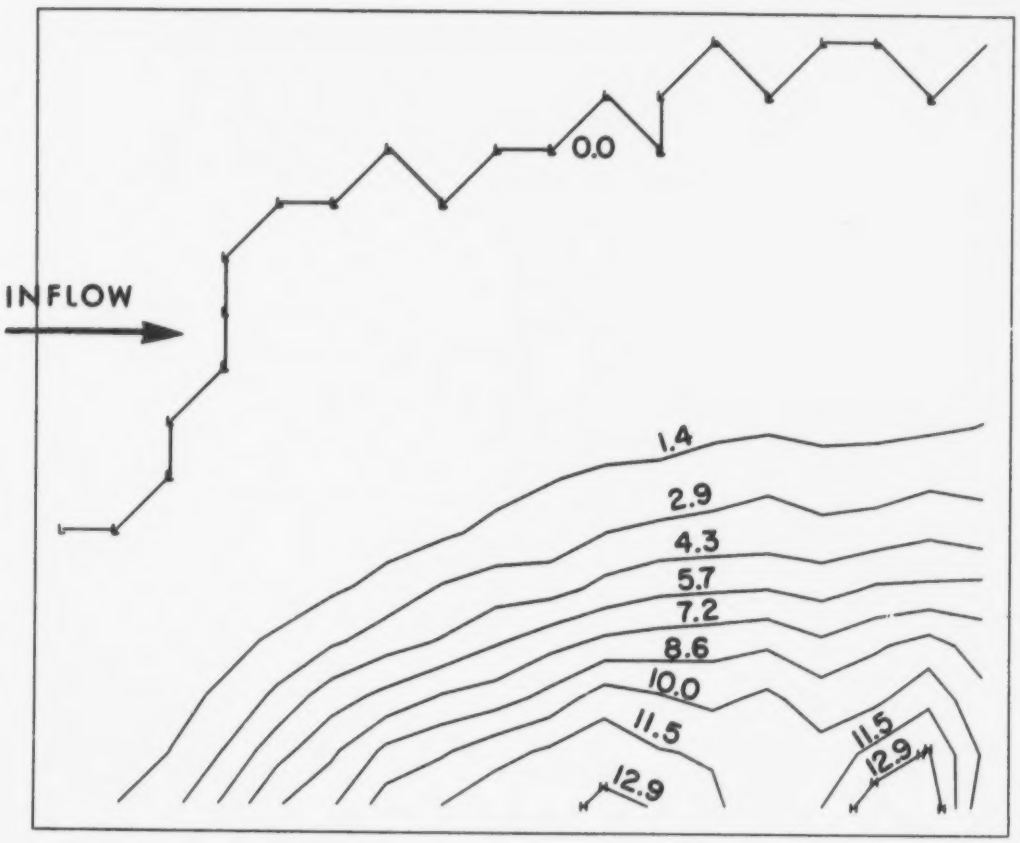

Fig. 45. Isopleths in a plane perpendicular to the y axis at a distance of 13.5 units from the origin. (Source perpendicular).

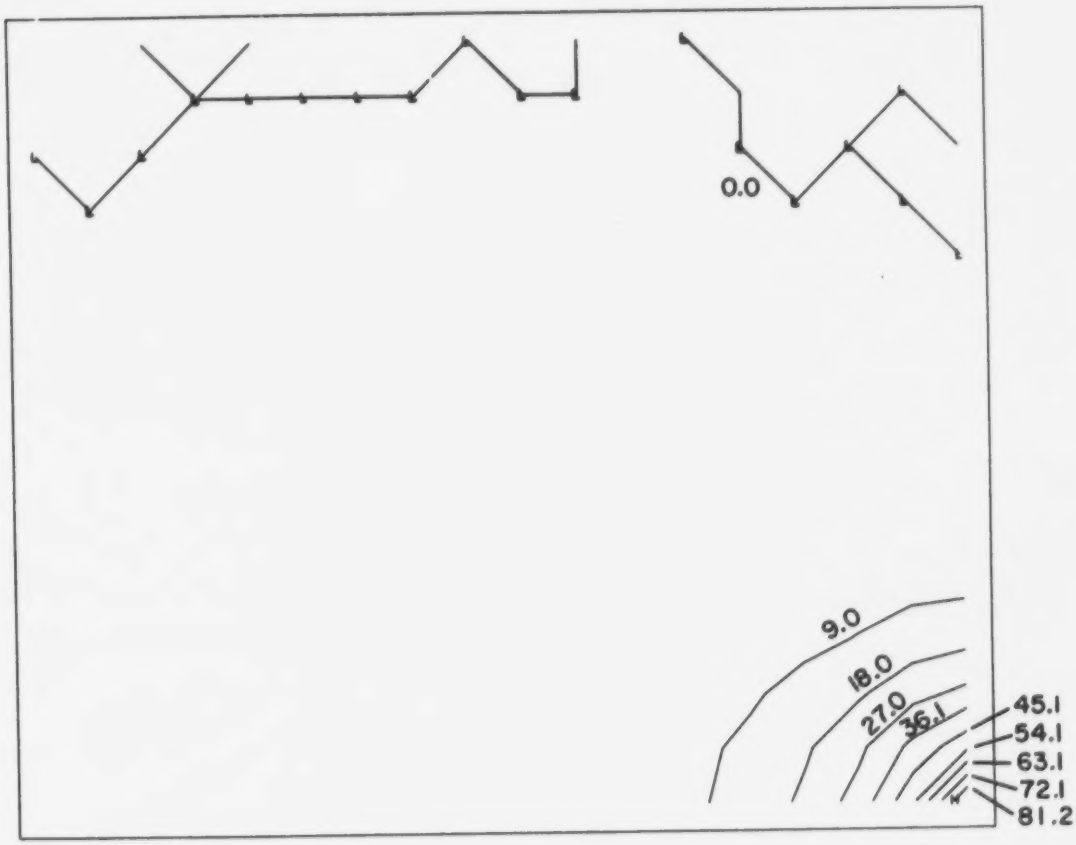

Fig. 46. Isopleths in a plane perpendicular to the x axis at a distance of 8.5 units from the origin. (Source perpendicular).

SECTION X

COMPUTER REQUIREMENTS

The calculations presented in this paper were all performed on a CDC 7600 computer with a 65,536 60-bit word small core memory and a 512,000 60-bit word large core memory. The computer program used to perform these calculations (entitled S-TRES) is designed to use almost all of both memories in order to reach its maximum resolution which is a mesh the equivalent of 27 cells cubed, and 30,000 particles.

The amount of computer time used in achieving steady state on a particular problem depends on such factors as the number of cells used in spanning the geometry, the size of the time step used, the size of the particle diffusivity and the amount and frequency of computer generated output. For example, the Broadway street canyon problem took approximately 90 min of computer time to reach hydrodynamic steady state and an additional 40 minutes to reach particle steady state; thus implying approximately 2.2 hours of total computer time to obtain the results presented. These numbers, of course, do not reflect setup of debugging time. S-TRES executes its function in an average time of approximately 5 sec for each hydrodynamic cycle and 3 sec for each particle moving cycle. These last numbers can vary greatly with the complexity of a problem.

SECTION XI

REFERENCES

1. Ludwig, F. L. and Dabberdt, W. F., "Evaluation of the APRAC-1A Urban Diffusion Model for Carbon Monoxide," Stanford Research Institute Final Report (February 1972).

2. Johnson, W. B., et al., "Field Study for Initial Evaluation of an Urban Diffusion Model for Carbon Monoxide," Stanford Research Institute Comprehensive Report (June 1971).

3. Hirt, C. W. and Cook, J. L., "Calculating Three-Dimensional Flows Around Structures and Over Rough Terrain," J. Comp. Phys. 10, 2 (1972).

4. Harlow, F. H. and Welch, J. E., Phys. Fluids 8, 2182 (1965), 9, 842 (1966); Welch, J. E., et al., "The MAC Method," Los Alamos Scientific Laboratory report LA-3425 (November 1965); Amsden, A. A. and Harlow, F. H., "The SMAC Method," Los Alamos Scientific Laboratory report LA-3470 (May 1970).

5. Hotchkiss, R. S. and Hirt, C. W., "Particulate Transport in Highly Distorted Three-Dimensional Flow Fields," Proceedings of the Summer Simulation Conference, San Diego, California, June 14-16, 1972.

6. Wang, P. N., Chang, P. C. and Lin, A., "Circulation and Diffusion of the Separated Flow in a Rectangular Trough," University of Utah Scientific Report for the Period 1 May 1970 to 30 April 1972, prepared for the Environmental Protection Agency under Grant AP 01126, May 1972.

7. Reiman, T. C. and Sabersky, R. H., "Laminar Flow Over Rectangular Cavities," Int. J. of Heat and Mass Transfer, 11 (1968).

8. Mills, R. D., "On the Closed Motion of a Fluid in a Square Cavity," J. of the Royal Aeronautical Society, 69, (1965).

9. Jacobs, H. R. and Sutton, S. B., "A Numerical Analysis of Steady Separated Flows in Rectangular Cavities With and Without Mass Additions," University of Utah Scientific Report for the Period 1 May 1970 to 30 April 1972, prepared for the Environmental Protection Agency under Grant AL 01126, May 1972.

10. Daly, B. J. and Harlow, F. H., "Transport Equations in Turbulence," Phys. Fluids, 13, 2634 (1970).

SECTION XII

APPENDIX

A PREPRINT OF

"Calculating Three-Dimensional Flows Around Structures And Over Rough Terrain," by C. W. Hirt and J. L. Cook, published in Journal of Computational Physics, 10, 2, 1972.

LA-DC – 13289

A -1-

CALCULATING THREE-DIMENSIONAL FLOWS AROUND STRUCTURES AND OVER ROUGH TERRAIN

by

C. W. Hirt and J. L. Cook

PREPRINT FROM

los alamos
scientific laboratory
of the University of California
LOS ALAMOS, NEW MEXICO 87544

UNITED STATES
ATOMIC ENERGY COMMISSION
CONTRACT W-7405-ENG. 36

A-1-a

CALCULATING THREE-DIMENSIONAL FLOWS AROUND STRUCTURES AND OVER ROUGH TERRAIN*

C. W. Hirt and J. L. Cook
University of California
Los Alamos Scientific Laboratory
Los Alamos, New Mexico 87544

November 12, 1971

Copies Submitted: 3
Manuscript Pages: 28
Figures: 11
Tables: 0

---

*This work was performed under the auspices of the United States Atomic Energy Commission.

Running Head: Three Dimensional Flows

C. W. Hirt
University of California
Los Alamos Scientific Laboratory
Los Alamos, New Mexico 87544

ABSTRACT

A computing technique for low speed fluid dynamics has been developed for the calculation of three dimensional flows in the vicinity of one or more block type structures. The full time-dependent Navier-Stokes equations are solved with a finite difference scheme based on the Marker-and-Cell method. Effects of thermal buoyancy are included in a Boussinesq approximation. Marker particles that convect with the flow can be used to generate streaklines for flow visualization, or they can diffuse while convecting to represent the dispersion by turbulence of particulate matter. The vast amount of data resulting from these calculations has been rendered more intelligible by perspective view and stero view plots of selected velocity and marker particle distributions.

I. INTRODUCTION

Finite difference solutions have been obtained for many complicated fluid flow problems,[1] but until recently, there have been relatively few of these involved with three-dimensional transient flows. The three dimensional calculations that have been reported have been restricted in scope, having been developed for the solution of specific problems, for example, the structure of the planetary boundary layer,[2] for Bénard convection,[3] and for flow between two concentric cylinders.[4] In this paper a method is described for calculating transient three-dimensional flows about large obstacles and over irregular boundaries. The technique is based on a simple variant of the Marker-and-Cell method[5] for the solution of the incompressible Navier-Stokes equations. Thermal buoyancy effects are included in a Boussinesq approximation, and a technique developed by Sklarew[6] is used to represent the convection and diffusion of particulate matter. Only confined flow calculations are reported here. Extensions to three-dimensional, free surface, flows over and around obstacles will be reported elsewhere.[7]

A major problem with three-dimensional calculations is the limited numerical resolution that may be obtained with the fast access memories of even the largest computers. Of course, additional external storage devices may be employed but these usually require much larger amounts of computer time. The program used for the examples in this paper is limited to a maximum of 3375 computational cells when run on a CDC 7600 computer with a 64,000 word fast core memory. This is not large, since 3375 cells is equivalent to a cubical

mesh with only 15 cells on an edge. Nevertheless, sample calculations show that meaningful and interesting calculations can be performed even with this limited resolution.

Another problem associated with three-dimensional calculations is how to reduce the vast amounts of computed data into easily assimilated forms. Displays of velocities, contours, and other kinds of data taken from two-dimensional slices through a three-dimensional mesh are not always sufficient to form a clear picture of the complete flow pattern. To reconstruct a composite three-dimensional mental picture from a collection of two dimensional slices is not an easy task. An alternative and more efficient means of displaying data is described in this paper. The technique is based on a hidden-line perspective view plot routine designed especially for finite difference calculations.[8] A perspective picture of, for example, velocity vectors associated with a given two dimensional plane of calculational cells shows not only the three-dimensional variations of the vectors, but also their orientation with respect to all nearby obstacles. An even better display method consists of making two perspective views from slightly different observation points. When correctly done the result can be combined into a stereoscopic view, which is the ideal way to see the structure of three-dimensional flows.

Examples of these various display methods are described in more detail in the text. In Section II a description of the basic fluid dynamic computing technique is presented together with some of its properties. Section III contains descriptions of the buoyancy and particulate transport models.

II. THE BASIC TECHNIQUE

A. Finite Difference Approximations

The Marker-and-Cell technique for the calculation of incompressible fluid flow[5] is an Eulerian finite difference approximation to the Navier-Stokes equations,

$$\frac{\partial u}{\partial t} + \frac{\partial u^2}{\partial x} + \frac{\partial uv}{\partial y} + \frac{\partial uw}{\partial z} = - \frac{\partial p}{\partial x} + g_x + \nu \left(\frac{\partial^2 u}{\partial x^2} + \frac{\partial^2 u}{\partial y^2} + \frac{\partial^2 u}{\partial z^2}\right)$$

$$\frac{\partial v}{\partial t} + \frac{\partial vu}{\partial x} + \frac{\partial v^2}{\partial y} + \frac{\partial vw}{\partial z} = - \frac{\partial p}{\partial y} + g_y + \nu \left(\frac{\partial^2 v}{\partial x^2} + \frac{\partial^2 v}{\partial y^2} + \frac{\partial^2 v}{\partial z^2}\right) \qquad (1)$$

$$\frac{\partial w}{\partial t} + \frac{\partial wu}{\partial x} + \frac{\partial wv}{\partial y} + \frac{\partial w^2}{\partial z} = - \frac{\partial p}{\partial z} + g_z + \nu \left(\frac{\partial^2 w}{\partial x^2} + \frac{\partial^2 w}{\partial y^2} + \frac{\partial^2 w}{\partial z^2}\right)$$

and the mass equation

$$\frac{\partial u}{\partial x} + \frac{\partial v}{\partial y} + \frac{\partial w}{\partial z} = 0 \quad , \qquad (2)$$

where p is the ratio of pressure to constant density, g_x, g_y, g_z are prescribed body accelerations and ν is the coefficient of kinematic viscosity. In addition to solving directly for the velocity components and pressures, the Marker-and-Cell method also uses marker particles that are convected

about by the fluid to record the locations of free surfaces. In this paper only confined flows are considered so that marker particles are not required for this purpose, but they are used to represent distributions of particulate matter as described in Section III-B.

The region in which computations are to be performed is divided into a set of small rectangular cells having edge lengths δx, δy, and δz. With respect to this set of computational cells, velocity components are located at cell faces and pressure values are at cell centers, see Fig. 1. Cells are labeled with an index (i,j,k), which denotes the cell number as counted from the origin in the x, y, and z directions respectively. Also $p_{i,j,k}$ is the pressure at the center of cell (i,j,k), while $u_{i+\frac{1}{2},j,k}$ is the x-direction velocity at the center of the face between cells (i,j,k) and (i+1,j,k), and so on.

A time dependent solution is obtained by advancing the flow field variables through a sequence of short time steps of duration δt. The advancement for one time step is calculated in two stages. First the velocity components are all advanced using the previous state of the flow to calculate the accelerations caused by convection, viscous stresses, body forces, pressure gradients, etc. In other words, stage one consists of a simple explicit calculation. However, this explicit time advancement does not necessarily lead to a velocity field with zero divergence, that is, to one that conserves mass. Thus, in stage two, adjustments must be made to insure mass conservation. This is done by adjusting the pressure in each cell in such a way that there is no net mass flow in or out of the cell. A change in one cell will affect neighboring cells so that this pressure adjustment

must be performed iteratively until all cells have simultaneously achieved a zero mass change.

In the original Marker-and-Cell method the pressures in stage two were obtained from the solution of a Poisson equation. A related technique developed by Chorin[3] involved a simultaneous iteration on pressures and velocity components. Viecelli[9] has shown that the two methods as applied to the Marker-and-Cell method are equivalent. In this paper we have chosen the second procedure and simultaneously iterate both pressures and velocities. This choice simplifies the applications of boundary conditions as discussed in Section II-C.

The specific finite difference expressions used for the steps described above may assume many forms. Those that follow are essentially direct extensions of the original Marker-and-Cell method. The stage one, explicit, advancement of velocities, resulting in quantities labeled by superscript tildes, is

$$\tilde{u}_{i+\frac{1}{2},j,k} = u_{i+\frac{1}{2},j,k} + \delta t \left\{ \frac{1}{\delta x} \left[(u_{i,j,k})^2 - (u_{i+1,j,k})^2 \right] \right.$$

$$+ \frac{1}{\delta y} \left[(uv)_{i+\frac{1}{2},j-\frac{1}{2},k} - (uv)_{i+\frac{1}{2},j+\frac{1}{2},k} \right] + \frac{1}{\delta z} \left[(uw)_{i+\frac{1}{2},j,k-\frac{1}{2}} \right.$$

$$\left. - (uw)_{i+\frac{1}{2},j,k+\frac{1}{2}} \right] + g_x + \frac{1}{\delta x} \left(p_{i,j,k} - p_{i+1,j,k} \right)$$

$$+ \frac{\nu}{\delta x^2} \left(u_{i+3/2,j,k} - 2u_{i+\frac{1}{2},j,k} + u_{i-\frac{1}{2},j,k} \right)$$

$$+ \frac{\nu}{\delta y^2} \left(u_{i+\frac{1}{2},j+1,k} - 2u_{i+\frac{1}{2},j,k} + u_{i+\frac{1}{2},j-1,k} \right)$$

$$\left. + \frac{\nu}{\delta z^2} \left(u_{i+\frac{1}{2},j,k+1} - 2u_{i+\frac{1}{2},j,k} + u_{i+\frac{1}{2},j,k-1} \right) \right\}$$

$$\tilde{v}_{i,j+\frac{1}{2},k} = v_{i,j+\frac{1}{2},k} + \delta t \{\frac{1}{\delta x}[(vu)_{i-\frac{1}{2},j+\frac{1}{2},k} - (vu)_{i+\frac{1}{2},j+\frac{1}{2},k}]$$

$$+ \frac{1}{\delta y}[(v_{i,j,k})^2 - (v_{i,j+1,k})^2] + \frac{1}{\delta z}[(vw)_{i,j+\frac{1}{2},k-\frac{1}{2}} - (vw)_{i,j+\frac{1}{2},k+\frac{1}{2}}]$$

$$+ g_y + \frac{1}{\delta y}(p_{i,j,k} - p_{i,j+1,k}) + \frac{\nu}{\delta x^2}(v_{i+1,j+\frac{1}{2},k} - 2v_{i,j+\frac{1}{2},k} + v_{i-1,j+\frac{1}{2},k})$$

$$+ \frac{\nu}{\delta y^2}(v_{i,j+3/2,k} - 2v_{i,j+\frac{1}{2},k} + v_{2,j-\frac{1}{2},k})$$

$$+ \frac{\nu}{\delta z^2}(v_{i,j+\frac{1}{2},k+1} - 2v_{i,j+\frac{1}{2},k} + v_{i,j+\frac{1}{2},k-1})\}$$

$$\tilde{w}_{i,j,k+\frac{1}{2}} = w_{i,j,k+\frac{1}{2}} + \delta t \{\frac{1}{\delta x}[(wu)_{i-\frac{1}{2},j,k+\frac{1}{2}} - (wu)_{i+\frac{1}{2},j,k+\frac{1}{2}}]$$

$$+ \frac{1}{\delta y}[(wv)_{i,j-\frac{1}{2},k+\frac{1}{2}} - (wv)_{i,j+\frac{1}{2},k+\frac{1}{2}}] + \frac{1}{\delta z}[(w_{i,j,k})^2 - (w_{i,j,k+1})^2]$$

$$+ g_z + \frac{1}{\delta z}(p_{i,j,k} - p_{i,j,k+1}) + \frac{\nu}{\delta x^2}(w_{i+1,j,k+\frac{1}{2}} - 2w_{i,j,k+\frac{1}{2}} + w_{i-1,j,k+\frac{1}{2}})$$

$$+ \frac{\nu}{\delta y^2}(w_{i,j+1,k+\frac{1}{2}} - 2w_{i,j,k+\frac{1}{2}} + w_{i,j-1,k+\frac{1}{2}})$$

$$+ \frac{\nu}{\delta z^2}(w_{i,j,k+3/2} - 2w_{i,j,k+\frac{1}{2}} + w_{i,j,k-\frac{1}{2}})\} \quad . \qquad (3)$$

Quantities needed at positions other than where they are defined are calculated as simple averages, e.g., $u_{i,j,k} = \frac{1}{2}(u_{i+\frac{1}{2},j,k} + u_{i-\frac{1}{2},j,k})$, and the square of a quantity, e.g., u^2 at (i,j,k) is the square of the average, $(u_{i,j,k})^2$, rather than the average of the squares, $u^2_{i+\frac{1}{2},j,k}$ and $u^2_{i-\frac{1}{2},j,k}$.

The computations indicated in (3) are made for all (i,j,k), and represent a straightforward explicit finite difference approximation to (1). Although centered differences have been used in approximating the convection terms, the resulting equations will be stable provided sufficient viscosity is applied. This is similar to the MAC method,[10] and is more fully described in Section II-E.

B. Pressure Iteration

Equations (3) do not necessarily result in a velocity field that satisfies (2), so that some adjustment of the tilde velocities must be made to insure mass conservation. An iterative process is used for this purpose, in which the cell pressures are modified to make the velocity divergence vanish. In each cell (i,j,k) the value of the velocity divergence, D, is calculated as

$$D_{i,j,k} = \frac{1}{\delta x}(u_{i+\frac{1}{2},j,k} - u_{i-\frac{1}{2},j,k}) + \frac{1}{\delta y}(v_{i,j+\frac{1}{2},k} - v_{i,j-\frac{1}{2},k})$$

$$+ \frac{1}{\delta z}(w_{i,j,k+\frac{1}{2}} - w_{i,j,k-\frac{1}{2}}) \quad . \qquad (4)$$

If the magnitude of D is less than some prescribed small value, ε, the flow is locally incompressible and no change in the cell velocity is necessary. However, if the magnitude of D is larger than ε then the pressure is changed by

$$\delta p = - \beta D \quad , \tag{5}$$

where β is given by

$$\beta = \frac{\beta_o}{2\delta t \left(\frac{1}{\delta x^2} + \frac{1}{\delta y^2} + \frac{1}{\delta z^2}\right)} \quad . \tag{6}$$

The constant β_o is a relaxation factor, where over-relaxation and under-relaxation correspond to β_o greater than or less than unity respectively. For iteration stability it is necessary to keep $\beta_o < 2$. A value of $\beta_o \approx 1.7$ is commonly used, but this is occasionally too large when there are strong flow distortions. The value of β_o giving the most rapid convergence can, in general, only be determined by experimentation.

Once δp has been calculated for a cell (i,j,k) it is necessary to add it to the pressure $p_{i,j,k}$, and to adjust the velocity components on the sides of cell (i,j,k) according to:

$$u_{i+\frac{1}{2},j,k} \rightarrow u_{i+\frac{1}{2},j,k} + \frac{\delta t}{\delta x}\,\delta p$$

$$u_{i-\frac{1}{2},j,k} \rightarrow u_{i-\frac{1}{2},j,k} - \frac{\delta t}{\delta x}\,\delta p$$

$$v_{i,j+\frac{1}{2},k} \rightarrow v_{i,j+\frac{1}{2},k} + \frac{\delta t}{\delta y}\,\delta p$$

$$v_{i,j-\frac{1}{2},k} \rightarrow v_{i,j-\frac{1}{2},k} - \frac{\delta t}{\delta y}\,\delta p$$

$$w_{i,j,k+\frac{1}{2}} \rightarrow w_{i,j,k+\frac{1}{2}} + \frac{\delta t}{\delta z}\,\delta p$$

$$w_{i,j,k-\frac{1}{2}} \rightarrow w_{i,j,k-\frac{1}{2}} - \frac{\delta t}{\delta z}\,\delta p \quad . \qquad (7)$$

This process is repeated successively in all cells until no cell has a magnitude of D greater than ε.

With the proper application of boundary conditions the pressure iteration will converge, and it will do so in relatively few sweeps of the mesh, provided the flow is not changing too rapidly from one cycle to the next, and provided ε is not chosen excessively small. For the problems illustrating this paper approximately 5 to 10 sweeps are necessary with an ε typically of magnitude 10^{-2} U/L, where U/L is a representative velocity to length ratio.

When the iteration has converged, the adjusted velocities satisfy the mass conservation condition (2), and this completes the necessary

calculations for advancing the flow field through one cycle in time.

If, in addition, it is desired to permit the transport of heat or pollution concentrations these field quantities must also be advanced one time step before beginning the next fluid dynamic cycle. Likewise, discrete marker particles used to define particulate distributions, or for flow visualization purposes, must be moved before starting the next cycle.

C. Boundary Conditions

The five principle kinds of boundary conditions to be considered are: rigid free-slip walls, rigid no-slip walls, inflow and outflow boundaries, and periodic boundaries. For simplicity it will be assumed that all physical boundaries coincide with cell boundaries. The inclusion of more general boundary configurations is a difficult problem, but a good start in this direction for two-dimensional flows has been made by Viecelli.[9]

The prescription of boundary conditions consists of a choice for both the normal and tangential velocities at the boundary. The normal velocity is easy to prescribe when the boundary coincides with a cell edge, since it is the normal velocity that is stored for each cell face. For a rigid boundary this velocity is set to zero, while for an input boundary it is assigned the desired input value. If the boundary is periodic the value must be chosen equal to the corresponding velocity one wavelength away.

For outflow boundaries, however, there is no unique prescription, but the general idea is to chose boundary conditions that have the least upstream influence. It has been found that for this purpose a useful prescription consists of setting the normal tilde velocity on the outflow boundary equal to the corresponding tilde velocity immediately upstream, and then letting the velocity on the boundary relax as it wishes during the pressure iteration. This appears to keep the flow going smoothly out of the boundary in the examples tested.

Tangential velocities are needed in cells immediately outside the fluid region in order to specify the appropriate viscous stress at the boundary. These velocities are set equal to the adjacent velocities inside the fluid when it is desired that the boundary represent a free-slip wall (plane of symmetry), and they are set equal to the negative of the adjacent fluid velocities when the boundary is to be no-slip. In other words, the external velocities tangent to a boundary are chosen to give either vanishing shear or vanishing velocity at a rigid wall. A more complete discussion of these alternatives and the conditions under which each should be used is contained in reference (11). If the boundary is periodic then these external velocities are set equal to their counterparts one wavelength away, and at an inflow boundary they are prescribed to give the desired input flow. At an outflow boundary they are set equal to the adjacent velocities inside the fluid, which encourages a smooth transition through the outflow boundary.

To aid in the identification of various kinds of boundaries a flagging scheme is employed in the computer program, which assigns to each cell a number that identifies it as an obstacle cell, inflow cell, outflow cell, etc. In this way it is easy to arrange a distribution of obstacles in a mesh, and to have various combinations of inflow and outflow boundaries.

Several examples illustrating different combinations of boundary conditions are shown in Figs. 2-6. In Fig. 2 a horizontal layer of velocity vectors is shown in perspective for steady flow around a simple rectangular structure. A uniform flow is entering the computing region (large rectangular box) through the left face and is leaving through the right face. Each vector (short line segment) is drawn from the corner of a computing cell with a direction and magnitude representing the average velocity about that corner.

A recirculation in the wake region is clearly evident in the figures. It consists of a pair of counter rotating eddies that are small near the top of the structure, but large near its base. The x-y components of the same set of velocity vectors have been plotted in Fig. 3. Here the double eddy structure is more clearly seen, but no indication of the distribution of z-component velocity is available in this kind of plot. Velocity vectors for a similar calculation, but involving a more complicated obstacle, are shown in Figs. 4-5. The three-dimensionality of the velocities is most clearly seen in Fig. 5.

In the previous examples the inflow is normal to the front face of the obstacle, but by making two adjacent sides of the mesh inflow boundaries and the opposite two sides outflow boundaries, the incident flow can be adjusted to any angle. Fig. 6, for example, shows the results of a calculation with the flow passing through the mesh from left to right, and oriented 45° to the large faces of the two obstacles.

D. Computer Requirements

In the previously described calculations the total number of computational cells used was 3344, requiring an average calculation time of 1-2 seconds per time cycle on a CDC 7600 computer. With this number of cells the computer program absorbed nearly all the storage available in a 64,000 word fast core memory. Fortunately, even with this limited resolution there are many interesting calculations that can be performed.

The problem of what to do when more resolution is needed, however, is an interesting one that deserves further comment. Clearly, the simplest approach is to use auxiliary memory units. Although more computer time is needed when operating with this kind of storage, because of the longer time needed to retrieve data, the calculation time for the examples illustrating this paper could easily be increased by an order of magnitude without becoming too unreasonable. An order of magnitude increase is roughly equivalent to doubling the finite difference resolution, since that requires a factor of eight increase in the number of cells and a somewhat larger increase in calculation time.

Nevertheless, it is easy to think of three-dimensional problems in which still larger increases in resolution are required, and aside from relying on the development of larger and faster computers, it is clear that more effort must be devoted to improving both computer programming and numerical approximation methods.

E. Numerical Stability

No additional stability conditions are introduced in the Marker-and-Cell method when it is used for three-dimensional computations, but the stability conditions previously reported[5,10,12] must be appropriately modified.

The basic restriction on the size of the time step, δt, is that fluid must not be permitted to flow across more than one computational cell in one time step, that is

$$\delta t < \min \left[\frac{\delta x}{|u|}, \frac{\delta y}{|v|}, \frac{\delta z}{|w|} \right] , \tag{8}$$

This is clearly a numerical accuracy condition, because the convective flux approximations used in the tilde calculations (3) assume exchanges between adjacent cells only. This condition must also be satisfied for numerical stability, as can be verified by linearizing the difference equations and performing a Fourier analysis on them.[12]

The linear analysis also reveals that the equations will always be unstable unless the kinematic viscosity, ν, is large enough; a good approximation is

$$\nu > \frac{\delta t}{2} \max [u^2, v^2, w^2] \quad . \tag{9}$$

This condition follows easily from a heuristic stability analysis,[10] which shows that ν should also satisfy the following approximate inequality,

$$\nu > \max [\frac{1}{2} \delta x^2 |\frac{\partial u}{\partial x}|, \frac{1}{2} \delta y^2 |\frac{\partial v}{\partial y}|, \frac{1}{2} \delta z^2 |\frac{\partial w}{\partial z}|] \quad . \tag{10}$$

The last two conditions imply a lower bound on the kinematic viscosity, which imposes an upper limit on the flow Reynolds number. This Reynolds number restriction is not unique to the Marker-and-Cell method, but is a necessary feature of all finite difference methods. The reasons for this can be shown in many ways. One way is to argue as follows: Truncation errors are unavoidable in finite difference approximations, and even though they do not always lead to instabilities that require restrictions like (9) or (10), they do influence the accuracy of a calculation. For purposes of accuracy, if the effects of ν are not to be obscured by truncation errors it is necessary that

$$\nu > \alpha \, \Delta x \, \Delta u \quad , \tag{11}$$

where α is some numerical factor of order unity, Δx is a typical cell

dimension, and Δu is a typical velocity change across a cell. This relation is based on the observation that a difference approximation of order $(p + 1)$ will have truncation error terms that modify ν by a contribution like,

$$\delta x^{p+1} \frac{\partial^p u}{\partial x^p} \quad .$$

In a finite difference approximation this quantity will be approximated by $\alpha \Delta x \Delta u$, which defines the value of α. For the order of magnitude estimate wanted here, α can be replaced by unity. Thus, (11) is simply the statement that ν must be larger than these errors for an accurate calculation. Now if a typical dimension in a flow, L, is resolved by N finite difference cells, $L = N\Delta x$, and if a typical velocity U is $N\Delta u$, then (11) also states that the flow Reynolds number, $R \equiv \frac{UL}{\nu}$, must be less than N^2. In other words, the condition

$$R < N^2 \tag{12}$$

is a necessary restriction for accurate finite difference calculations.

It may be noted that a few finite difference approximations, for example, those using the so called donor cell approximation,[13] have even larger truncation errors that lead to the more restrictive condition,

$$R < N \quad . \tag{12a}$$

Condition (12) is a rough estimate for the maximum allowable Reynolds number obtainable with any finite difference approximation. It is primarily an accuracy condition, but it often happens, as in the present case, that it is a condition for stability as well.

Finally, when very low Reynolds number flows are to be simulated the time step is additionally restricted by the condition

$$\nu\delta t < \frac{1}{2\left(\frac{1}{\delta x^2} + \frac{1}{\delta y^2} + \frac{1}{\delta z^2}\right)} \quad . \tag{13}$$

In analogy with the interpretation of (8) this restriction may be roughly described as limiting the distance over which momentum diffuses during one time step to be less than one cell width.

III. AUXILIARY FEATURES

A. Thermal Buoyancy

A heat equation may be simultaneously solved with the fluid equations in order to simulate the effects of thermal buoyancy that are important for many meteorological applications. The differential equation governing convection and diffusion of temperature, T, is

$$\frac{\partial T}{\partial t} + \nabla \cdot T\vec{u} = \nabla \cdot (\lambda \nabla T) \quad , \tag{14}$$

where λ may be chosen to represent both turbulent and molecular diffusion processes. The finite difference expression used to approximate (14) assumes that $T_{i,j,k}$ is located at the center of cell (i,j,k),

$$\begin{aligned} T^{n+1}_{i,j,k} = T_{i,j,k} + \delta t \{ & \frac{1}{\delta x} [\langle Tu \rangle_{i-\frac{1}{2},j,k} - \langle Tu \rangle_{i+\frac{1}{2},j,k}] \\ & + \frac{1}{\delta y} [\langle Tv \rangle_{i,j-\frac{1}{2},k} - \langle Tv \rangle_{i,j+\frac{1}{2},j}] + \frac{1}{\delta z} [\langle Tw \rangle_{i,j,k-\frac{1}{2}} - \langle Tw \rangle_{i,j,k+\frac{1}{2}}] \\ & + \lambda [\frac{1}{\delta x^2} (T_{i+1,j,k} - 2T_{i,j,k} + T_{i-1,j,k}) \\ & + \frac{1}{\delta y^2} (T_{i,j+1,k} - 2T_{i,j,k} + T_{i,j-1,k}) \\ & + \frac{1}{\delta z^2} (T_{i,j,k+1} - 2T_{i,j,k} + T_{i,j,k-1})]\} \end{aligned} \tag{15}$$

A constant diffusion coefficient has been assumed for simplicity, but this can be easily changed. The notation $\langle Tu \rangle_{i+\frac{1}{2},j,k}$ means that the flux between cell (i,j,k) and (i+1,j,k) is to be evaluated by the donor cell rule,[13] that is,

$$\langle Tu \rangle_{i+\frac{1}{2},j,k} = \begin{cases} T_{i,j,k}\, u_{i+\frac{1}{2},j,k}, & \text{if } u_{i+\frac{1}{2},j,k} \geq 0 \\ T_{i+1,j,k}\, u_{i+\frac{1}{2},j,k} & \text{if } u_{i+\frac{1}{2},j,k} < 0 \end{cases} .$$

Donor cell fluxes are used here to insure numerical stability and to avoid negative temperatures upstream from a local hot spot.

The most common boundary condition on the temperature is that of zero flux, which corresponds to a nonconducting wall or a plane of symmetry. Heat sources can be added in a variety of ways. Either selected portions of the boundaries can be given prescribed temperatures, or prescribed energy fluxes, or energy can be deposited directly into selected regions of the fluid.

The effects of temperature variation are assumed to influence the fluid motions through a Boussinesq approximation, which consists of the addition of buoyancy terms to the right sides of the tilde equations (3). For example, the following term is added to the w-tilde equation,

$$\beta g_z \, (T_o - T_{i,j,k+\frac{1}{2}}) \quad .$$

The constant T_o is an initial reference temperature and β is the coefficient of thermal expansion. This term requires a temperature at the boundary between two cells, which is equal to the average of the two cell temperatures.

An additional numerical stability condition is needed when equation (15) is used. This condition, which is analagous to (13), is

$$\lambda\delta t < \frac{1}{2\left(\frac{1}{\delta x^2} + \frac{1}{\delta y^2} + \frac{1}{\delta z^2}\right)} \quad . \tag{16}$$

The temperature equation can also be used to represent the transport of particulate matter when temperature effects are not of interest, in which case T is interpreted as the particulate concentration. For example, Fig. (7) shows a particulate distribution calculated in this way (with β equal to zero). The air flow is incident at 45^o to the buildings, as shown in Fig. (6). There is a constant source of particulate matter being inserted at the center of the base of the large obstacle on the side furthest from view. The particulate concentration is shown in Fig. 7 as a distribution of particles. This was made by plotting in each cell a number of particles proportional to the cell concentration, T, and with positions distributed randomly within the cell.

B. Marker Particles

The above technique for particulate transport is not very refined and does not work well for problems having sharply defined regions of particulate

matter. A better technique has been devised by R. C. Sklarew.[6] He keeps track of individual particles and uses a clever trick to move them so that their distribution represents a solution of (14). The trick is to rewrite this equation as

$$\frac{\partial T}{\partial t} + \nabla\cdot(\vec{u} - \frac{\lambda}{T}\nabla T)T = 0 \qquad (17)$$

Now it is evident that if particles are moved (convected) with the effective velocity

$$\vec{u} - \frac{\lambda}{T}\nabla T \qquad (18)$$

they will approximate a solution of (17). Another way to say this is that the total flux of T resulting from convection and diffusion is equivalent to a pure convection with the velocity (18). The concentration, T, in a cell is then proportional to the number of marker particles in the cell. The diffusion coefficient can vary arbitrarily in space and time, and the method is stable provided no particle moves more than one cell width in one time step.

Figure 8 shows an application of the Sklarew method to the flow of a slowly dispersing plume passing over the top of a rectangular structure. The flow is the same as that shown in Figs. (2-3). Particles are seen trapped and recirculated in the wake region.

A similar calculation is shown in Fig. 9 for a more complex building and with particulates emitted from a vent centrally located on top of the principle structure. The flow field for this problem is identical to that of Figs (4-5).

The numerical prescription used for moving particles is based on a straightforward extension of the technique used in the original Marker-and-Cell method.[5] Each particle is moved with a velocity obtained from a linear interpolation among the eight nearest cell velocities. The same interpolation is used whether the particles are to move with the fluid or with the effective velocity (18).

The only difficult problem in moving particles is to account for the presence of various boundary conditions. In the examples shown here, this has been accomplished by suitably adjusting the velocity interpolation factors when particles are near a boundary.

C. Data Display Techniques

Most of the figures have displayed data in the form of perspective views. These views give a much better picture of the three-dimensional flow fields than could be obtained from sets of purely two-dimensional plots. In addition to the velocity vectors and particle distributions shown, it can be useful to plot perspective views of contour lines, streak lines, and, in general, anything having a three-dimensional distribution.

The perspective plots used here[8] have been designed especially for three dimensional finite difference calculations. They are so efficient

that movies of transient flow phenomena can be made at little additional expense to a calculation. Movies can also be made with the observation point continually changing position, to give an even better feel for the three-dimensionality of a problem.

Stereo pictures of velocity vectors and particle distributions have proven themselves to be extremely useful, but unfortunately they are not easily presented in journal articles. The usual procedure is to print, side by side, two perspective views made from slightly shifted observation points, as in Fig. 10a. The left view is the correct perspective for the left eye and the right view is correct for the right eye. To see in stereo it is necessary to hold the figure approximately 18 inches in front of the eyes and to let the eyes move apart so that the combined eye images merge together at some distance beyond the page. Unfortunately, many persons cannot keep their eyes in focus while forcing them to move apart (walleyed). On the other hand, a large fraction of these people can keep them focused when they are moved together (crossed). Thus, in Fig. 10b the left and right images shown in Fig. 10a have been reversed. This figure will appear in stereo when the eyes are crossed to bring the images together at a point in front of the page. Admittedly it takes some practice to get a stereo view in either case, but the results are generally worth the effort.

IV. ACKNOWLEDGMENT

The authors would like to express their appreciation to Robert Hotchkiss who has supplied many valuable additions to the program, and who performed the calculations illustrated in Figs. (8-10).

REFERENCES

1. F. H. Harlow, "Numerical Methods for Fluid Dynamics -- An Annotated Bibliography," Los Alamos Scientific Laboratory Report LA-4281 (1969).
2. J. W. Deardorff, Geophys. Fluid Dynamics 1, 377 (1970); J. Fluid Mech. 41, 453 (1970).
3. A. J. Chorin, AEC Research and Development Report, NYO-1480-61 (1966).
4. G. P. Williams, Jour. Fluid Mech. 37, 727 (1969).
5. F. H. Harlow and J. E. Welch, Phys. Fluids 8, 2182 (1965); J. E. Welch, F. H. Harlow, J. P. Shannon, and B. J. Daly, Los Alamos Scientific Laboratory Report, LA-3425 (1966).
6. R. C. Sklarew, Paper presented at 63rd Annual Meeting Air Pollution Control Assoc., St. Louis, Missouri, June (1970).
7. B. D. Nichols and C. W. Hirt, Manuscript in preparation.
8. C. W. Hirt and J. L. Cook, Manuscript in preparation.
9. J. A. Viecelli, Jour. Comp. Phys. 8, 119 (1971).
10. C. W. Hirt, Jour. Comp. Phys. 2, 339 (1968).
11. B. D. Nichols and C. W. Hirt, To be published in Jour. Comp. Phys.
12. B. J. Daly and W. E. Pracht, Phys. of Fluids 11, 15 (1968).
13. R. A. Gentry, R. E. Martin, and B. J. Daly, Jour. Comp. Phys. 1, 87 (1966).

LIST OF SYMBOLS

ν	Nu
δ	Delta
β	Beta
$\rightarrow$	Arrow
$>$	Greater than
$<$	Less than
$\lvert \ldots \rvert$	Absolute value
α	Alpha
Δ	Cap. delta
λ	Lambda

FIGURE CAPTIONS

1. Location of velocity components on a typical Eulerian cell (i,j,k).
2. Perspective view of velocity field about a single building.
3. Projection of velocity vectors seen in Fig. 2 on a z = constant plane.
4. Perspective view of velocity field near the bottom of a complicated structure.
5. Perspective view of velocity field near the top of a complicated structure.
6. Perspective view of velocity field in vicinity of two buildings. Incident flow is oriented 45° with respect to large faces of the buildings.
7. Perspective view of particulate distribution in flow field shown in Fig. 6.
8. The dispersal of a narrow plume passing over a single building. Recirculation in wake region is clearly evident.
9. The dispersal of pollutant from a flush vent on the top of a complex building structure.
10. The two perspective views in (A) appear in stero when viewed "walleyed", while those in (B) appear in stero when viewed "crosseyed".

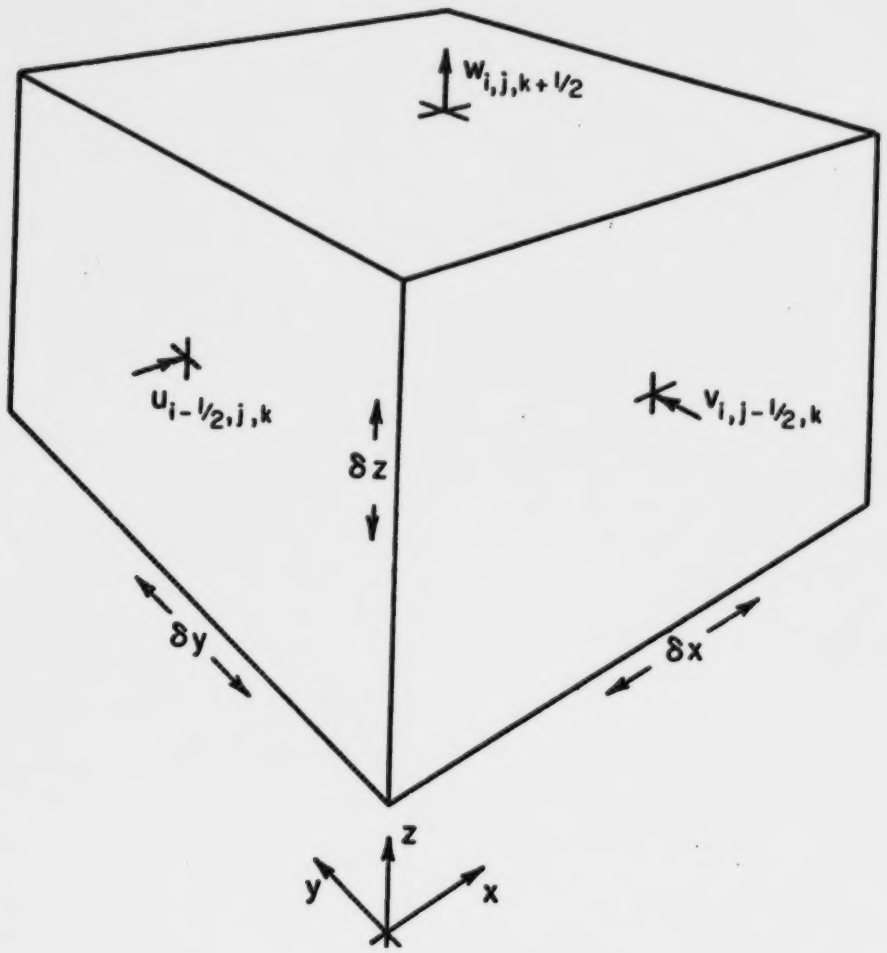

Fig 1

Hint -

TOP

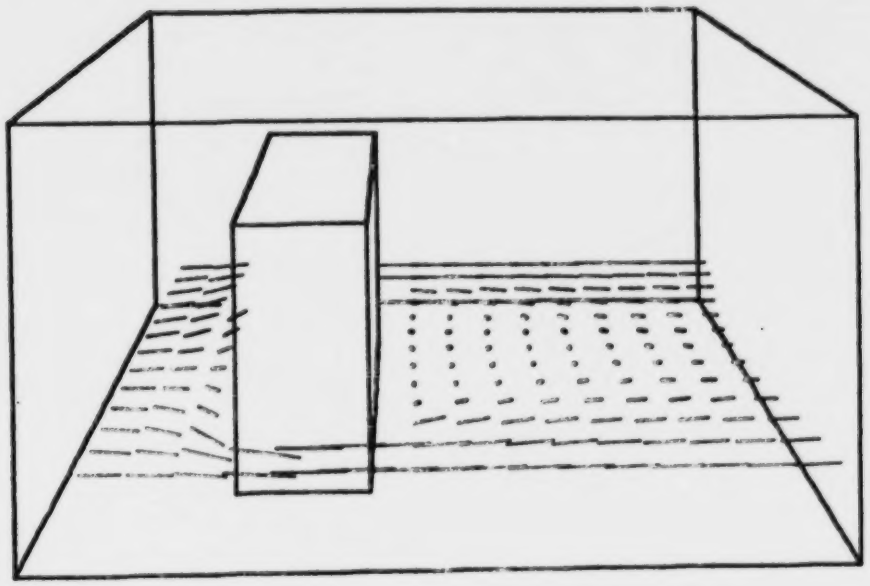

Fig 2
Hint

Top ↑
Hint

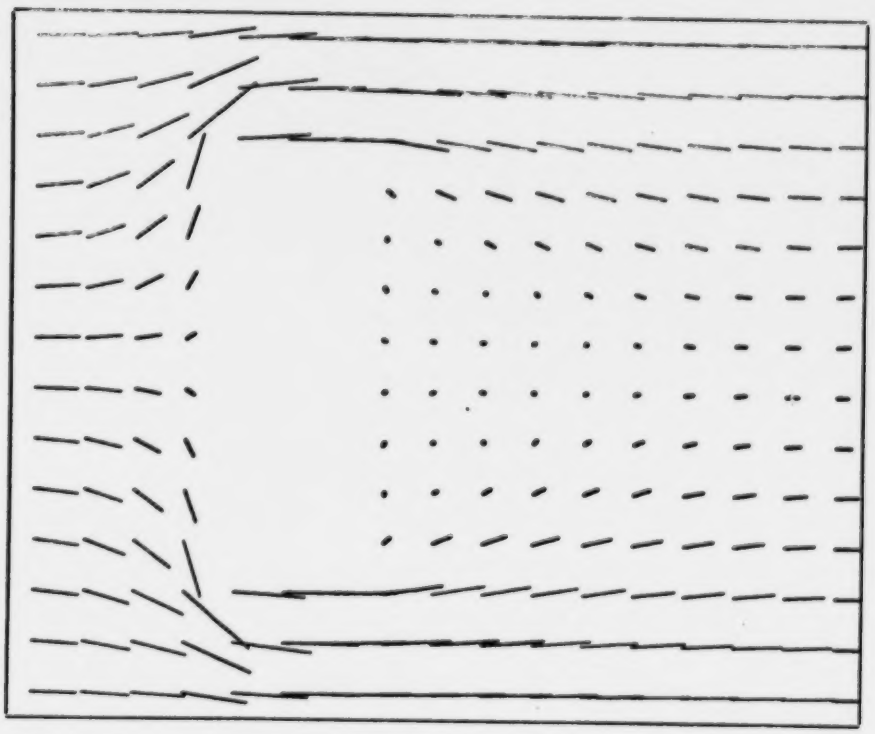

Fig 3

Hint

Top ↑

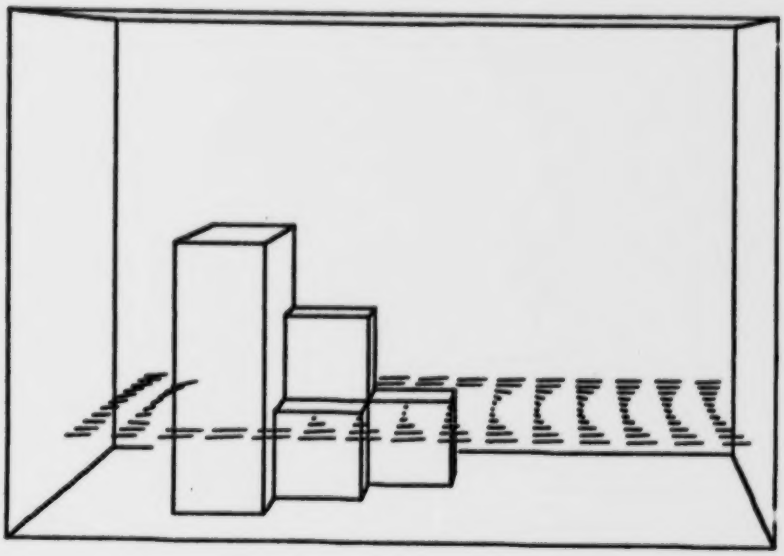

Fig 4

Hint

Top ↑

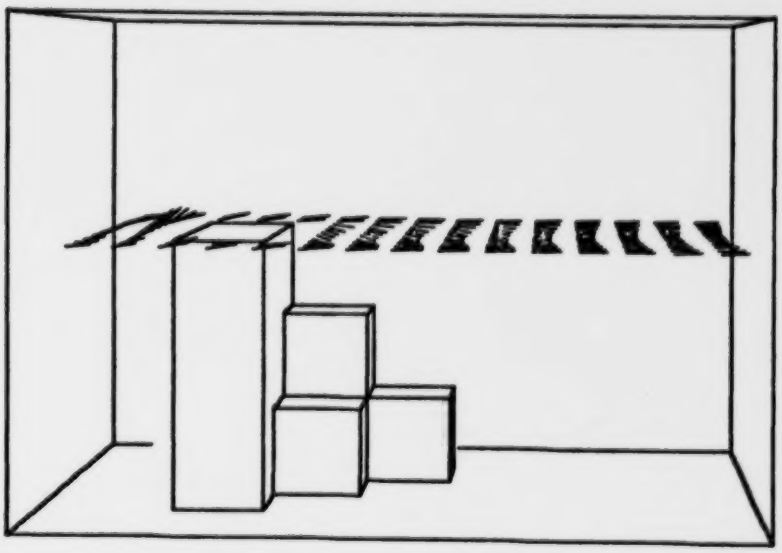

Fig 5

Hint

Top ↑

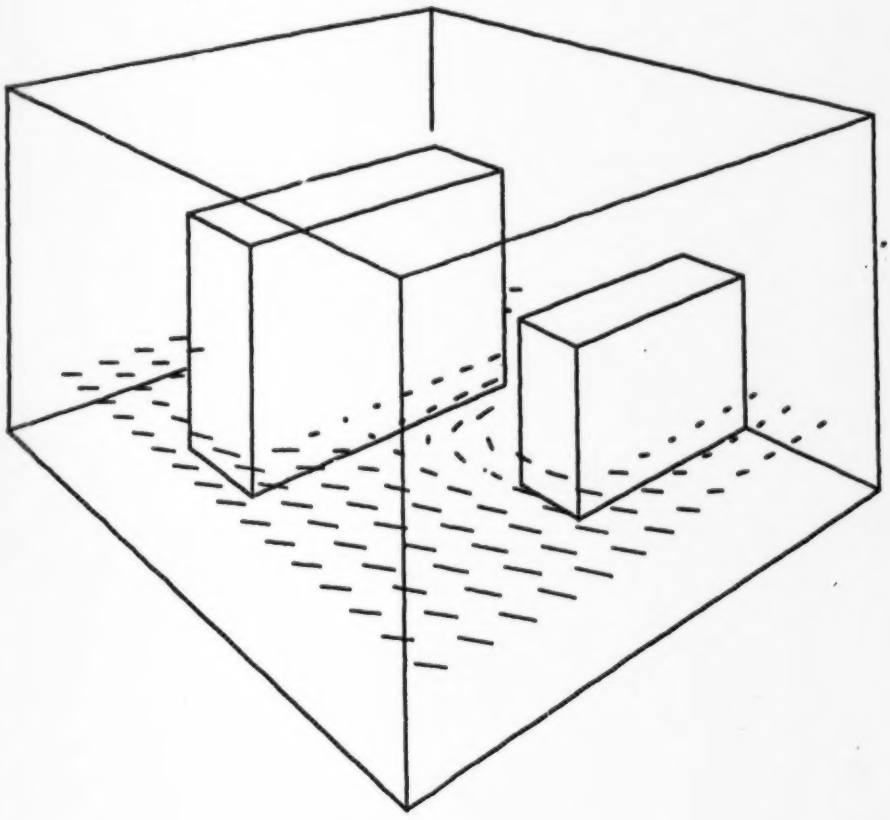

Fig 6

Hint

Top ↑

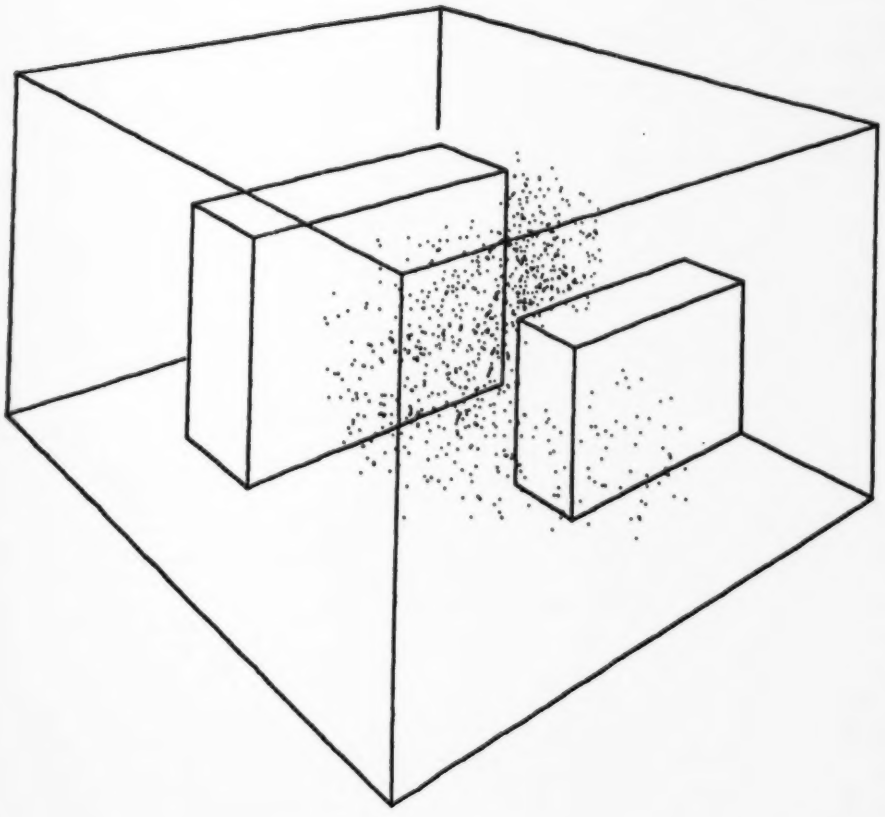

Fig 7

Hint

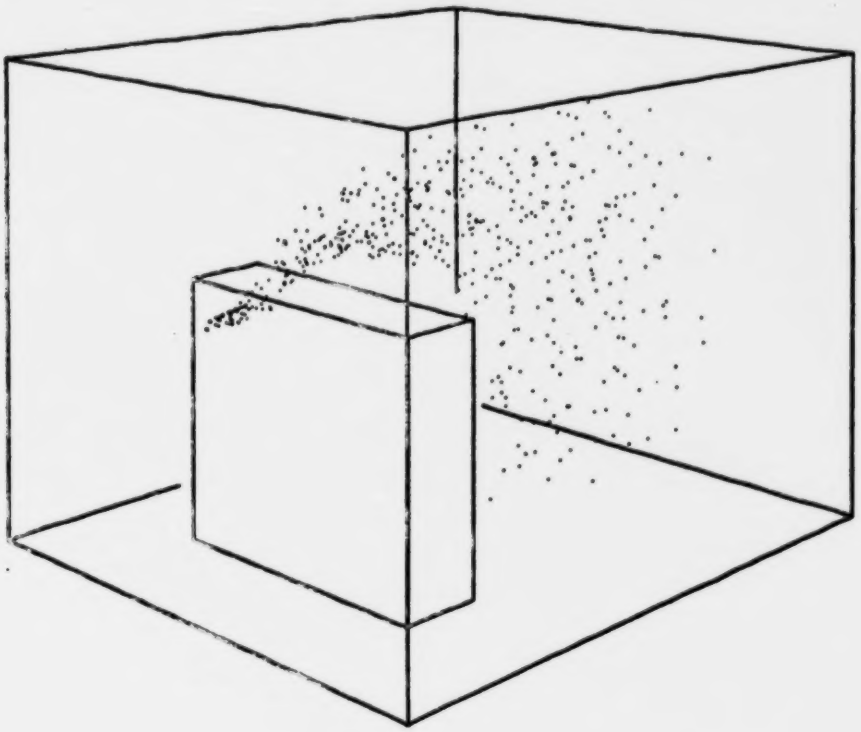

Fig 8

Hint

Top ↑

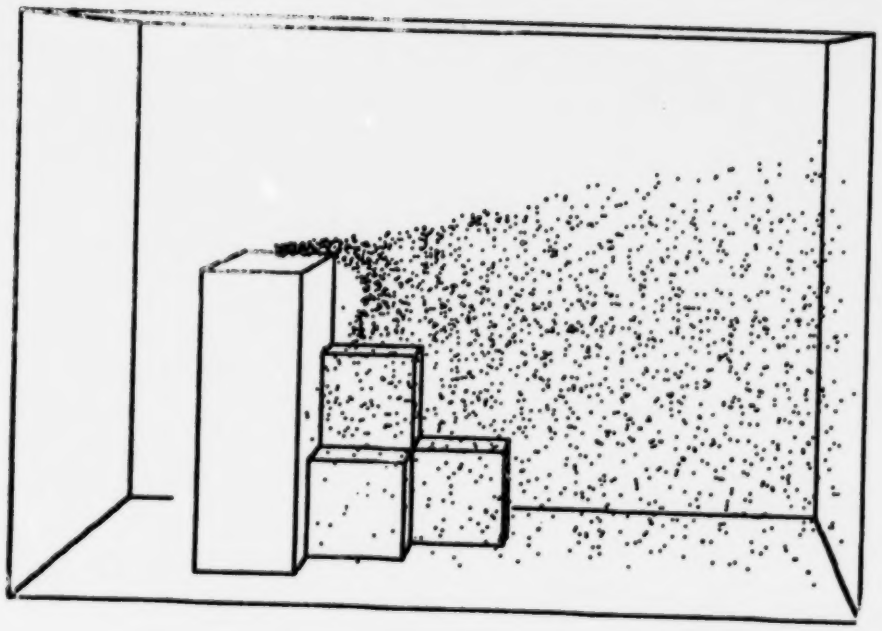

Fig 9

Hint

Top ↑

Fig 10a {

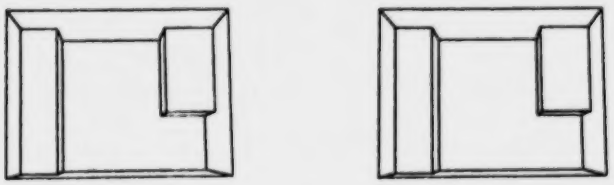

A

Fig 10b {

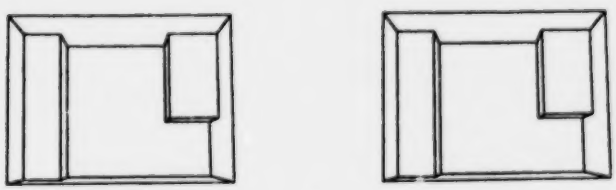

B

Hint